Validation of Discrete Ordinate Radiation Model for Application in UV Air Disinfection Modeling

---

By

Pak Chein (Jefferey) Hoi

Supervisor

Dr. Siamak Elyasi

This thesis is submitted in partial fulfillment of the requirements for the degree of

MASTER OF SCIENCE in Environmental Engineering

Faculty of Engineering

Lakehead University, Thunder Bay, Ontario, Canada

Abstract:

Hoi, Pak Chien (Jeffrey). Validation of Discrete Ordinate Radiation model for applications in UV Air Disinfection modeling. (Under the supervision of Siamak Elyasi.)

This study investigated one of the most important aspect of ultra-violet (UV) air disinfection modeling which is radiation modeling. Radiation modeling is a topic of interest in the domain of UV air disinfection research. Researchers in this field uses various types of radiation models to perform radiation modeling work including: Multiple Point Source Summation (MPSS), Multiple Segment Source Summation (MSSS), Line Source Integration (LSI), View Factor model and Discrete Ordinate (DO) model; among the radiation models discussed, DO model is the only numerical iterative radiation model that can fully utilize the ever increasing power of computing of today. Advantages of properly utilizing the DO model for radiation modeling include solving complex radiation problems in a full 3-dimensional space that provides ways to study fluence rate distribution easily. This work aims to properly utilize and validate the DO model by:

- demonstrating DO model's consideration for basic optical principles (refraction, reflection, shadowing effecting and partial absorption)
- studying fluence rate simulated values by comparing it with previously published experimental work
- performing a 3-dimensional multi-lamp radiation experiment in conjunction with the complex DO model radiation simulation case setup

The work performed shows that DO model is capable of considering basic optical principles (refraction, reflection, shadowing effecting and partial absorption) which are all integral to

developing an accurate radiation model. Previously published use of the DO model in fluence rate studies concluded that DO model was inaccurate because some of the basic optical considerations could not be included in the solution; however, the findings of this work prove otherwise. A detailed description of utilizing DO model to account for these optical principles was outlined in this paper. With sufficient understanding of utilizing the DO model for UV lamp radiation cases, the scalability of using this newly described method to solve complex UV radiation cases was demonstrated. Additionally, DO model simulated results (with all basic optical considerations) are shown to match UV fluence rate values based on a published actinometer radiation experiment to a good agreement.

This method was studied further by performing a complex multi lamp 3D radiation experiment and comparing the experimental readings to the DO model simulated result. The complexity of this UV radiation experiment is unprecedented as there are no published UV radiation lamp experimental work that could be found (during the time of writing). Unfortunately, the comparison between radiometer readings and simulated values did not show good agreement. Although the DO model simulation results did not match the experimentally measured data completely, a lot of important optical considerations to include in a DO model simulation was explored. Findings from this study is significant to the application and utilization of DO model in radiation modeling work for UV air disinfection.

VALIDATION OF DISCRETE ORDINATE RADIATION MODEL FOR APPLICATION IN UV AIR DISINFECTION MODELING

by

JEFFREY (PAK CHIEN) HOI

A dissertation submitted to the Graduate Faculty of

Lakehead University

In partial fulfillment of the

Requirements for the degree of

Masters in Applied Sciences

Department of Environmental Engineering

Thunder Bay, ON

2014

REVIEWED BY:

Dr. Siamak Elyasi (supervisor)

Dr. Leila Pakzad

Dr. Dimiter Alexandrov

Table of Contents

Chapter 1: Literature Review 1-1

1.1 Introduction to Ultra Violet Disinfection 1-1

1.1.1 UV Inactivation Theory 1-2

1.1.2 UV Photoreactivation and UV defend mechanisms 1-3

1.2 Modeling Work 1-4

1.2.1 Mathematical Microbial Decay Models 1-5

1.2.2 Hydrodynamic Modeling 1-11

1.2.3 Radiation Modeling 1-13

1.2.4 Numerical radiation models in CFD 1-16

1.3 Thesis Objectives 1-20

1.3.1 DO Model Validation 1-21

1.4 Significance of Work 1-22

1.5 References 1-23

Chapter 2: Foundations of DO model 2-27

2.1 Basic terms 2-27

2.2 Radiative Transfer Equation (RTE) 2-30

2.3 Finite Volume (FV) Approach 2-31

2.4 Formulation of Discrete Equations 2-34

2.5 Solution Procedure 2-37

2.5.1 Boundary conditions 2-38

2.5.2 Angular grid 2-38

2.5.3 Isotropic Scattering 2-39

2.5.4 Energy equation 2-39

2.5.5 Iterative Solution 2-40

2.6 Using DO model in FLUENT 2-41

2.7 References 2-42

Chapter 3: Obtaining accurate result from DO model for radiation distribution modeling 3-43

3.1 Abstract 3-43

3.2 Introduction 3-43

3.3 Theory 3-45

3.4 Procedures and Methods 3-50

3.4.1 Basic Optic Principles 3-50

3.4.2 Past Experimental Study Validation 3-52

3.4.3 Complex Case Simulation Validation 3-54

3.5 Results 3-56

3.5.1 Basic Optic Principles Validation 3-56

3.5.2 Past Experimental Study Validation 3-58

3.5.3 Complex Case Simulation Validation 3-61

3.6 Discussion 3-62

3.7 Conclusion 3-66

3.8 References 3-68

3.9 Appendix 3-70

3.9.1 Setting up model in FLUENT for simulation 3-70

Chapter 4: Validating DO model with multi-lamp 3-dimensional radiation measurement experiment 4-73

4.1 Abstract 4-73

4.2 Introduction 4-73

4.3 Procedures and Methods 4-75

4.3.1 Main experimental setup 4-75

4.3.2 Simulation setup 4-79

4.3.3 Initial experimental setup 4-81

4.4 Results 4-83

4.4.1 Stability test results 4-83

4.4.2 Main experiment results 4-84

4.4.3 Additional experiments for simulation 4-86

4.4.4 DO model Simulation results 4-89

4.5 Discussion 4-90

4.6 Conclusion 4-97

4.7 References 4-100

Chapter 5: Conclusion of study and future work 5-102

5.1 References 5-105

List of Figures

Figure 1-1: Illustration of multi-hit variable model for a typical S vs D plot (Kowalski, Bahnfleth, Witham, Severin, & Whittam, 2000) 1-10

Figure 3-1: Angular discretization of a quadrature 3-49

Figure 3-2: Illustration of overhanging control angle issue in 2D cases 3-49

Figure 3-3: Reactor simulation setup used as described in a study evaluating several fluence rate models by Liu et al. 3-53

Figure 3-4: Details of lamp models used with included quartz housing and source light from surface of lamp core 3-54

Figure 3-5: Complex Radiation Case with Non-specular and Specular Enclosure and multiple Lamps Setup 3-55

Figure 3-6: Qualitative simulation results demonstrating DO model accounting for basic optic principles: (a) reflection; (b) refraction; (c) shadowing effect; (d) partial absorption 3-57

Figure 3-7: Simulation results from fluence rate experimental setup experiment conducted by Liu et al. 3-59

Figure 3-8: Value comparisons between simulated DO model results to experimentally measured actinometer fluence rate values 3-60

Figure 3-9: Cross-sectioned incident radiation (W/m^2) results at different locations for complex case simulation with non-specular enclosure 3-61

Figure 3-10: Cross-sectioned incident radiation (W/m^2) results at different locations for complex case simulation with specular enclosure 3-62

Figure 4-1: Lamp position and dimension details 4-76

Figure 4-2: 3D Scanner Apparatus with attached radiometer on probe 4-77

Figure 4-3: Positions of planes and grid system used for gathering data 4-78

Figure 4-4: Full general overview of experimental setup and a snapshot of experiment running. 4-79

Figure 4-5: Geometry and mesh of complex multi-lamp experimental setup in ANSYS 4-80

Figure 4-6: Initial experimental setup to determine lamp intensity variations 4-82

Figure 4-7: Lamp plasma absorption experiment 4-83

Figure 4-8: Initial UV lamps stability test 4-84

Figure 4-9: Contoured radiation readings obtained for z-plane distance = 50mm 4-85

Figure 4-10: Contoured radiation readings obtained for z-plane distance = 100mm 4-85

Figure 4-11: Contoured radiation readings obtained for z-plane distance = 150mm 4-85

Figure 4-12: Contoured radiation readings obtained for z-plane distance = 200mm 4-86

Figure 4-13: Radiometer reading profiles along longitudinal (Y-axis) of each lamp used in the experiment..... 4-87

Figure 4-14: Incident radiant flux contours from DO model simulation of z-plane distance away = 50mm (a) and 100mm (b)..... 4-89

Figure 4-15: Incident radiant flux contours from DO model simulation of z-plane distance away = 150mm (a) and 200mm (b)..... 4-89

Figure 4-16: Comparison between incident radiant flux (W/m^2) contours of DO model simulation (a), experimental data (b), and overlaid contours (c) at z-plane distance = 50mm..... 4-93

Figure 4-17 Comparison between incident radiant flux (W/m2) contours of DO model simulation (a), experimental data (b), and overlaid contours (c) at z-plane distance = 100mm..... 4-94

Figure 4-18 Comparison between incident radiant flux (W/m2) contours of DO model simulation (a), experimental data (b), and overlaid contours (c) at z-plane distance = 150mm..... 4-94

Figure 4-19 Comparison between incident radiant flux (W/m2) contours of DO model simulation (a), experimental data (b), and overlaid contours (c) at z-plane distance = 200mm..... 4-95

List of Tables

Table 2-1: Nomenclature terms 2-27

Table 4-1: Intensity ratio between lamps against lamp 3 4-87

Table 4-2: Summary of radiometer readings obtained from absorption experiment..... 4-88

Chapter 1:Literature Review

1.1 Introduction to Ultra Violet Disinfection

Ultra Violet (UV) can be defined as a spectrum of electromagnetic radiation with wavelengths ranging from 100-400nm (just under visible light). UV can be classified into four primary bands within this range. They are UVA (320-400nm), UVB (280-320nm), UVC (200-280nm), and VUV (100-200nm). Between these primary bands, only UVB and UVC are of interest when considering UV for disinfection purposes (Bedford, 1927). Both UVB and UVC lie within the germicidal range for disinfection of microorganisms (Kowalski W. , 2009).

The use of UV for disinfection has many industrial applications, primarily in the water treatment industry. A lot of research effort has been focused on developing effective UV systems for water treatment (AWWA, 2011), (Bolton & Colton, 2011). However, another important application of UV disinfection is the disinfection of air and surfaces. This was significantly apparent when the center for disease control and prevention (CDC) acknowledged the effectiveness of UV for *Tuberculosis* (TB) control during the worldwide TB epidemic in 1994 (Jensen, Lambert, Iademarco, & Ridzon, 2005). To help distinguish between research efforts related to water and air UV disinfection, the term "UVGI" (Ultra violet Germicidal Irradiation) was established and adopted by CDC. UVGI is used in the field of UV disinfection research for air and surface applications specifically.

Early research efforts in UV disinfection focused heavily on water treatment systems. Unfortunately, the design of UVGI systems for water and air applications differs significantly from design of UV disinfection in water systems. Therefore, the research knowledge accrued from past research in water UV disinfection systems cannot be directly translated into design of

UV air disinfection systems (Bolton & Colton, 2011). Generally speaking, the design of UV systems for water treatment requires closely packed arrays of UV lamps as the attenuation of UV irradiance in water only occurs within 15 cm (Bolton & Colton, 2011). UVGI disinfection for air systems occurs in a much broader range compared with UV disinfection for water.

The use of UV to disinfect air has the potential to be efficient and cost-effective method to improve air quality in commercial applications. Schools and hospitals (surgery rooms) have begun implementing UV disinfection systems since 1940s (Goldner & Allen Jr, 1937-1973). However, UVGI was not taken seriously by the health care industry until the global leading health authority, CDC, endorsed it in 1994. This presents an important opportunity to study and understand UVGI systems for us today. Recent research has reaffirmed that UV technology can have a major impact on the reduction of various types of nosocomial and commercially acquired disease (Menzies, Popa, Hanley, Rand, & Milton, 2003) (Ritter, Olberding, & Malinzak, 2007) (Varma, et al., 2013).

1.1.1 UV Inactivation Theory

Both UVC (200-280nm) and UVB (280-320nm) have been identified to lie within the germicidal range of microorganisms (Kowalski W. , 2009). It is theorized by researchers that inactivation of microorganisms is a result of UV Irradiation being absorbed by the proteins in the microorganisms (Bolton & Colton, 2011) (Turtoi, 2013). The mutation caused by the absorption of UV Irradiation is particularly damaging to the microorganism population as it would commonly prevent the cells from re-producing or could lead to cell death. The germicidal effectiveness of UVC and UVB varies from species to species; however, the UV absorption peak usually lies between 260-265nm (highest germicidal effectiveness) (Sommer, et al., 2001).

Coincidently, this range is close to the peak energy wavelength output from low pressure (LP) mercury lamps, which is at 253.7nm (IESNA, 2000).

There are generally two types of nucleic acids in a cell, ribonucleic acid (RNA) and deoxyribonucleic acid (DNA). Both RNA and DNA are composed of nucleotides containing nucleobases (guanine, adenine, cytosine, thymine (DNA only) and uracil (RNA only)). These nucleobases are held in place by hydrogen bonds. When exposed to UV radiation, a photochemical reaction can cause the formation of thymine-thymine base bond, which is more stable than the hydrogen bond, altering the structure of the nucleic acid. As RNA and DNA are proteins in a cell responsible for reproductive functions and protein synthesis, the mutation caused by UV radiation exposure results in inactivation of the cell (unable to re-produce) (Casarett, 1968).

1.1.2 UV Photoreactivation and UV defend mechanisms

There is a common phenomenon exhibited by microorganisms population when exposed to UV irradiation, it is known as photoreactivation. The phenomenon of photoreactivation refers to the ability of microorganism to self-repair the damages incurred by UV exposure. Photoreactivation occurs when microorganisms are exposed to visible light after UV irradiation (Setlow & I., 1966) (Fletcher, Noakes, Beggs, Sleigh, & Kerr, 2003).

One study indicates the decay rate of *Mycobacterium parafortuitum* under UV exposure in liquid suspensions is significantly decreased by simultaneous exposure to visible light. The same study suggests that airborne microbial populations can recover significantly if allowed sufficient time (Peccia and Hernandez, 2002). The photoreactivation phenomenon is still a relatively new field of study and not understood very well yet; however, Linden & Darby has demonstrated that

photoreactivation can be preempted by using high-enough UV doses to cause extensive damage to the cell that no photorepair mechanism can occur (Linden & Darby, 1994).

Another recent study pertaining to photoreactivation have noted that there are evidence that suggests broad-band UV lamps (medium pressure mercury lamps) are more effective in suppressing photoreactivation compared with a narrow band UV lamps (low pressure mercury lamps) (Massachelein, 2002).

Microorganisms also have mechanisms to defend against UV irradiation. The nucleocapsid surrounding the nucleus and cytoplasm of the cell might absorb UV irradiation before the nucleic acid is exposed to the radiation. Some microorganisms may also have dark proteins within the cell to that are able to absorb the UV irradiation. Fungal spores for example, are considered one of the UV resistant microbes as it often has melanin-containing dark pigmented conidia (Durrell & Shields, 1960) (Bell & Wheeler, 1986), (Boyd-Wilson, Perry, & Walter, 1998) (Valero, et al., 2007).

1.2 Modeling Work

UVGI is a field of research with many opportunities to improve and develop upon. Understanding and employing models governing the disinfection of microorganisms is key to designing an effective UVGI disinfection system. Conventionally, efficiency of a UVGI system design can be evaluated by experimental bioassay tests; however, this physical process would be a concern when considering large-scale complex UV air disinfection systems. The advancements in the fast-paced development of the computing industry, lead to high performing computers today could strongly aid in the understanding and evaluation of UVGI system if leveraged properly. Numerical models modeling UV disinfection systems can be established and solved using powerful computers available today.

A fully integrated UVGI system model comprise of three main components:

1. Mathematical Decay Model
2. Hydrodynamic Model
3. Radiation or Fluence Rate Model

The mathematical decay model describes the behavior of microorganism population when exposed to set UV dosage. UV dosage, or fluence is an important parameter of concern when considering modeling UVGI systems. It is covered in more detail in the upcoming section. Accurate prediction of UV dosage is key to developing a good UVGI model. Modeling of UV dosage requires integration of a fluence rate model with hydrodynamic model. These models will be discussed in more detail in the upcoming section.

1.2.1 Mathematical Microbial Decay Models

To effectively study UVGI disinfection, it is important to analytically describe the mechanics of disinfection as an expression or model.

1.2.1.1 Dosage Calculations

Microorganisms exposed to UV irradiation are subject to UV dose or fluence. UV Dosage received by the microorganism can be expressed as:

$$D = I_f \cdot t$$

where,

D = Dosage, (J/m^2)

I_f = Fluence rate (W/m^2)

t = exposure time (s)

(Kowalski, Bahnfleth, Witham, Severin, & Whittam, 2000)

The fluence rate, I_f refer to the radiative flux passing through the surface of the microorganism (in a simplified assumption, a cross section of a sphere). This parameter is also referred to as spherical irradiance by other researchers in this field. The dosage parameter is an important and widely used parameter when considering modeling disinfection rates.

1.2.1.2 Single-stage Decay Model

The efficiency of a UVGI system can be evaluated by calculating the survival fraction of microorganisms, S after being exposed to a set dosage, D of UV irradiation. The primary model used to evaluate the survival of microorganisms subject to UV exposure is a single-stage exponential decay model as represented below:

$$S = e^{-kD} \qquad (2)$$

where,

S = Survival, fractional

k = Rate constant (m^2/J)

D = Dosage, (J/m^2)

(Kowalski, Bahnfleth, Witham, Severin, & Whittam, 2000)

The single-stage decay model is generally adequate for most UVGI design purposes because disinfection rates of 90-99% can be achieved in the first stage decay. The dosage required to achieve 90% disinfection rate is termed D_{90} (Kowalski W. J., 2001).

UV rate constant, k, is an experimentally determined value. High values of k, implies faster decay and rapid disinfection; lower UV rate constant implies that the microorganism of interest is more UV resistant. Generally speaking, bacteria and viruses (both RNA and DNA viruses) have high k values, while fungal spores have low k values. Many researchers in this field have studied the UV rate constants of various types of bacteria, viruses, and fungi as well as other microbes. In 2009, Dr. Kowalski consolidated and compiled over 600 k values for these common microorganisms from prior research work in this field. The k values described only apply to UVGI air and surface disinfection studies. It should be noted that the UV rate constant for water UV disinfection is significantly different from the air disinfection counterpart. A full list of k values for bacteria, viruses, fungi and other microbes can be found in appendices of "Ultraviolet germicidal irradiation handbook: UVGI for air and surface disinfection" by Dr. Kowalski. (Kowalski W. , 2009)

1.2.1.3 Two-stage Decay Model

Although most microbial population decay behavior can be described with a single stage decay model, it is common for a small fraction in the microbial population that exhibits higher level of UV resistance. The fraction of microbial population that is more UV resistant could have a UV rate constant, k that is up to 10 times lower than the rest of the microbial population (Sharp, 1939). This will result in a significant distinguishing of stages in the decay curve, a rapid decay stage and slow decay stage. An alternative model to account for this behavior was proposed by Hiatt in 1964:

$$S = (1 - f)e^{-k_1 D} + fe^{-k_2 D} \qquad (3)$$

where,

f = fraction of microbial population that is more UV resistant

k_1= UV rate constant for 1st stage of decay (rapid decay), (m^2/J)

k_2= UV rate constant for 2nd stage of decay (slow decay), (m^2/J)

(Hiatt, 1964)

This is commonly known as the two-stage decay model, where the survival response of the population is a summation of two stages of decay within the microbial population. Two UV rate constants are used to describe the rapid and slow decay in the respective stages of decay. Similar to UV rate constants for the single stage decay, the values obtained experimentally. Values of k_1 and k_2 as well as $(1-f)$ and f have to be fitted to data by trial and error for different species of microbial population. Dr. Kowalski has also consolidated and compiled appendices of these values for common microorganisms (Kowalski W. , 2009). It should be noted that the values of k_1 for a two-stage decay model is different from the value of k in a single-stage decay model. These terms cannot be used interchangeably.

1.2.1.4 Shoulder Effect

Another decay behavior commonly observed in UVGI disinfection studies is a slight delay before conforming to typical single-stage and two-stage decay models described above. The delay of response to UV exposure is commonly known as the shoulder by researchers in this field. The delay behavior was given the term shoulder because it results in a horizontal line in the decay curve, shaping the curve similar to a shoulder. Implications of the shoulder effect observed could suggest microorganisms have defense mechanisms as described in the previous section. A threshold of UV exposure dose is required before effects of exposure (decay) can be significantly

observed (Casarett, 1968) (Cerf, 1977) (Munakata, Saito, & Hieda, 1991) (Pruitt & Kamau, 1993).

There are generally two types of mathematical models that could be used to account for the shoulder effects into decay modeling: classic model and target model. Various researchers proposed several types of target models: recovery models, split-dose recovery models, empirical models and more recently, the multi-hit target model (Harm, 1980) (Russell, 1982) (Severin & Suidan, 1983) (Kowalski, Bahnfleth, Witham, Severin, & Whittam, 2000). The multi-hit target model was first proposed by Severin & Suidan and is described below:

$$S(t) = 1 - (1 - e^{-kD})^n \qquad (4)$$

where,

n = multi-hit target exponent

(Severin & Suidan, 1983)

The multi-hit target exponent, n, can be determined by extrapolating decay curve data with a solid line until it intercepts the axis where dosage, D = 0 J/m^2 in a survival fraction, S vs. D plot. This is illustrated by the graph image below, Figure 1-1.

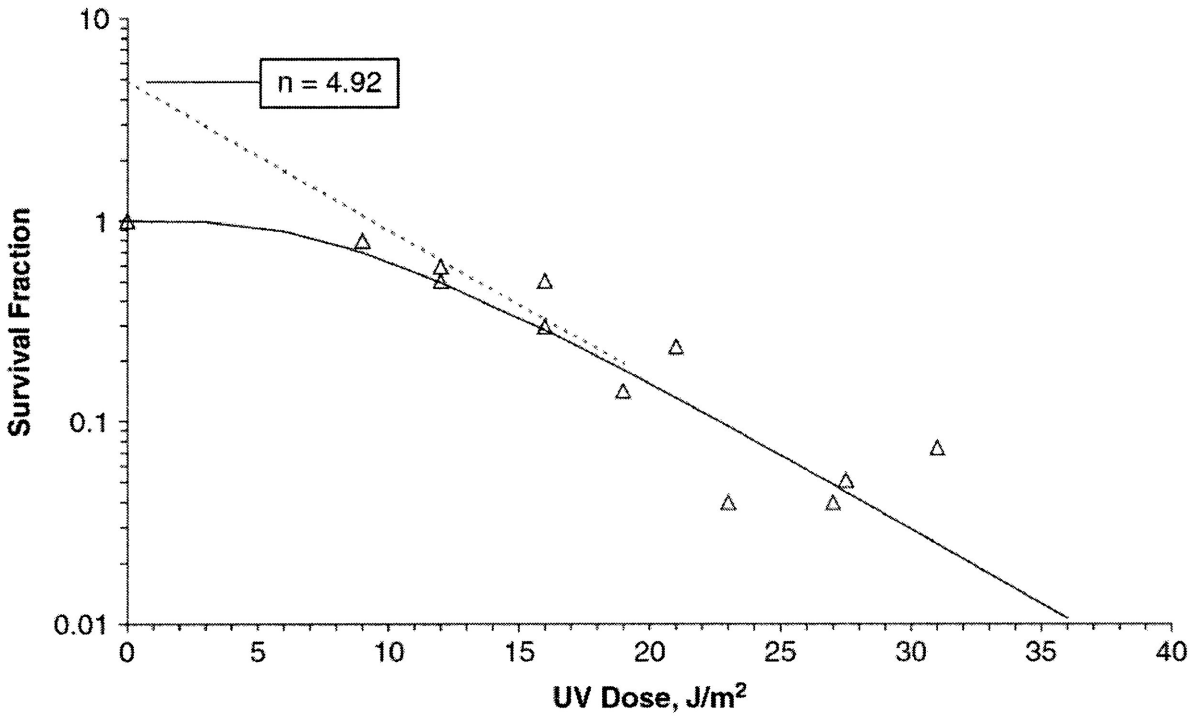

Figure 1-1: Illustration of multi-hit variable model for a typical S vs D plot (Kowalski, Bahnfleth, Witham, Severin, & Whittam, 2000)

The equation above only applies for single-stage decay model behavior. The parameter n, represents the number of discrete critical sites that must be hit to inactivate the microorganism. Theoretically, the value of n is an integer, but practically, this is not typically true. The value of n ranges widely from 1 up to over 1000 (Kowalski, Bahnfleth, Witham, Severin, & Whittam, 2000).

The shoulder effect can also extend to two-stage decay models in some cases. The combination of the two-stage decay model with multi-hit target model can be used to model this behavior.

$$S = (1 - f)[1 - (1 - e^{-k_1 D})^{n_1}] + f[1 - (1 - e^{-k_2 D})^{n_2}] \quad (5)$$

n_1 = multi-hit target exponent for 1st stage (rapid decay)

n_2 = multi-hit target exponent for 2nd stage (slow decay)

(Kowalski, Bahnfleth, Witham, Severin, & Whittam, 2000)

Limited data is available in literature to sufficiently determine these values for most microbes. Dr. Kowalski's consolidated data of rate constants only has a few examples of microbial population that exhibit this behavior (both shoulder and two-stage decay). It should be noted that parameter n_2 generally have little or no effect on the shape of decay curve; therefore, the assumption of $n_2 = 1$ can be established without loss in predictive accuracy (Kowalski, Bahnfleth, Witham, Severin, & Whittam, 2000).

1.2.2 Hydrodynamic Modeling

UV Dosage, D is expressed previously as a function of fluence rate, I (W/m^2) and exposure time, t (s) Equation (1). The exposure term, t can be determined through hydrodynamic modeling of the microorganism particle travelling in the UVGI system. The velocity field can be simulated using computational fluid dynamics (CFD), which establishes and solves a system of equations based on conservation of mass and momentum.

The general form of single-phase conservation of momentum is:

$$\frac{\partial}{\partial t}(\rho u) + \nabla \cdot (\rho u) = \nabla p - \nabla \cdot \tau + \rho g + F \qquad (6)$$

where,

ρ = medium density (kg/m^3)

u = velocity vector (m/s)

p = pressure (Pa)

τ = viscous stress tensor (Pa)

g = gravitational constant (9.81 m/s^2)

F = body force (N)

(Ranade, 2002)

The numerical solution to the conservation equation above Equation (6) can be solved numerically for low Reynolds flow conditions; however, for flow conditions with higher Reynolds number (turbulent), the solution of from conservation of momentum gets more complicated. Several turbulence models were developed to address this issue. Some examples are the standard (STD) k-ε model, re-normalisation group (RNG) k-ε model, the k-ω model as well as Reynolds-Stress Model (RSM) for multi-phase for even more complex flow problems (Yakhot & Orszag, 1986) (Wilcox, 1998) (Ranade, 2002) (Cokljat, Slack, & Vasquez, 2003).

Before the use of turbulence models, researchers in the field of UV systems simulations studied microbial kinetics with traditional residence time models (RTD). Average values of fluence rate were used with the RTD model, which resulted in bad prediction of disinfection rates that didn't match experimental results (Chiu, Lyn, Savoye, & Blatchey III, 1999) (Kowalski W. , 2009). Recent research has indicated that turbulence models are the most promising technique of analyzing mixing and turbulent flow behavior in a UV system (Liu D. , 2004). Several authors have shown that incorporating turbulence models (as part of a CFD package) to simulate the hydrodynamic behavior of microorganisms in UV systems have shown reasonable agreement with conventional bioassay experiments (Baas, 1996) (Buffle, Chiu, & Taghipour, 2000) (Rokjer, Valade, Keesler, & Borsykowsky, 2002) (Neofotistos, Do-Quang, & Perrin, 2002) (Do-Quang, Janex, & Perrin, 2002) (Ducoste, Liu, & Linden, 2005).

1.2.3 Radiation Modeling

Hydrodynamic modeling is an important component in dosage modeling; however, extensive modeling research has already been performed in this field already. Another component that is integral to dosage modeling is radiation (fluence rate) component. Researchers in the field of radiation modeling have acknowledged the complexity of accurately modeling UV lamp radiation that has to account for optical principles such as absorbance, scattering, reflection and refraction (Bolton, 2000).

There are a few known approaches to radiation modeling. Some common fluence rate models include multiple points source summation (MPSS), line source integration (LSI), multiple segment source summation (MSSS), view factor and discrete ordinate (DO) model (Liu, Ducoste, Jin, & Linden, 2004).

In 1970, Jacob and Dranoff developed the MPSS approach. The MPSS approach is based on dividing the linear lamp into a series of equally spaced point sources along the absorbing media. Each point along the absorbing media is assumed to emanate uniformly in all directions (Jacob & Dranoff, 1970). In 1997, Blatchey introduced the LSI model. LSI model is conceptually similar to the MPSS. LSI model integrates over an infinite number of point sources as compared to finite number of points with MPSS approach (Blatchley III, 1997). MPSS and LSI model becomes identical as the number of points sources approaches infinity.

Both the MPSS and LSI radiation models do not consider reflection and refraction effects. In 2000, Bolton highlighted the importance of accounting reflection and refraction into radiation models. He improved the MPSS model to include the effects of refraction, reflection and absorption; however, using a large number of point sources can be computationally intensive (Bolton, 2000). In 2002, Bolton introduced the MSSS model, which incorporated much of the

improvements he introduced to MPSS model (reflection and refraction considerations); however, MSSS model corrected the over-prediction problem experience by MPSS when modeling the lamp as a series of linear point sources. The MSSS approach corrected the over-prediction problem by modeling the lamp as a series of cylindrical segments (Liu, Ducoste, Jin, & Linden, 2004).

Another common approach to radiation modeling is view factor method. Using view factor algebra, Modest developed a model to calculate the irradiance intensity from a cylindrical surface to a differential element in space (Modest, 1993). This approach was later adopted by Kowalski to simulate light intensity field for studying disinfection of air streams (Kowalski, Bahnfleth, Witham, Severin, & Whittam, 2000). According to Kowalski's research, view factor simulation resulted is in better agreement with experimental data than other radiation models like point source, line source, LSI.

Fluence rate of a UV system can also be modeled using DO method. DO model solves a systems of equations based on the radiative transfer equation (RTE) for an absorbing, emitting and scattering medium at position $\vec{r}$ in the direction $\vec{s}$ for a finite number of discrete solid angles (defined by the user as angular discretization).

The RTE equation is shown below:

$$\frac{dI(\vec{r},\vec{s})}{ds} = an^2\frac{\sigma T^4}{\pi} + \frac{\sigma_s}{4\pi}\int_0^{4\pi} I(\vec{r},\vec{s}')\Phi(\vec{s}\cdot\vec{s}')d\Omega' - (a+\sigma_s)I(\vec{r},\vec{s}) \qquad (7)$$

where,

$\vec{r}$ = position vector

$\vec{s}$ = direction vector

$\vec{s}'$= scattering direction vector

s = path length (m)

a = absorption coefficient (m^{-1})

n = refractive index

σ_s = scattering coefficient

σ = Stefan-Boltzmann constant (5.672×10^{-8} $W/m^2\text{-}K^4$)

I = radiation intensity, (as a function of position, $\vec{r}$ and direction, $\vec{s}$) (W/m^2-sr)

T = local temperature (K)

Φ = phase function

Ω'= solid angle (sr)

(Fluent Inc, 2006)

The discrete-ordinate (DO) method for solving radiative heat transfer was first introduced by Chandrasekhar (Chandrasekhar, 1960). Regrettably, early computer implementations of the method at the time were plagued with numerical difficulties (Liou K. N., 1973); however, Stamnes developed a numerically stable DO model algorithm, which invigorated interest back into DO model. Stamnes et. al. improved the DO model by developing a stable algorithm which incorporated reflection at interfaces of layers for a multi-layered media (Stamnes, Chee Tsay, Wiscombe, & Jayaweera, 1988). In 1996, Liou and Wu, further extended DO model by consider interactions of interface in multi-layered medium as Fresnal interfaces. This consideration allows DO model to account for reflection and refraction based on Fresnal equations (Liou & Wu, 1996). In 1999, further development of the model expanded DO model for solving radiative heat transfer problems involving semitransparent media (Murthy & Mathur, 2000).

MPSS, LSI, and MSSS are well-researched and accurate radiation models; however, these models are based on analytical approaches to solving radiation problems. It would be difficult and time-consuming to scale these models for analysis of complex UV system setup. View factor and DO radiation models on the other hand, solves radiation problems numerically. This translates into easy scalability from simple to complex radiation problems. It would then be beneficial to utilize these numerical models for complex UV radiation problems instead of analytical models.

1.2.4 Numerical radiation models in CFD

The advancement in high performance computers has made historically computational intensive tasks much more accessible today. One field of research that benefited from a lot from this advancement is the field of computational fluid dynamics (CFD). Several general-purpose commercial CFD software packages were developed and published over the past decade. Popular CFD software packages include: FLUENT (part of ANSYS), CFX (part of ANSYS), OpenFOAM, OpenFlower, COMSOL, and Flow-3D to name a few (ANSYS Inc, n.d.) (ANSYS Inc, n.d.) (OpenCFD Ltd, n.d.) (Dice Holdings Inc, n.d.) (COMSOL Inc, n.d.) (Flow Science Inc, n.d.).

Among the listed CFD software packages, FLUENT is one of the leading CFD software package with broad range of physics modeling including flow, turbulence, heat transfer, and reactions for industrial applications (ANSYS Inc, n.d.). As a result, FLUENT is the platform of choice in this study. Several radiation models are available in FLUENT:

1. Discrete Ordinate (DO) model
2. Discrete Transfer radiation model (DTRM)
3. P-1 radiation model

4. Rosseland radiation model
5. Surface to surface (S2S) radiation model

(Fluent Inc, 2006)

Each radiation model listed has advantages and disadvantages that should be taken into consideration when choosing a radiation model to use.

1.2.4.1 DO model

DO model solves RTE for discrete solid angles as discussed previously. The implementation of DO model in FLUENT uses a conservative finite-volume approach which will be discuss thoroughly in the upcoming chapter. The solution method of DO model is similar to that of fluid flow and energy. Advantages of utilizing DO include:

1. DO model spans the entire range of optical thickness and can account for principle optical laws such as absorption, scattering, reflection and refraction. (Applicable to radiation problems with semi-transparent media, specular and diffuse surfaces)
2. DO model can be used to solve gray or non-gray radiation problems (using gray-band model).
3. Computational load for implementing DO model can be controlled by adjusting angular discretization and overhanging control angle pixelation.

DO model is a comprehensive radiation model that can account for most radiation problems; however, solutions with fine angular discretization is very CPU intensive. (Fluent Inc, 2006)

1.2.4.2 DTRM model (Ray Tracing)

DTRM model solves radiation problems by performing ray tracing. The main assumption used in DTRM is that radiation leaving the surface element can be approximated by a single ray (in a

certain range of solid angles). Similar to DO model, an advantage of DTRM is control over computational load. Accuracy of DTRM simulations can be improved by increasing number of rays. DTRM is primarily a simple model and applies to a wide range of optical thickness; however, there a few limitations to utilizing DTRM model:

1. DTRM model assumes all surface are diffuse. (isotropic reflection)
2. Effect of scattering is not considered.
3. DTRM only assumes gray radiation model.
4. DTRM is not compatible with non-conformal interface or sliding meshes.
5. DTRM is not programmed for parallel processing.

(Fluent Inc, 2006)

1.2.4.3 P-1 radiation model

P-1 radiation model is one of the simplest case for a general P-N model, which is based on expansion of radiation intensity I into an orthogonal series of spherical harmonics. P-1 radiation model solves RTE as a diffuse equation, which requires little computational demand. This radiation model can also include the effects of scattering; however, there are limitations to utilizing P-1 radiation model:

1. P-1 model assumes all surface are diffuse. (similar to DTRM model)
2. P-1 model only assumes gray radiation model.
3. Accuracy of model is compromised with complicated geometry and small optical thickness.
4. P-1 model also has a tendency to over-predict local radiative flux from local sources or sinks.

(Fluent Inc, 2006)

1.2.4.4 Rosseland model

Rosseland radiation model is similar to P-1 model as it can be derived from P-1 model equations (with some approximations). Rosseland model has two main advantages over P-1 model. Rosseland model does not consider an extra transport equation for incident radiation; therefore, it is more computationally less demanding than P-1. Rosseland model solution can be achieved faster with less required memory compared with the P-1 radiation model; however, there are limitations to Rosseland model:

1. Rosseland model only applies to optically thick media ($\alpha L \gg 1$, where L is the length of the domain). It is recommended for use when optical thickness exceed 3 by FLUENT's user guide.
2. Rosseland model is also not available when a density-based solver is used, only when pressure-based solver is used.

(Fluent Inc, 2006)

1.2.4.5 S2S model

Surface to surface (S2S) model is designed to model enclosed radiation problems with gray-diffuse surfaces and no participating media. The approach taken by S2S model is based on view factor method. The main assumption in S2S model is based on neglecting effects of absorption, scattering or emission in participating media; the only considerations of this model is size, distance and orientation of one surface to another.

Limitations of utilizing S2S model include:

1. S2S model assumes all surface are diffuse (similar to DTRM model)

2. S2S model only assumes gray radiation
3. S2S model cannot be used for radiation problems with participating media
4. S2S model cannot be used for symmetric or periodic boundary conditions.
5. S2S model cannot support non-conformal interfaces, hanging nodes and grid adaption.

(Fluent Inc, 2006)

1.2.4.6 Choosing a radiation model

FLUENT provides a wide range of numerical radiation models; however, as discussed, each radiation model has advantages and disadvantages. Depending on the radiation problem of interest, utilizing one radiation model may be more appropriate than others. In this study, DO model is the numerical radiation model of choice because it is the most comprehensive radiation model in FLUENT.

DO model is the only radiation model in FLUENT that can account for the major optical problem considerations involving absorption, scattering, or emission of a gray or non-gray medium with semi-transparent interfaces and specular as well as diffuse surfaces. DO model also allows for modeling of localized heat sources and optically thick media problems. DO model has also been developed and improved to account for unstructured and asymmetric meshes which will be detailed in the next chapter.

1.3 Thesis Objectives

The overall objective of this research is to develop a reliable model that integrates a numerical radiation model (DO model) and a hydrodynamic turbulence model for UV dosage calculations. The focus of the research would be on the validation of DO model as an accurate and reliable numerical radiation model. The results generated from DO model simulations can also be translated into a full dosage model when integrated with particle tracking and a hydrodynamic

turbulence model. Implications of this research can be applied to better understanding and aid in designing effective UV air disinfection systems.

1.3.1 DO Model Validation

DO model is the numerical radiation model of interest in this work. DO model was studied in detail because it is a robust numerical radiation model that accounts for absorption, emission, scattering, reflection and refraction. The flexibility of scaling a numerical model for larger and complex UV radiation systems is a valuable to the field of radiation modeling. Although it is theoretically a powerful numerical radiation model, it is still underutilized in the field of radiation modeling. Therefore, it is important to establish better understanding and validate of the use of the model.

The DO model is readily available in a commercial CFD software package known as ANSYS. ANSYS is the platform of choice for use in this validation study. A set of simple radiation cases is studied to perform qualitative validation of DO model against basic optic principles such as reflection, refraction, shadowing and absorption. The importance of accounting for these basic optic principles in radiation models can significantly improve the accuracy of simulation results generated (Bolton, 2000).

Additionally, quantitative validation of DO model is also important. A study conducted by Liu (Liu, Ducoste, Jin, & Linden, 2004) detailed comparison between various fluence rate models including MPSS, LSI, MSSS, view factor and DO models. In the study, Liu concluded that the commercial application of DO model in FLUENT (part of ANSYS) does not account for refraction and resulted in over-prediction of fluence rate values. The effects of refraction will be accounted for in this work and the quantitative values of fluence rate obtained from this paper's

implementation of DO model will be compared against experimental values published by Liu et al (Liu D. , 2004).

A full 3-dimensional radiometry experimental study will also be conducted as an effort to validate the DO model. The experimental setup consists of multiple lamp fixtures and multiple radiometers (instruments used to measure UV irradiance incident to the photoelectric detector). This experiment aims to study accuracy of DO model simulations with a controlled UV lamp system design in full 3-dimensional space. More details about the experimental setup will be discussed in Chapter 4.

1.4 Significance of Work

The research on UV air disinfection modeling is directly be applicable to disinfection systems using of UV radiation to control the spread of pathogens transmitted through air. As discussed previously, UV air disinfection modeling is primarily divided into hydrodynamic modeling and radiation modeling. The focus of this work is the radiation modeling aspect of UV air disinfection modeling; specifically the proper use of and validation of DO radiation model. DO radiation model is potentially a comprehensive and robust radiation model that can leverage the ever increasing power of computing today. This advantage allows DO model to be easily scaled for use in simple or complex radiation problems.

The modeling work performed in this study aims to provide a deeper understanding of utilizing DO model to study UV radiation. This research will address the advantages and disadvantages of employing DO model as a radiation model through validation studies on DO model. The findings from this study is important to advance the use of DO model in UV radiation modeling.

1.5 References

ANSYS Inc. (n.d.). Retrieved January 2014, from http://www.ansys.com/Products/Simulation+Technology/Fluid+Dynamics/Fluid+Dynamics+Products/ch.ANSYS+CFX.pl

ANSYS Inc. (n.d.). Retrieved January 2014, from http://www.ansys.com/Products/Simulation+Technology/Fluid+Dynamics/Fluid+Dynamics+Products/ch.ANSYS+Fluent.pl

AWWA. (2011). *Water Quality & Treatment: A Handbook on Drinking Water.* New York: McGraw-Hill.

Baas, M. M. (1996). Latest Advances in UV Disinfection Hydrodynamic Simulation and Relation to Practical Experiences. *Proceedings AQUATECH.* Amsterdam.

Bedford, T. B. (1927). The nature of the action of ultra-violet light on microorganisms. *British journal of experimental pathology, 8*(6), 437.

Bell, A., & Wheeler, M. (1986). Biosynthesis and function of melanin. *Annual Review of Phytopathology, 24*, 411-451.

Blatchley III, E. R. (1997). Numerical modeling of UV intensity: application to collimated-beam reactors and continuous-flow system. *Wat. Res., 31*, 2205-2218.

Bolton, J. R. (2000). Calculation of Ultraviolet Fluence Rate Distributions in an Annular Reactor: Signifiance of Refraction and Reflection. *Wat. Res., 34*, 3315-3324.

Bolton, J. R., & Colton, C. A. (2011). *The ultraviolet disinfection handbook.* American Water Works Assoc.

Boyd-Wilson, K., Perry, J., & Walter, M. (1998). Persistence and survival of saprophytic fungi antagonistic to Botrytis cinerea on kiwifruit leaves. *Proc of the 51st Conf on the New Zealand Plant Prot Soc, Inc*, (pp. 96-101).

Buffle, M. O., Chiu, K. P., & Taghipour, F. (2000). UV reactor conceptualization and performance optimization with computational modeling. *Proceedings of the Water Environmental Federation, 2*, pp. 401-410.

Casarett, A. P. (1968). *Radiation Biology.* Eaglewood: Prentice-Hall.

Cerf, O. (1977). A review: Tailing of survival curves of bacterial spores. *Journal of Applied Bacteria, 42*, 1-19.

Chandrasekhar, S. (1960). *Radiative Transfer.* New York: Dover.

Chiu, K., Lyn, D. A., Savoye, P., & Blatchey III, E. R. (1999). Integrated UV Disinfection Model Based on Particle Tracking. *Journal of Environmental Engineering ASCE, 125*(1), 7-16.

Cokljat, D., Slack, M., & Vasquez, S. A. (2003). Reynolds-Stress Model for Eulerian Multiphase. *Proceedings of the 4th Intenational Symposium on Turbulence Heat and Mass Transfer* (pp. 1047-1054). Begell House, Inc.

COMSOL Inc. (n.d.). Retrieved January 2014, from http://www.comsol.com/comsol-multiphysics

Dice Holdings Inc. (n.d.). Retrieved January 2014, from http://sourceforge.net/projects/openflower/

Do-Quang, Z., Janex, M. L., & Perrin, D. (2002). Predictive tool for UV dose distribution assessment: Validation of CFD models by bioassays. *Proceedings AWWA National Convention.* New Orleans.

Ducoste, J. J., Liu, D., & Linden, K. (2005). Alternative Approaches to Modeling Dose Distribution and Microbial Inactivation in Ultraviolet Reactors: Lagrangian vs Eulerian. *Journal Environmental Engineering.*

Durrell, I., & Shields, L. (1960). Fungi isolated in culture from soil of the Nevada test site. *Mycologia, 52,* 636-641.

Fletcher, I. A., Noakes, C. J., Beggs, C. B., Sleigh, P. A., & Kerr, K. G. (2003). The ultraviolet susceptibility of aerosolised microorganisms and the role of photoreactivation. *IUVA.* Vienna.

Flow Science Inc. (n.d.). Retrieved January 2014, from http://www.flow3d.com

Fluent Inc. (2006, 09 20). *Fluent 6.3 User's Guide.* Retrieved January 2014, from http://aerojet.engr.ucdavis.edu/fluenthelp/html/ug/main_pre.htm

Goldner, J. L., & Allen Jr, B. L. (1937-1973). Ultraviolet light in orthopedic operating rooms at Duke University: Thirty-five years' experience. *Clinical Orthopaedics and Related Research, 96,* 195-205.

Harm, W. (1980). *Biological effects of ultraviolet radiation.* New York: Cambridge University Press.

Hiatt, C. (1964). Kinetics of inactivation of viruses. *Bacteria Review, 28*(2), 150-163.

IESNA. (2000). *Lighting Handbook: Reference & Application IESNA HB-9-2000.* New York: Illumination Engineering Society of North America.

Jacob, S. M., & Dranoff, J. S. (1970). Light intensity profiles in a perfectly mixed photoreactor. *A.I.C.H.E,* 359-363.

Jensen, P. A., Lambert, L. A., Iademarco, M. F., & Ridzon, R. (2005). *Guidelines for preventing the transmission of Mycobacterium tuberculosis in health-care settings.* US Department of Health and Human Services, Public Health Service, Centers for Disease Control and Prevention.

Kowalski, W. (2009). *Ultraviolet germicidal irradiation handbook: UVGI for air and surface disinfection.* Springer.

Kowalski, W. J. (2001). *Design and Optimization of UVGI Air Disinfection System.* PhD Thesis, State College: The Pennslyvania State University.

Kowalski, W. J., Bahnfleth, W. P., Witham, D. L., Severin, B. F., & Whittam, T. S. (2000). Mathematical modeling of UVGI for air disinfection. *Quant Microbiol, 2*(3), 249-270.

Linden, K. G., & Darby, J. L. (1994). Ultraviolet disinfection of wastewater: effect of dose on subsequent reactivation. *Water Res, 28,* 805-817.

Liou, B. T., & Wu, C. Y. (1996). Radiative transfer in a multi-layer medium with fresnel interfaces. *Heat and Mass Transfer, 32,* 103-107.

Liou, K. N. (1973). A Numerical Experiment on Chandrasekhar's Discrete-Ordinate Method for Radiative Transfer: Applications to Cloudy and Hazy Atmosphere. *Journal of Atmospheric Science, 30*, 1303.

Liu, D. (2004). *Numerical Solution of UV Disinfection Reactors: Impact of Fluence Rate Distribution and Turbulence Modeling.* Thesis.

Liu, D., Ducoste, J., Jin, S., & Linden, K. (2004). Evaluation of alternative fluence rate distribution models. *Journal of Water Supply: Research and Technology AQUA, 53*(6), 391-408.

Massachelein, W. J. (2002). *Ultraviolet Light in Water and Wastewater Sanitation.* Boca Raton: Lewis Publishers.

Menzies, D., Popa, J., Hanley, J. A., Rand, T., & Milton, D. K. (2003). Effect of ultraviolet germicidal lights installed in office ventilation systems on workers' health and wellbeing: double-blind multiple crossover trial. *The Lancet, 362*(9398), 1785-1791.

Modest, M. (1993). *Radiative Heat Transfer.* New York: McGraw-Hill.

Munakata, N., Saito, M., & Hieda, K. (1991). Inactivation action spectra of Bacillus subtilis spores in extended ultraviolet wavelengths (50-300nm) obtained with synchrotron radiation. *Photochemitry and Photobiology, 54*(5), 761-768.

Murthy, J. Y., & Mathur, S. R. (2000). A finite volume scheme for radiative heat transfer in semitransparent media. *Numerical Heat Transfer, 37*, 25-43.

Neofotistos, P., Do-Quang, Z., & Perrin, D. (2002). Ultraviolet Light: CFD Modeling Overlay with Fluence Rate Modeling as a Predictor of Reactor Performance for Drinking Water UV systems. *Proceedings AWWA National Convention.* New Orleans.

OpenCFD Ltd. (n.d.). Retrieved January 2014, from http://www.openfoam.com

Pruitt, K. M., & Kamau, D. N. (1993). Mathematical models of bacterial growth, inhibition and death under combined stress conditions. *J Ind Microb, 12*, 221-231.

Ranade, V. (2002). *Computational Flow Modelling for Chemical Reactor Engineering.* London: Academic Press.

Ritter, M. A., Olberding, E. M., & Malinzak, R. A. (2007). Ultraviolet lighting during orthopaedic surgery and the rate of infection. *The Journal of Bone & Joint Surgery, 89*(9), 1935-1940.

Rokjer, D., Valade, M., Keesler, D., & Borsykowsky, M. (2002). Computer modeling of UV reactors for validation process. *Proceedings AWWA WQTC.* Seattle.

Russell, A. D. (1982). *The Destruction of Bacterial Spores.* New York: Academic Press.

Setlow, R. B., & I., C. W. (1966). Pyridimine dimers in ultraviolet-irradiated DNA's. *J Mol Biol, 17*, 237-254.

Severin, B. F., & Suidan, M. T. (1983). Kinetic modeling of UV disinfection of water. *Water Res, 17*(11), 1669-1678.

Sharp, G. (1939). The lethal action of short ultraviolet rays on several common pathogenic bacteria. *Journal of Bacteria, 37*, 447-459.

Sommer, R., Pribil, W., Appelt, S., Gerringer, P., Eschweiler, H., Leth, H., . . . Haider, T. (2001). Inactivation of bacteriophages in water by means of non-ionizing (UV-253.7nm) and ionizing (gamma) radiation: a comparative approach. *Water Research, 35*, 3109-3116.

Stamnes, K., Chee Tsay, S., Wiscombe, W., & Jayaweera, K. (1988). Numerically stable algorithm for discrete-ordinate-method radiative transfer in multiple scattering and emitting layered media. *Appl. Opt., 27*(12), 2502-2509.

Turtoi, M. (2013). ULTRAVIOLET LIGHT POTENTIAL FOR WASTEWATER DISINFECTION.

Valero, A., Begum, M., Leong, S., Hocking, A., Ramos, A., Sanchis, V., & Marin, S. (2007). Fungi isolated from grapes and raisins as affected by germicidal UVC light. *Lett Appl Microbial, 45*, 238-243.

Varma, G., Savard, P., Coles, C., Ross, T., Carroll, K., Perl, T., & Labrique, A. (2013). Hospital room sterilization using far-ultraviolet radiation: a pilot evaluation of the Sterilray device in an active hospital setting. *Hospital, 34*(5), 536-538.

Wilcox, D. C. (1998). *Turbulence Modeling for CFD.* DCW Industries, Inc, La Canada.

Yakhot, V., & Orszag, S. A. (1986). Renormalization Group Analysis of Turbulence I. Basic Theory. *J. Sci. Compt, 1*(1).

Chapter 2:Foundations of DO model

In order to use DO model effectively, it is important to understand the foundations of DO model. DO model as implemented by FLUENT uses a conservative approach finite-volume scheme (Fluent Inc, 2006). The theories and mathematical formulations of this method will be discussed and covered extensively in this chapter. A nomenclature of common terms used in this thesis is presented below.

Nomenclature			
$\vec{r}$	position vector	N_θ	divisions in polar angle direction
$\vec{s}$	direction vector	N_ϕ	divisions in azimuthal angle direction
$\vec{s}'$	scattering direction vector		
s	path length (m)		
a	absorption coefficient (m^{-1})		
n	refractive index		
σ_s	scattering coefficient (m^{-1})		
σ	Stefan-Boltzmann constant (5.672×10^{-8} $W/m^2\text{-}K^4$)		
I	radiation intensity (W/m^2-sr)		
T	local temperature (K)		
Φ	phase function		
Ω'	control solid angle (sr)		
I_b	black-body intensity (W/m^2-sr)		

Table 2-1: Nomenclature terms

2.1 Basic terms

Before going into deep discussion about the theories and mathematical formulations behind DO model, it is important to establish definitions of basic terms and concepts used in radiation modeling.

Solid angle, Ω can be defined as the area from a section of sphere divided by r^2, where r is the radius of the sphere. Solid angle has units of steradians (sr). The maximum solid angle is 4π sr.

Radiative power, P can be defined as the radiant energy emitted in all directions by a light source. Radiative power has units of W. Generally, radiative power refers to radiant energy from a full range of spectral waves emitted by the source; however, in UVGI disinfection applications, radiative power is described for a specific spectral wave range.

Radiative Intensity, I can be defined as radiative power flow per unit solid angle and unit area normal to the rays. Radiative Intensity has units of W/m^2-sr. Spectral intensity refers to intensity in an interval of $d\lambda$ around a single wavelength. The total intensity is the integral of spectral intensity over all wavelengths. An important note of common misconception with radiative intensity is that radiative intensity does not decay with distance as it is travelling in the direction of solid angle (in non-absorbing media).

Radiative flux, q can be defined as radiative power flow per unit of controlled area or surface. Radiative flux has units of W/m^2. Similar to radiative power and intensity can also be defined for a specific spectral wave range or full range of spectral wave.

Absorption coefficient, α is the property of a medium to quantify the degree of absorption of radiation per unit path length travelled within the medium. Absorption coefficient has units of m^{-1}. It can also be interpreted as the inverse of the mean free path that a photon will travel before being absorbed (for constant absorption coefficient along travel path).

Scattering coefficient, σ_s is the property of a medium to quantify the degree of scattering of radiation per unit path length travelled within the medium. Scattering coefficient has units of m^{-1}. It can also be interpreted as the inverse of mean free path that a photon will travel before undergoing scattering (for constant scattering coefficient along travel path).

Scattering phase function, Φ is a function that describes the probability that a ray from one direction, $\vec{s}$ to be scattered into another direction, $\vec{s}'$. The scattering phase function must satisfy:

$$\int_{4\pi} \Phi(\vec{s}', \vec{s}) d\Omega = 4\pi \tag{2}$$

Scattering phase functions can be categorized into linear phase functions and Rayleigh phase function. Linear phase function can be classified further into isotropic and anisotropic scattering. Isotropic scattering scatters energy in all directions equally while anisotropic scattering scatters energy favoring forward (forward scattering) or backward (backward scattering) direction. Rayleigh phase function describes scattering behavior that is proportional to the inverse fourth power of the wavelength. Rayleigh scattering is important when describing scattering by gas molecules when the scattering particle (gas) diameter is considerably smaller than the wavelength of the radiation passing the particle. (Chai & Rath, 2006)

Optical thickness, t_{op} or optical depth is a measure of transparency, and it is defined as the negative logarithm of the fraction of radiation (i.e. light) that is not scattered or absorbed on a path.

$$t_{op} = -\ln\left(\frac{I_0}{I}\right) \tag{2}$$

The optical depth is a measure of the proportion of radiation absorbed or scattered along a path through a partially transparent medium. The optical depth expresses the quantity of light removed from a beam by scattering or absorption during its path through a medium. A medium is considered optically thick when $t_{op} \gg 1$.

Refractive index, n is the property of a medium to quantify the degree of refraction of a ray passing into the medium. Refractive index is non-dimensional and can be defined as:

$$n = \frac{c_0}{c} \tag{3}$$

where,

c_0 = speed of light in vacuum (2.998×10^8 m/s)

c = speed of light in medium (m/s)

Refractive indices for most gases are close to unity; for example, refractive index of air is 1.00029 (over visible light spectrum). Therefore, light propagates through gases nearly as fast as in vacuum.

Diffuse-gray surface, refers to surfaces that absorbs and/or emits a fraction of incident radiation hitting the surface without depending on direction (diffuse) or range of wavelength (gray).

2.2 Radiative Transfer Equation (RTE)

DO model was derived from solving RTE equation as briefly discussed in the previous chapter. RTE was developed to describe the steady state conservation of radiant energy of a single ray traveling in direction $\vec{s}$ from position $\vec{r}$. RTE equation is shown below with parts of the equation labeled to provide reference for the detailed description to follow:

$$\frac{dI(\vec{r},\vec{s})}{ds} = aI_b + \frac{\sigma_s}{4\pi}\int_0^{4\pi} I(\vec{r},\vec{s}')\Phi(\vec{s}\cdot\vec{s}')d\Omega' - (a+\sigma_s)I(\vec{r},\vec{s}) \tag{4}$$

where,

$I(\vec{r},\vec{s})$ is radiation intensity (W/m^2-sr)

a is absorption coefficient (m^{-1})

I_b is black-body intensity (W/m2-sr)

σ_s is scattering coefficient (m^{-1})

$\Phi(\vec{s} \cdot \vec{s}')$ is a phase function

Ω' is control solid angle (sr)

The left term of Equation (3) describes the overall intensity gradient along the propagation direction, $\vec{s}$ from position, $\vec{r}$. The first term on the right side of Equation (3) describes the gain of intensity due to black-body emission of the medium where:

$$I_b = n^2 \frac{\sigma T^4}{\pi} \qquad (5)$$

where,

n is refractive index

σ is Stefan-Boltzmann constant (5.672×10^{-8} W/m^2-K^4)

T is temperature (K)

The emitted black-body intensity is proportional to the local energy content (which is a function of temperature) in the medium. The second term on the right side of Equation (3) describes the gain of intensity due to in-scattering effects (governed by scattering phase function). In-scattering effects has contributions from all directions (spans the entire range of solid angles, 0 - 4π sr). The last term on the right side of Equation (3) describes the loss of intensity due to absorption and out-scattering effects. Loss of intensity is a result of absorbed energy along travel path and re-direction energy from scattering effects.

2.3 Finite Volume (FV) Approach

The finite volume approach to DO model in FLUENT is a more conservative variant of the model. The FV approach was implemented in FLUENT as it lead to exact satisfaction of the conservation laws over the region (the finite volume) surrounding each node. The methods for solving fluid flows in CFD is conceptually similar to solving DO model using the FV approach.

The concept of strict conservation of radiant energy (or momentum), defining boundary conditions and formation as well as solution of discrete equations are common for all processes: fluid flow, convective heat transfer and radiation (Raithby & Chui, 1990).

The first step for solving a problem using FV approach is to subdivide the computational domain into finite volumes (meshing). This can be achieved in many ways, but the finite volumes should fill the entire domain without overlap. The volumes could be in any shapes for example, tetrahedral, hexahedra, wedges or pyramids. One node could be established within each volume in which dependent variables (like temperature) are computed. The fundamental constraint for this variable in the volume is governed by an integral equation expressing conservation of that variable for that volume.

These terms can be written as surface integrals (using divergence theorem); each integral over the entire surface is split into the sum of integrals for each face of the volume. To obtain an algebraic equation for the variable, the transport across each face is approximated by an algebraic equation that involves geometry and nodal variables. It is the key to always use the same equation for each face, to ensure that the energy which leaves one control volume through that face is exactly the same energy that enters the other control volume that shares the same face.

A similar methodology is employed to solve fluid flows and convective heat transfer problems in a commercial CFD software; this allows commercial CFD software to apply the same calculation algorithm to solve radiation problems. Radiation energy can be thought of as "convected" through a medium at a different rate. The main conceptual difference between convection of radiant energy and the convection of thermal energy is that convection of radiant energy occurs simultaneously in all directions (as protons propagate in all directions). Another difference is

that, in any given direction, the interaction of radiant energy with the medium and with radiation from other directions depends on the frequencies of the radiation; however, for the sake of simplicity, frequency dependence is ignored in this discussion by invoking gray approximation. The dependent variable in radiation problems is intensity, I, which is comprised of 6 independent variables: location in space (r_x, r_y, r_z), direction vector (θ, ϕ), and frequency (λ) (Raithby, 1999).

RTE describes conservation of radiant energy using intensity, I as the dependent variable. The FV approach is to perform efficient directional spatial discretization based on dividing the computational domain into a range of solid angles (also known as angular discretization). The first step is to subdivide the spatial domain into finite volumes, and the directional domain (4π sr) into finite solid angles. The solid angles should exactly fill the directional domain without overlap. This can be done in many ways, but it is easiest to choose the solid angles associated with areas on the surface of a sphere defined by lines and longitude and latitude. For each spatial node, there is one dependent variable (intensity) associated with each finite solid angle.

The fundamental constraint for the dependent variable (of a particular volume and solid angle) is the integral, over the spatial finite volume and over the finite solid angle of RTE equation as described previous. It is important that the transport of energy equation be evaluated as a (double) surface integral, over the surface of finite volume and over the finite solid angle; the integral can be written as a double sum over all faces of the finite volume, and over any number of sub-solid angles that make up the finite solid angle.

To obtain algebraic equations for intensity (of particular volume and solid angle), the transport across each face within each solid angle is approximated by an algebraic equation that involves

geometry and nodal values. It is key that radiant energy transport within the finite solid angle that crosses the boundary of any control volume to be exactly conserved, and that boundary conditions be applied in an exactly conservative manner (Raithby & Chui, 1990).

2.4 Formulation of Discrete Equations

The RTE equation as described previously Equation (4) is used to formulate discrete equations to calculate conservation of radiant energy using a finite volume approach. To facilitate exact conservation of radiant energy, the energy transport terms are converted to surface integrals. The computational domain can be discretized both spatially and in angular directions as described in the previous section. Observing a node, P in a control volume, an RTE equation can be integrated over control volume dV and control discrete angle $d\omega^l$.

Integrating Equation (4) over control volume, dV:

$$\int_{V_P} \frac{dI_P}{ds}\, dV = \int_{V_P} \nabla I_P \cdot s\, dV = \int_{V_P} \nabla \cdot (I_P s)\, dV = \int_S I_P (s \cdot n)\, dS \qquad (6)$$

where,

$I_P = I(\vec{r}, \vec{s}')$ Intensity at node P

S = surface area of volume V_P (dS is the surface area of the control volume dV) at node P

n = is the unit vector normal to surface

It should be noted that divergence theorem was used in the last step.

Integrating Equation (6) over control discrete angle, $d\omega^l$:

$$\int_{\omega^l} \int_S I(s \cdot n)\, dS\, d\omega = \int_{\omega^l} \int_{V_P} \left[aI_b - (a + \sigma_s)I + \frac{\sigma_s}{4\pi} \int_{4\pi} I\Phi(\vec{s} \cdot \vec{s}')d\Omega' \right] dV\, d\omega$$

In the finite-volume approach, the spatial solution domain is subdivided into discrete non-overlapping volumes, and a single node (P) is located within each volume where location of this node in the volume depends on the selected type of grid (i.e cell-centered or vertex-centered). To be consistent with the spatial discretization, direction, which is also an independent variable, is subdivided into L discrete, non-overlapping solid angles of size, ω^l, $l = 1, 2, \ldots L$, which sums to 4π. The number of angles and their size distribution can be specified by user (angular discretization). By reasonably approximating all variables is constant over control volume dV and control discrete angle $d\omega^l$, the right side of Equation (7) can be written as:

$$\int_{\omega^l}\int_V \left[aI_b - (a+\sigma_s)I + \frac{\sigma_s}{4\pi}\int_{4\pi} I\Phi(\vec{s}\cdot\vec{s}')d\Omega'\right]dV\,d\omega \approx \left[a_P I_{b,P} - (a_P + \sigma_{s,P})I_P^l + \sigma_{s,P}\bar{I}_P^l\right]V_P\omega^l \tag{8}$$

where,

$$\bar{I}_P^l = \frac{1}{4\pi}\sum_{l'=1}^{L} I_P^{l'}\bar{\Phi}^{l'l} \tag{9}$$

and

$$\bar{\Phi}^{l'l} = \frac{\int_{\omega^l}\int_{\omega^{l'}}\Phi(l',l)d\omega' d\omega}{\omega^l} \tag{10}$$

Consider the surface of the control volume surrounding node P to be divided into surface panels (or faces) and an integration point (ip) is located at the center of each panel. The panel surface area associated with integration point ip is S_{ip}, and the normal surface at ip is n_{ip}. Treating each variable as constant over the panels, the left side of Equation (8) can be written as:

$$\int_{\omega^l}\int_{S} I(s\cdot n)\,dS\,d\omega \approx \sum_{ip=1}^{N_{ip}} S_{ip}\int_{\omega^l} I_{ip}(s\cdot n_{ip})\,d\omega \tag{11}$$

therefore, by considering these assumptions, Equation (11) can be re-written as:

$$\sum_{ip=1}^{N_{ip}} S_{ip}\int_{\omega^l} I_{ip}(s\cdot n_{ip})\,d\omega = \left[a_P I_{b,P} - (a_P+\sigma_{s,P})I_P^l + \sigma_{s,P}\bar{I}_P^l\right]V_P\omega^l \tag{12}$$

To complete the discretization, relations should be found between the I_{ip} values and nodal point values like I_P^l and I_{ip}^l because intensities are calculated at each computational node. Many differencing methods such as the diamond, step and exponential schemes have been suggested to find I_{ip}. However, the simplest and most common differencing scheme used is step spatial differencing scheme or upstream differencing scheme, UDS (which set the downstream boundary intensities equal to the upstream nodal intensities). In this method, the I_{ip} values are approximated by the values at the upstream nodes, which is consistent with physical propagation of RTE.

The main advantages of this scheme is its simplicity; however, it is a first order and not accurate in strongly participating media (where there is a significant change of intensity from upstream node and integration point). This method is also susceptible to false scattering, which was the topic of discussion over the use of DO model for computing radiative heat transfer.

Relating I_{ip} values with nodal values using any spatial "differencing" scheme, the resulting algebraic equation has the form:

$$a_P^l I_P^l = \sum_{nb} a_{nb}^l I_{nb}^l + b_P^l \quad (13)$$

The numerical procedure for solving this equation is presented in the next section.

(Georgios & Nikolos, 2012) (Chai & Rath, 2006) (Kim, Baek, & Park, 2001) (Murthy & Mathur , 1998).

2.5 Solution Procedure

The discretization procedure leads to a set of (nominally) linear equations relating the value of I_i at the cell center to its cell neighbors.

$$a_P\, I_{iP} = \sum_{nb} a_{nb} I_{inb} + b \quad (14)$$

where,

nb = number of cell neighbors

b = Intensities associated with other discrete directions

The algebraic set for each i is solved iteratively, looping through all the discrete directions in turn until convergence. The system is solved using a multi-grid procedure, which constructs course-level equations by clustering a fine-level cell with the neighbor for which the influence coefficient is the highest as discussed in detailed by Hutchison and Raithby. Typically, Brandt cycle is used for intensity calculations and Gauss-Seidel relaxation procedure is used at each multigrid level (Hutchinson & Raithby, 1986).

2.5.1 Boundary conditions

The equations set of algebraic equations still need a boundary condition to form a closed system of equations. For a gray-diffuse surface at temperature T_S, the boundary condition for the surface intensity I_S^l leaving the surface into the medium, $s^l \cdot n < 0$, is:

$$\varepsilon_S S\sigma {T_S}^4 + (1 - \varepsilon_S) \sum_{s^l \cdot n > 0} Q^{l'} = \sum_{s^l \cdot n < 0} Q_S^l = S\pi I_S^l \qquad (15)$$

where,

s^l = unit direction in the center of discrete solid angle, ω^l

n = unit surface normal from medium to surface

ε_S = surface emissivity

Q^l = radiative heat transfer rate

This equation shows that the intensity leaving the surface to the medium I_S^l is the sum of of the emitted radiation from the surface (ε_S term) and reflected radiation from the surface ($1 - \varepsilon_S$ term). The reflected radiation depends on incident intensities on the surface. For black surface (fully absorbent),$\varepsilon_S = 1$, the boundary condition becomes:

$$I_S^l = \frac{\sigma {T_S}^4}{\pi} \qquad (16)$$

2.5.2 Angular grid

An important aspect to forming a system of equations to solve in DO model is the construction of a spatial grid. Baliga and Patankar and Schneider and Raw proposed methods to spatially discretize heat transfer problems (Baliga & Patankar, 1983) (Schneider & Raw, 1987). A similar approaches described in those papers is employed in FLUENT's DO model according to the FLUENT user guide (Fluent Inc, 2006). Unfortunately as the end user of the product, it is

difficult to determine the exact type of angular grid used in FLUENT's DO model. However, with an established angular grid, Equation 14 is applied to the spatial volume surrounding each node and to each solid angle, to obtain Equation 15. More in-depth coverage of this topic is discussed by Raithby (Raithby, 1999).

2.5.3 Isotropic Scattering

For isotropic scattering, $\Phi = 1$; therefore:

$$\vec{I}_P^{\,l} = \frac{1}{4\pi} \sum_{l'=1}^{L} I_P^{l'} \omega^{l'} \tag{17}$$

where the right-hand side is the discrete form of average intensity I_a:

$$I_a(r) = \frac{1}{4\pi} \int_{4\pi} I(r, s') d\omega' \tag{18}$$

Hence, $\vec{I}_P^{\,l} = I_a(r)$ for isotropic scattering. This means that for isotropic scattering, scattering does not contribute to net radiant flux through the control volume faces.

2.5.4 Energy equation

Radiation contributes to internal energy equation through a source term, q_r''' known as the radiant source term.

$$q_r''' = \int_0^{\infty} \iint_{4\pi} a_\lambda (I_{\lambda,b} - I_\lambda)\, d\omega\, d\lambda \tag{19}$$

To account for the increase in internal energy due to radiation crossing the boundaries of the control volume, Equation 12 can be integrated over $\omega^l = 4\pi$:

$$\int_{4\pi}\int_{S} I(s\cdot n)\,dS\,d\omega = -4\pi\int_{V_P} a(I-I_b)dV \approx -4\pi a_P\left(I_{b,P}-I_P\right)V_P \qquad (20)$$

which is approximately $q_r'''V_P$. The scattering contribution isn't part of the energy balance because scattering can change the directional distribution but does not affect the level of radiative energy.

In radiative equilibrium condition, the temperature field adjusts to make the net surface heat transfer zero, which means $q_r''' = 0$ and $I_{b,P} = I_P$. In this condition, the fluid temperature and radiation fields are disconnected. This simple condition allows the radiation method to be solved independent from solving the internal energy equation.

2.5.5 Iterative Solution

In RTE, emission is a function of temperature of the medium and in-scattering depends on intensities from all directions. Therefore, the radiant intensity in any given direction depends on both of the temperature and complete intensity field (from all directions). To avoid solving the equations for all directions simultaneously by a direct solver, these equations are solved iteratively.

To obtain intensity in a given direction, the temperature field and intensities in all the other directions are assumed known from the previous iteration. They appear as a source term. The newly obtained intensity they then used to update the temperature field and in-scattering terms. This is repeated until convergence is achieved. This iterative solution method is referred to as explicit or sequential.

For optically thin media, the lagged terms are very small and convergence can be achieved faster. As optical thickness increases, the angular coupling becomes stronger and the lagged

terms dominate. At a given node, solving the RTE in each direction conserves the energy in that direction, but updating the temperature field and in-scattering terms with the newly obtained intensity destroys the conservation of energy in the previously solved directions. This can dramatically slow down convergence. Raithby and Chui noted this problem for finite-volume method. (Raithby & Chui, 1990)

An acceleration scheme was later developed to couple the energy and radiation model by Mathur and Murthy. This method was named couple ordinates method (COMET) and is based on the multigrid idea, which solves the internal energy equation and RTE together. This method is implemented in FLUENT for solving optically thick radiation problems. It should be noted that studies implied that the complexity of this method increases sharply as the scattering phase function becomes more complicated. (Murthy & Mathur,1998)

2.6 Using DO model in FLUENT

The discussion in this chapter covers the foundation equations that DO model represents. The complexity of developing this model has been extensively studied and improved over the years of research (especially by Raithby, Chui, Mathur, and Murthy). The goal of the work for this thesis is proper application of the DO model as implemented in commercial CFD software such as FLUENT. With proper understanding of the foundations behind DO model, the validation efforts or DO model use will be discussed in the upcoming chapters.

2.7 References

Baliga, B. R., & Patankar, S. V. (1983). A Control Volume Finite Element Method for Two-Dimensional Fluid Flow and Heat Transfer. *Numerical Heat Transfer, 6*, 245-261.

Chai, J. C., & Rath, P. (2006). *Discrete-Ordinates and Finite-Volume Methods for Radiative Heat Transfer.* Retrieved January 2014, from http://dspace.nitrkl.ac.in:8080/dspace/bitstream/2080/341/1/ISHMT-06-2.pdf

Chui, E. H., & Raithby, G. D. (1993). Computation of radiant heat transfer on a nonorthogonal mesh using the finite-volume method. *Numerial Heat Transfer, 23*(3), 269-288.

Fluent Inc. (2006, 09 20). *Fluent 6.3 User's Guide*. Retrieved January 2014, from http://aerojet.engr.ucdavis.edu/fluenthelp/html/ug/main_pre.htm

Georgios, N. L., & Nikolos, I. K. (2012). Using the Finite-Method and Hybrid Unstructured Meshes to Compute Radiative Heat Transfer in 3-D Geometries. *Numerical Heat Transfer, 62*, 289-314.

Hutchinson, B. R., & Raithby, G. D. (1986). A Multigrid Method Based on the Additive Correction Strategy. *Numerical Heat Transfer, 9*, 511-537.

Kim, M. Y., Baek, S. W., & Park, J. H. (2001). Unstructured finite-volume method for radiative heat transfer in a complex two-dimensional geometry with obstacles. *Numerical Heat Transfer, 39*, 617-635.

Murthy, J. Y., & Mathur, S. R. (1998). Finite volume method for radiative heat transfer using unstructured meshes. *Journal of thermophysics and heat transfer, 12*(3), 313-321.

Murthy, J. Y., & Mathur, S. R. (2000). A finite volume scheme for radiative heat transfer in semitransparent media. *Numerical Heat Transfer, 37*, 25-43.

Raithby, G. D. (1999). Discussion of the finite-volume method for radiation and its application using 3D unstructured meshes. *Numerical Heat Transfer, 35*, 389-405.

Raithby, G. D., & Chui, E. H. (1990). A finite volume method for predicting a radiant heat transfer in enclosures with participating media. *Journal of Heat Transfer, 122*(2).

Schneider, G. E., & Raw, M. J. (1987). Control Volume Finite-Element Method for Heat Transfer and Fluid Flow Using Colocated Variables. 1. Computational Procedure. *Numerical Heat Transfer, 1*, 363-390.

Chapter 3:Obtaining accurate result from DO model for radiation distribution modeling

3.1 Abstract

In this chapter, the validation of discrete ordinate (DO) radiation model is addressed. DO model is an iterative numerical model for solving radiation problems by considering conservation of radiant energy. Studies with DO model were conducted on FLUENT as a platform. Numerical solution of DO model was demonstrated to take into consideration multiple optic principles (reflection, refraction, shadowing effect and partial absorption). Accounting for these optical principles are integral to establishing an accurate radiation model. Previous use of this model by researchers failed to consider some optical principles which resulted in poor conclusion and results generated from DO model. The proper use of DO model is explained in detail and validated against published radiation experimental data. Additionally, a common misconception of studying fluence rate from DO model results is discussed. Finally, a study on the scalability of DO model to solve complex problems was detailed to encourage use of DO model in future UV air disinfection studies that involve complex UV systems.

3.2 Introduction

UV air disinfection modeling is a field of study that can be divided into two major components: Radiation and Hydrodynamic modeling. These components are important for the calculation of UV dosage received by a microorganism. Dosage, D (J/m^2) can be calculated by a simple function of Fluence Rate, I_f (W/m^2) × Exposure time, t (s) (Kowalski W. , 2009). Radiation modeling would provide values for fluence rate; hydrodynamic modeling would provide values for residence time of microorganism in the radiant field (exposure time). The combination of these two values would be used to develop a proper dosage model for study.

Hydrodynamic modeling is a field of research that studies flow and establish velocity profiles in fluid bodies. This is important to describe the flow behaviours of microorganism traveling in a UV air disinfection systems. Computational fluid dynamic (CFD) is a common tool used for hydrodynamic modeling. CFD modeling is based on solving a system of partial equations that describe conservation of momentum and mass. Before the use of CFD, researchers used traditional residence time distribution (RTD) models for UV disinfection systems simulations which resulted in poor prediction of disinfection rates that didn't match experimental results (Blatchley III, 1997) (Chiu, Lyn, Savoye, & Blatchey III, 1999). However, the use of CFD for hydrodynamic modeling in UV disinfection studies have shown reasonable agreement with conventional bioassay experiments (Baas, 1996) (Buffle, Chiu, & Taghipour, 2000) (Rokjer, Valade, Keesler, & Borsykowsky, 2002) (Neofotistos, Do-Quang, & Perrin, 2002) (Do-Quang, Janex, & Perrin, 2002) (Liu, Ducoste, Jin, & Linden, 2004).

Radiation modeling is a field of research that studies radiative energy transfer and establish radiation energy profiles. This is important to determine/calculate the radiation energy received by microorganism (fluence rate). There are several approaches to radiation modeling employed by researchers in the past including variations of point and line source models (MPSS, MSSS, LSI), view factor model, Monte Carlo model, P-1 model and DO model (Jacob & Dranoff, 1970) (Blatchley III, 1997) (Bolton, 2000) (Stamnes, Chee Tsay, Wiscombe, & Jayaweera, 1988) (Mishra & Rajamani, 1992) (Modest, 1993) (Kowalski W. , 2009).

This paper focuses on the radiation modeling aspect of UV air disinfection modeling, more specifically the discrete ordinate (DO) model. DO model is based on solving sets (all angular directions) of radiative transfer equations (RTE) that describes the conservation of radiant energy in a specific angular direction. DO model has been utilized as a radiation model in previous UV

air disinfection studies but still lacks thorough published validation work. This led to poor implementation of DO model. A study of multiple fluence rate distribution models (including DO model) was conducted by Liu et al (Liu, Ducoste, Jin, & Linden, 2004); the improper use of DO model led to a poor conclusion that DO model could not account for refraction. However, DO model is able to account for refraction as detailed by Liou & Wu (Liou & Wu, 1996).

The validation methodology followed through this paper begins by demonstrating DO model account for many important aspects of radiative energy transfer including partial or total reflection, refraction, shadowing effects and partial absorption. This is achieved by isolating and testing each optical principle independently in simple 2D simulation cases. Incorporating these aspects into DO model, it is compared with past implementation of DO model in Liu et al's work. Using a similar platform (FLUENT), the numerical solution of DO model simulation in our study was compared against experimentally measured fluence rate in Lie et al's study. Additionally, a common misconception of obtaining fluence rate distribution from DO model simulation is addressed. This misconception assumes the incident radiation values obtained from the DO model simulation directly corresponds to fluence rate values. This study is also performed on the scalability of DO model to solve complex radiation problems with considerations of these optical aspects to the solution. This case is performed to show the ease and flexibility of DO model to solve complex radiation cases.

3.3 Theory

DO model is based on solving RTE that accounts for emission, absorption and scattering effects in discretized angular directions. DO model as implemented in FLUENT uses a conservative finite-volume approach (Fluent Inc, 2006). The finite-volume approach satisfy conservations laws over the region (finite volume) surrounding a node. This approach for numerically solving

RTE follows the same underlying principles of solving hydrodynamic models in CFD (Raithby, 1999). The foundations behind DO model (formation of discrete equations and spatial discretization) is a complex topic.

The fundamentals of DO model was first introduced by Chandrasekhar in 1960 (Chandrasekhar, 1960). Early computer implementations of this method at the time were plagued with numerical difficulties because of limited computing resources (Liou K. N., 1973). However, Stamnes et al developed a numerically stable DO model algorithm, which invigorated interest back into development of DO model; Stamnes et al also improved the DO model by incorporating reflection at interfaces of layers for a multi-layered media in the algorithm (Stamnes, Chee Tsay, Wiscombe, & Jayaweera, 1988). In 1996, Liou and Wu, further extended DO model by consider interactions of interface in multi-layered medium as Fresnal interfaces. This consideration allows DO model to account for reflection and refraction based on Fresnal equations (Liou & Wu, 1996). In 1999, further development of the model expanded DO model for solving radiative heat transfer problems involving semitransparent media and interfaces (Murthy & Mathur, 2000).

The improvements to DO model over the past 50 years resulted in a comprehensive numerical radiation model that can utilized for radiation cases that spans the entire range of optical thicknesses, and solves problems ranging from surface-to-surface radiation to participating radiation in combustion problems. It also allows the solution of radiation at semi-transparent walls (Murthy & Mathur, 2000). Computational cost is moderate for typical angular discretization (i.e $N_\theta \times N_\phi = 5 \times 5$), and memory requirements are modest; however, solving a problem with a fine angular discretization can be CPU-intensive.

The governing equation that describes the conservation of radiant energy at position $\vec{r}$, in the direction $\vec{s}$, is known as RTE which is:

$$\frac{dI(\vec{r},\vec{s})}{ds} = aI_b + \frac{\sigma_s}{4\pi}\int_0^{4\pi} I(\vec{r},\vec{s}')\Phi(\vec{s}\cdot\vec{s}')d\Omega' - (a+\sigma_s)I(\vec{r},\vec{s}) \quad (3)$$

where,

$I(\vec{r},\vec{s})$ is radiation intensity (W/m^2-sr)

a is absorption coefficient (m^{-1})

I_b is black-body intensity (W/m2-sr)

σ_s is scattering coefficient (m^{-1})

$\Phi(\vec{s}\cdot\vec{s}')$ is a phase function

Ω' is control solid angle (sr)

The left term of Equation (3) describes the overall intensity gradient along the propagation direction, $\vec{s}$ from position, $\vec{r}$. The first term on the right side of Equation (3) describes the gain of intensity due to black-body emission of the medium where:

$$I_b = n^2\frac{\sigma T^4}{\pi} \quad (4)$$

where,

n is refractive index

σ is Stefan-Boltzmann constant (5.672×10^{-8} W/m^2-K^4)

T is temperature (K)

The emitted black-body intensity is proportional to the local energy content (which is a function of temperature) in the medium. The second term on the right side of Equation (3) describes the gain of intensity due to in-scattering effects (governed by scattering phase function). In-scattering effects has contributions from all directions (spans the entire range of solid angles, 0 - 4π sr). The last term on the right side of Equation (3) describes the loss of intensity due to

absorption and out-scattering effects. Loss of intensity is a result of absorbed energy along travel path and re-direction energy from scattering effects.

Equation (3) is a general RTE equation that describes conservation of radiant energy for a single band of radiative wavelength (gray model). Equation (3) only describes conservation of radiant energy in a single angular direction or solid angle. To obtain the incident radiation on any surface, contributions of intensity magnitude from the entire range of solid angles (0-4π) has to be integrated.

To consider multiple bands in the range of a radiation wavelengths, a simple non-gray model can be implemented. The non-gray models sums of the intensity contribution of several wavelength bands and can be represented as:

$$I(\vec{r},\vec{s}) = \sum_{k} I_{\lambda k}(\vec{r},\vec{s})\Delta\lambda_k \qquad (5)$$

where,

λ is the wavelength

k is the index of sets wavelengths under consideration in calculation

For the sake of simplicity, this paper will only consider a single band (gray model).

Solving RTE numerically, the computational domain should be discretized into finite volumes and angular directions that fills the entire domain without overlaps. The level of discretization can be controlled by adjusting divisions of polar N_θ and azimuthal N_ϕ angle values. In two-dimensional cases, four octants are solved due to symmetry, making a total of 4 $N_\theta N_\phi$ directions; in three-dimensional cases, eight quadratures are solved making a total of 8 $N_\theta N_\phi$ directions.

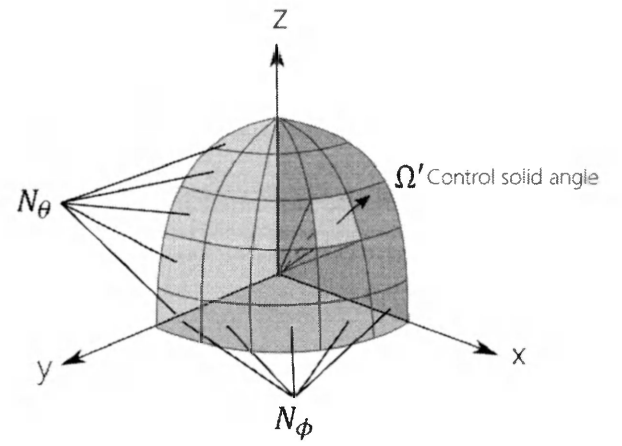

Figure 3-1: Angular discretization of a quadrature

When Cartesian co-ordinates are used, it is possible to align the angular grids with control volume faces; however, for cases with unstructured meshes, control volumes often do not align with the global angular discretization as illustrated in Figure 3-2. This phenomena leads to a problem known as control angle overhang. Control angle overhang may also occur from considerations of Fresnel interfaces (reflection and refraction) in a multi-layered optical media cases. The problem of control angle overhang was addressed by several researchers in this field (Murthy & Mathur, 1998) (Kim, Baek, & Park, 2001) (Georgios & Nikolos, 2012).

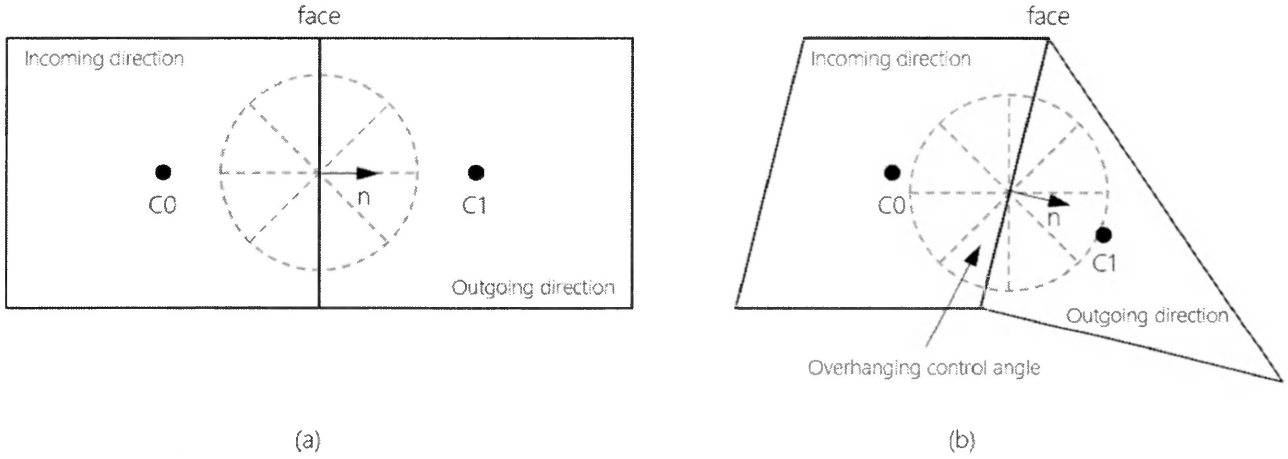

Figure 3-2: Illustration of overhanging control angle issue in 2D cases

Part (a) of Figure 3-2 shows a 2D case where angular grid fully aligns with control volume faces and no overhanging angle is present. Part (b) of Figure 3-2 shows a 2D case where angular grid does not align with unstructured control volumes and overhanging control angle is present. The issue of overhanging angles is addressed in FLUENT by the implementation of pixelation based on research performed by Murthy and Mathur (Murthy & Mathur, 1998). This method divides the overhanging control angle into $N_{\theta_p} \times N_{\phi_p}$ pixels. The energy contained in each pixel is treated as incoming or outgoing to the face. The influence of overhang angles can accounted for within the pixel resolution. High pixelation resolution could reduce errors from overhanging control angles but at the cost of computational power. FLUENT recommends pixelation of 3×3 for radiation problems involving symmetry, periodic, specular, or semi-transparent boundaries (Fluent Inc, 2006).

3.4 Procedures and Methods

The methodology taken to validate the DO model in this paper includes a study against simple basic optic principles, comparison with past experimental work in this field and performing sample radiation field studies involving a set of complex radiation cases. The qualitative and quantitative analysis simulations will be presented in the following section and discussed thoroughly.

3.4.1 Basic Optic Principles

Characterizing the fluence rate from the lamp requires incorporating many basic optical principles. Based on RTE, DO model accounts for effects of absorption, scattering and emission of a medium in any specific angular direction, $\vec{s}$. However, further improvements and development to DO model allows for consideration of Fresnel interfaces, semi-transparent media. These considerations are important when considering radiation problems with rays

passing media of different densities and interfaces that reflects and/or refracts rays. The importance of considering these basic optic principles to develop an accurate radiation model was highlighted by Bolton (Bolton, 2000). A study conducted by Liu et al, evaluated several fluence rate models including DO model; however, the implementation of DO model did not include the consideration of refraction which resulted in poor computational results (Liu, Ducoste, Jin, & Linden, 2004). More discussion on this study will be presented later in this paper. This section aims to demonstrate the implementation of DO model with considerations of basic optic principles such as reflection, refraction, shadowing effect as well as absorption of a semi-transparent media.

A simple two-dimensional rectangular enclosure was used for these simulations where irradiated collimated beam(s) was introduced into the enclosure filled with media. The media considered for this case is assumed to be air with absorption coefficient, a of 0, scattering coefficient, σ_s of 0 and refractive index, n of 1. The behaviour of collimated beam is assumed to follow a single gray band model. The simulation setup uses fine angular discretization of 10 x 10 ($N_\theta \times N_\phi$) for each quadrature of the angular space and pixelation of 6x6. The angles θ and ϕ are the polar and azimuthal angles respectively. The fine angular discretization and high pixelation was used as the cases simulated for this section is relatively simple and the computation cost for implementing these conditions were as computationally demanding as more complex cases.

To demonstrate the principle of reflection, the collimated beam was introduced to the enclosure at an angle towards the top of the enclosure. The wall boundary conditions for the top of the enclosure were set to be completely reflective/specular ($\varepsilon = 0$) while the rest of the wall boundary conditions were set to be completely absorbent ($\varepsilon = 1$). To demonstrate the principle of refraction, two collimated beams were passed straight forward into the enclosure media that

will pass a glass media shaped as a convex lens. The glass media has transparent boundaries and a refractive index of 1.5. The beams are passed near the top and bottom of the lens to observe the refracting effects of glass lens media inside the enclosure media by focusing the beams to focal point.

The next optic principle to account for is the shadowing effects in DO model simulations. Three collimated irradiated beams are passed into the 2D box media with similarly modeled convex lens media model as the previously tested principle (refraction); however, the properties of the lens media are changed. The boundaries of the lens are set to be completely opaque and absorbent (without reflection/specular effects). The absorption effect of semi-transparent media was studied next. To test this principle of absorption, the enclosure was modeled with a circular semi-transparent media inside; the properties of the circular media has absorption coefficient of ($0.1\ m^{-1}$).

3.4.2 Past Experimental Study Validation

The previously described validation tests were mostly qualitative analysis of DO model. In order to account for the accuracy and values obtained from the DO model simulation, it is compared with a fluence rate distribution study conducted by Liu et al. (Liu, Ducoste, Jin, & Linden, 2004). Liu et al conducted a study evaluating several fluence rate distribution models including analytical and numerical models such as line source integration (LSI), multiple point source summation (MPSS), multiple segment source summation (MSSS), UVCalc3D, RAD-LSI, view factor and DO model.

The experimental setup as performed by Liu et al was a test reactor with single lamp and potassium iodide (KI) actinometers (similar to the experiment conducted by Rahn (Rahn, 1997). Experimental researches in the past have shown that the use of spherical actinometry would

better represent the fluence rate experienced by microorganisms (Linden & Mofidi, 1999) (Rahn, Stefan, & Bolton, 2000) as opposed to measuring UV fluence from a radiometer.

The actinometer solution was housed in a spherical quarts container suspended parallel to the low pressure (LP) mercury UV lamp at three specific positions with radial distances, X of 5, 10 and 15 cm from the lamp as shown in Figure 3-3.

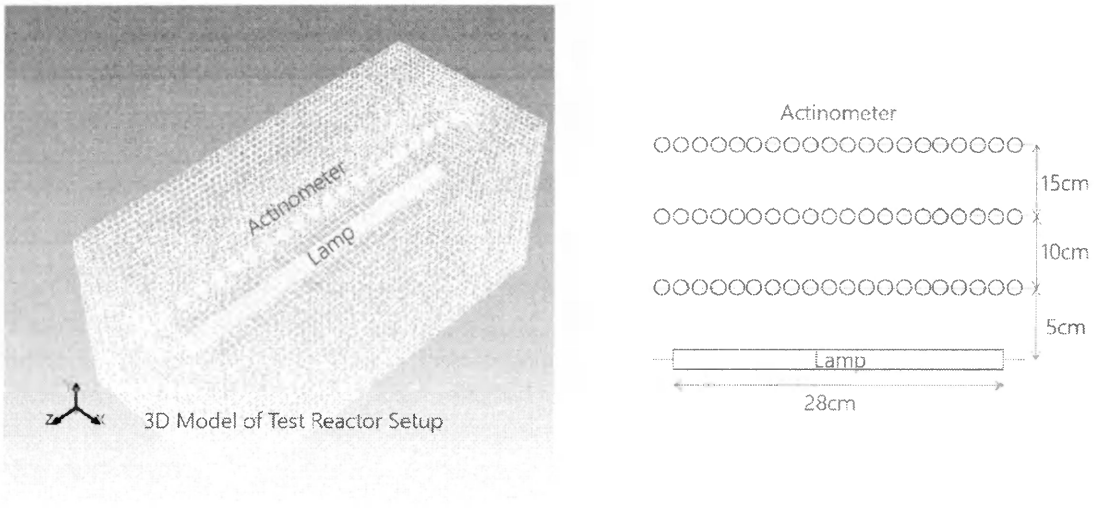

Figure 3-3: Reactor simulation setup used as described in a study evaluating several fluence rate models by Liu et al.

The arc length of the lamp used was 28 cm with a total output power of 16 W (with measured efficiency of 41.35%) at 254 nm wavelength. The authors measured the UVC output power using an International light IL1700 radiometer at a distance of 1.5m from the lamp centerline in air and calculated the power using the measured radiometer reading using the inverse square law.

The authors used a 0.1M KlO_3/0.6M KI in 0.01M $Na_2B_4O_7$ $10H_2O$ (Fisher scientific) solution as the KI/KIO_3 actinometer solution. The authors determined the molar absorption coefficient to be between 26,400 – 27,636 (M^{-1} cm^{-1}). They noted that reflection of light by the quartz is also taken into consideration and is based on the approach developed by Bolton (as 8.9%).

The setup used and describe by the Liu et al. was virtually constructed in the simulation software for the purpose of our study. Dimensions and properties of the actinometers and lamps were not

provided in detail in the published paper; therefore, dimensions of the actinometers, emissivity and absorption coefficients values had to be assumed for the simulation case. Actinometer sizes were assumed to be 1cm in diameter housed by a thin layer (0.05cm) of spherical quartz containers. Actinometer absorption coefficient is set to a high value ($a = 1 \times 10^6\ m^{-1}$). Additionally, the lamp is also modelled with a thin layer of quartz (0.05cm) housing the lamp core. Figure 3-4 shows details of the lamp setup that was used for this simulation. It should also be noted that setup by Liu et al did not have any particulates in the optical medium and therefore scattering effects are not studied.

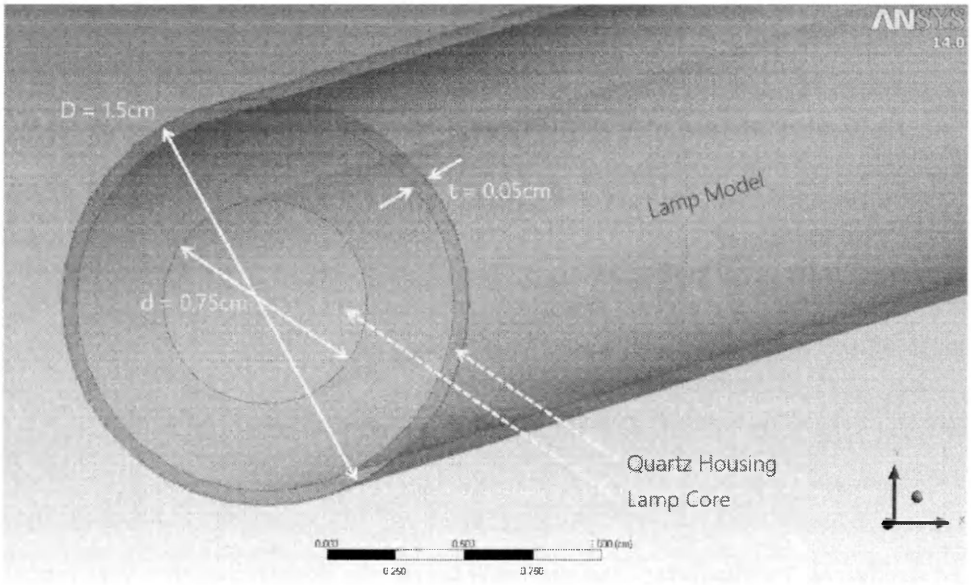

Figure 3-4: Details of lamp models used with included quartz housing and source light from surface of lamp core

3.4.3 Complex Case Simulation Validation

Another important validation case is needed to address the scalability and practicality of using DO model for a complex radiation problem/case. To consider a complex radiation problem, three tubular lamps were modeled in a tubular container. The wall boundary conditions of the tubular container are varied between a completely absorbent (non-reflective) and a completely specular (reflective) surface. The lamps are distanced 7 cm radially from the center of the tubular media. Each lamp is 25cm long with an outer diameter of 2.5cm. A thin quartz housing is modeled with

the lamp as well with a thickness of 0.1cm. Figure 3-5 below shows the simulation setup for this complex simulation condition.

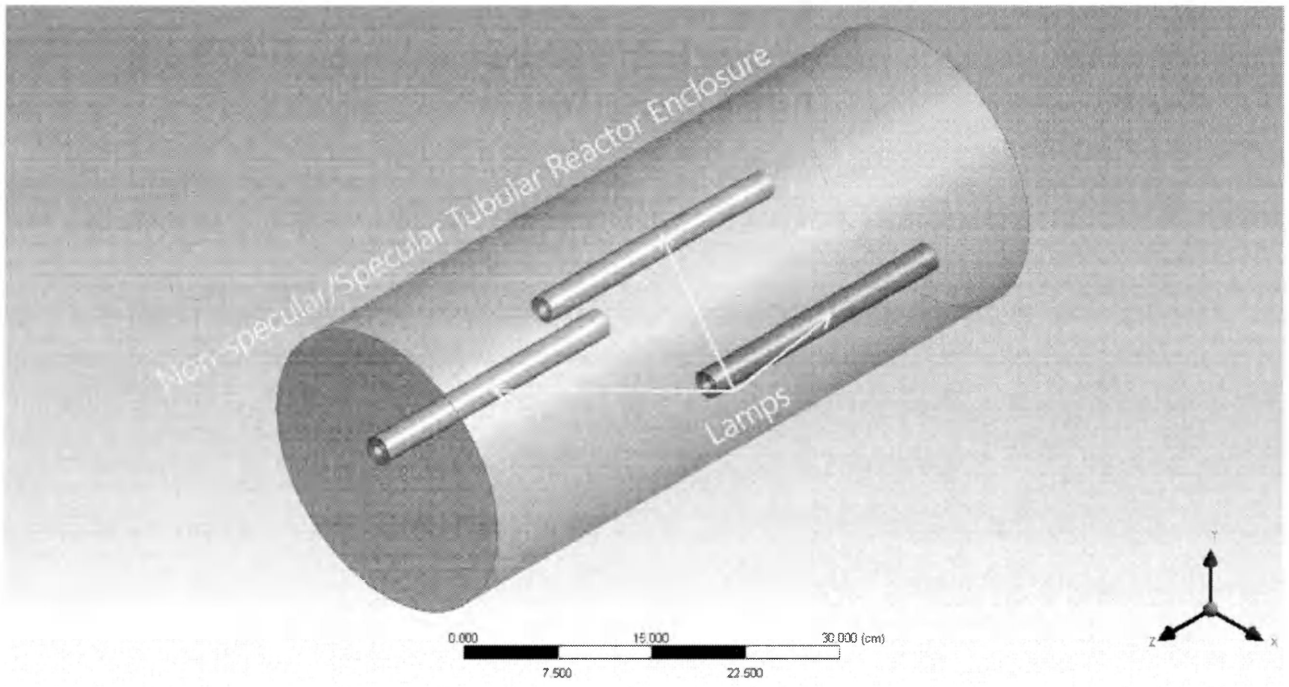

Figure 3-5: Complex Radiation Case with Non-specular and Specular Enclosure and multiple Lamps Setup

The surrounding media of the tubular container is assumed to be air with absorption coefficient, a of 0, scattering coefficient, σ_s of 0 and refractive index, n of 1. Additionally, the quartz housing for the lamps are modeled with a refractive index, n of 1.5 with emissivity, ε of 0.92. A diffuse irradiation boundary condition was applied to the surface boundaries of the lamp core as the source of radiation in this simulation (similar to previous simulation). Additionally, the simulation setup uses angular discretization of 10 x 10 ($N_\theta \times N_\phi$) for each quadrature and pixelation of 3x3. Two cases were considered:

1. Lamps enclosed in a tubular reactor with non-reflective walls
2. Lamps enclosed in a tubular reactor with completely specular walls

The solution to these radiation cases is very complex and would be very difficult to study analytically. Each lamp in the system is enclosed with quartz that will reflect and refract a portion of optical intensity. In the case of specular walls, the reflected intensity from the walls will also interact and contribute to the radiation field in the computation domain. As complex as this case seem to be, the DO model set-up approach to solving the simple cases are used to solve the complex cases as well (this is detailed in the appendix).This study demonstrates the flexibility and advantages of using DO model to model radiation in simple cases as well as complex cases.

3.5 Results

ANSYS 14 was used to conduct the simulation cases described in the previous section. This section will report the findings from the simulation setups.

3.5.1 Basic Optic Principles Validation

There were a set of simple 2D simulation cases that involve studying reflection, refraction, shadowing effect as well as partially absorbing media. The simulation results are summarized by Figure 3-6.

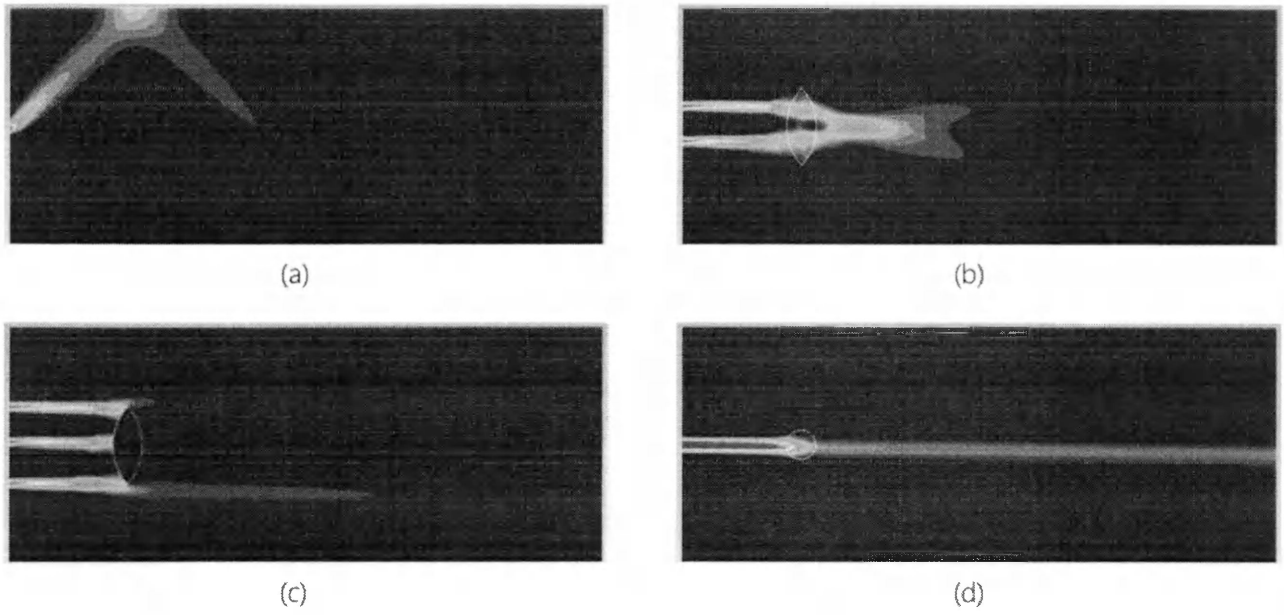

Figure 3-6: Qualitative simulation results demonstrating DO model accounting for basic optic principles: (a) reflection; (b) refraction; (c) shadowing effect; (d) partial absorption.

Considering Figure 3-5:

- Part (a) shows the simulation result for the case of demonstrating the principle of reflection. The collimated beam introduced into the media is angled towards the top surface of the enclosure which has boundary properties of a specular non-diffuse surface. The results follows the expected trajectory of the collimated optical beam as it is reflected back into the media at the same angle of incidence. The implications of this result mean DO model can consider reflection effects.
- Part (b) shows the simulation result for the case of demonstrating the principle of refraction. Two collimated beams are introduced into the media passing a convex lens glass media that refracts the beam into a focal point. The implications of this result suggests DO model can consider refraction effects as it passes from one media to another media with different refractive indices.

- Part (c) shows the simulation result for the case of demonstrating shadowing effect. In this simulation, three collimated beams are introduced into the media passing a convex lens opaque media that fully absorbs light intensity and does not allow it to pass the media. The implications of this result suggests DO model can account for shadows generated by media or walls. This is an important optical principle that should be accounted for in radiation simulations.
- Part (d) shows the simulation result for the case of demonstrating partial absorption effect. This simulation sends a collimated beam pass a media that is partially absorbing the intensity of the beam. As observed in the results, the intensity of the beam is reduced after passing the circular partially absorbing media but retained its intensity in the surrounding air media that has absorption coefficient, $a = 0$.

The simulation results presented are qualitative validation of DO model's capabilities to account for various basic optic principles. The following section will describe the quantitative validation of DO model as values from the simulation will be compared to measure experimental data obtained from past research.

3.5.2 Past Experimental Study Validation

A summary of the simulated radiation profile of the cross-section past the center of the reactor is shown in Figure 3-7 below. The reported results is a cross-sectional of the experimental setup across the center of the reactor.

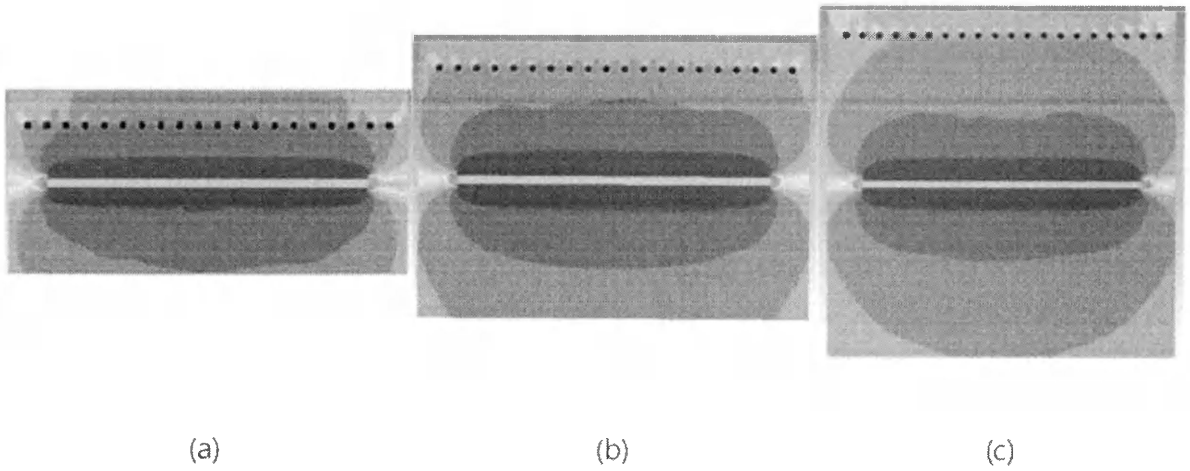

(a) (b) (c)

Figure 3-7: Simulation results from fluence rate experimental setup experiment conducted by Liu et al.

Part (a), (b) and (c) of Figure 3-7 shows the radiation profiles the cases with a row of actinometer radially distance from lamp by 5cm, 10cm and 15cm respectively. For each actinometer, the integral of incident radiation surrounding the surface of the actinometer can be calculated in the FLUENT. This value corresponds to the fluence rate values obtained experimentally in Liu et al's paper. The simulated DO model fluence rate values from our simulation were compared against the fluence rate values measured experimentally in Figure 3-8. Additionally, in the published work, Liu et al used the DO model to simulate fluence rate distribution as well and is summarized in the chart below.

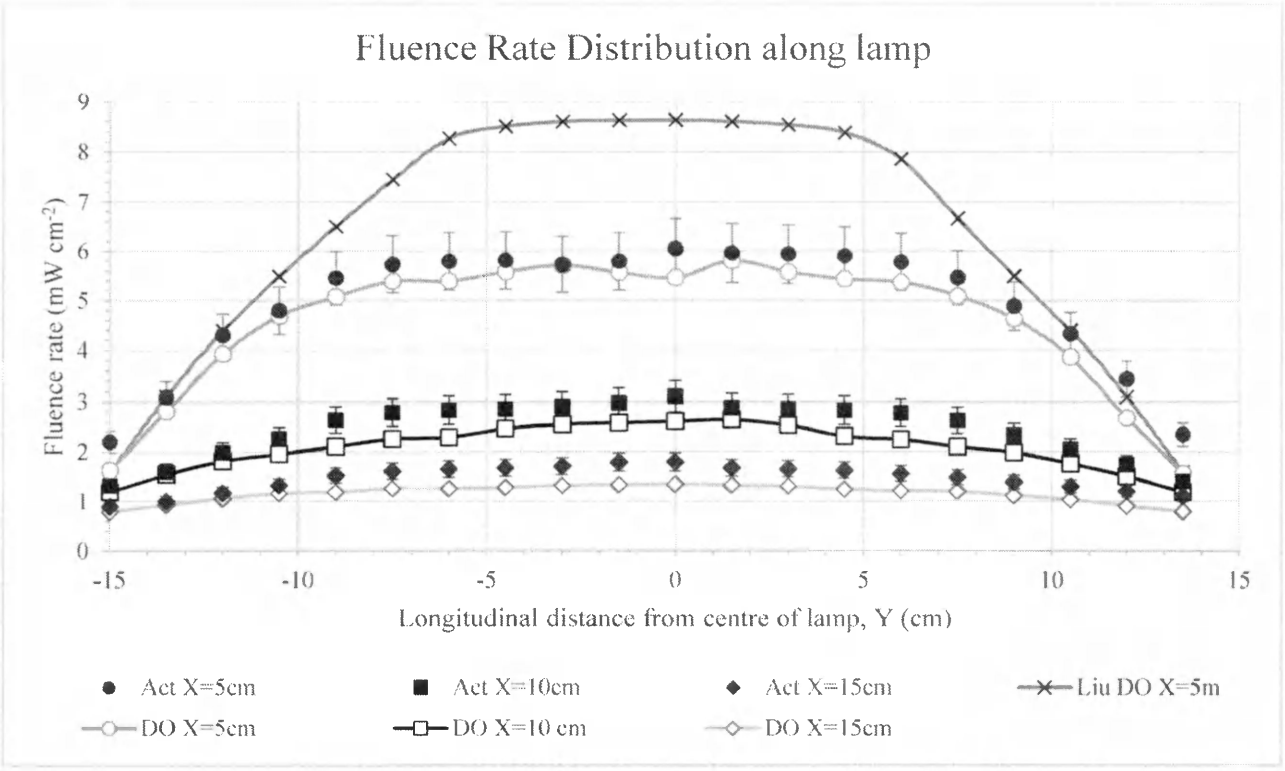

Figure 3-8: Value comparisons between simulated DO model results to experimentally measured actinometer fluence rate values.

Using the measured experimental fluence rate values from Liu et al's published work is indicated by prefix "Act" in the legend of the chart. The simulated DO model result from Liu et al is indicated by prefix "Liu DO" in the legend. The simulated DO model result from this study is indicated by prefix "DO" in the legend. The values of DO model simulated by this study and Liu et al are very different. This discrepancy is discussed in the following section. One detail that should be noted is the DO simulation results plotted in Figure 3-8 were the integral of incident radiation values over the entire surface of the actinometer (as opposed to the default incident radiation values reported by FLUENT). It can be observed that the simulated DO model values from this study is in agreement with the measured experimental fluence rate values from the published work.

3.5.3 Complex Case Simulation Validation

The following are the complex case DO model simulations results. The reported radiation profiles are taken from cross-sections of different locations within the annular reactor. Results for the non-specular enclosure case is shown in Figure 3-9 and specular enclosure case is shown in Figure 3-10.

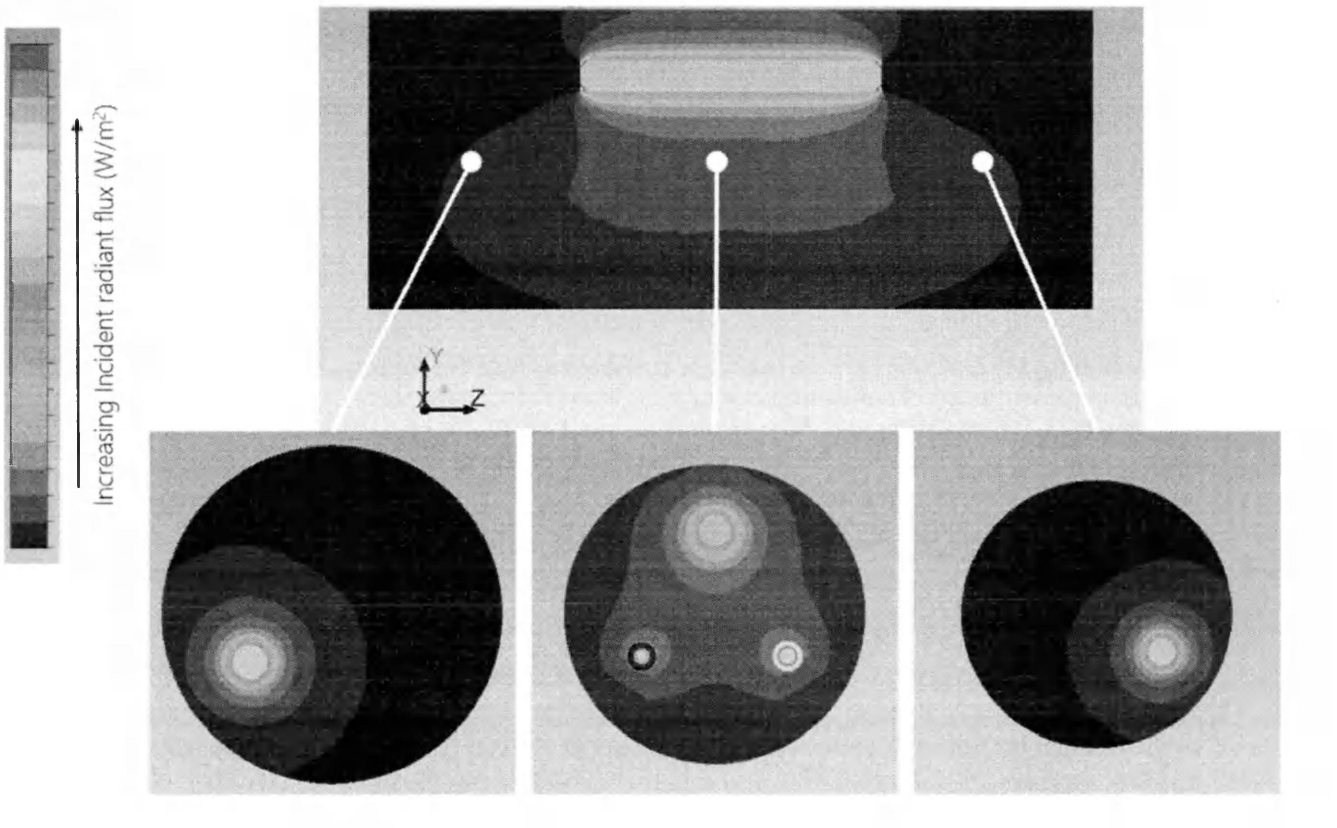

Figure 3-9: Cross-sectioned incident radiation (W/m^2) results at different locations for complex case simulation with non-specular enclosure

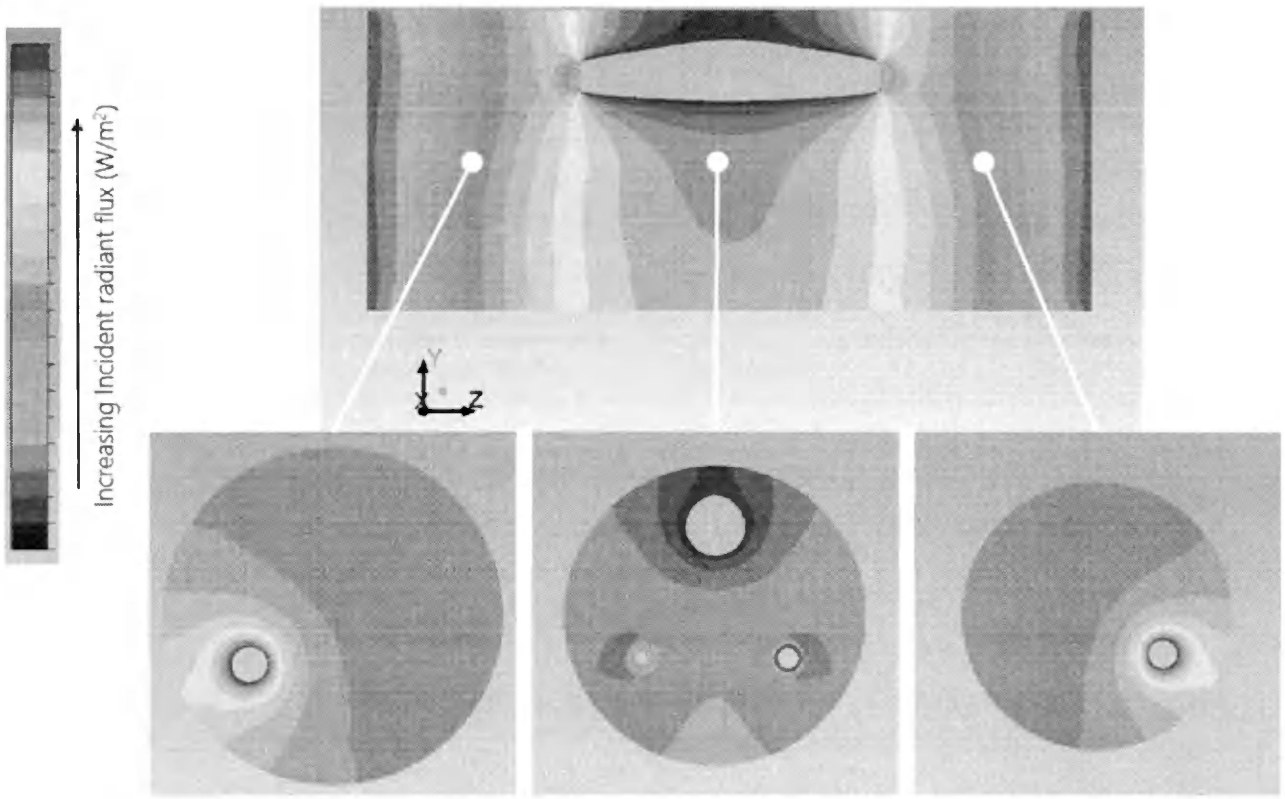

Figure 3-10: Cross-sectioned incident radiation (W/m^2) results at different locations for complex case simulation with specular enclosure

Observing these results, it can noted that the radiation profile obtained from the specular and non-specular cases are very different. It can also be noted that the incident radiation values also differ greatly in this scenario.

3.6 Discussion

Three sets of studies were considered in this paper to validate DO model for use as a viable alternative to analytical approach to radiation modeling (basic optic principles validation, past experimental study validation and complex case simulation validation). The first set of study involves basic optic principles validation. This study is important because the consideration of these basic optic principles improves the accuracy of the radiation model. Bolton addressed this importance of consideration of reflection and refraction in radiation modeling as mentioned previously (Bolton, 2000).

The strategy taken to validate DO model's consideration for these basic principles is to run a set of simple simulations with a collimated beam(s) to address a basic optic principles: reflection, refraction, shadowing and absorption. Figure 3-6 summarizes the simulation results. The behaviour of collimated optical beam simulated by DO model is shown to account for the effects of reflection, refraction, shadowing and absorption qualitatively. It should be noted that simulating a direct collimated optical beam to travel horizontally ($\vec{s} = (1,0,0)$) requires fine angular discretization and pixelation. A fine angular discretization (10×10) and pixelation (6×6) was used in this simulation but slight tilting of the collimated beam can still be observed in the simulation result. This error is apparent in Figure 3-6(d).

Another general observation that could be made from the simulation results is the collimated optical beam slightly diffuses radiant energy into directions normal to beam direction. This error can be observed especially in Figure 3-6(b). As the collimated beam is travelling close to the convex lens, the collimated optical beam diffuses radiant energy to directions normal to beam direction. The error could be attributed to the unstructured meshes around the lens, leading to more overhanging control angles. However, this error did not significantly change the expected refractive behaviour of the simulation as the collimated beams still converged into a focal point.

These simple basic optic principle simulations have significant implications to the capabilities of DO model. By altering the boundary conditions of the walls or media, the DO model can account for these basic optic principles, which are the foundation for solving more complex radiation problems.

The second set of studies looked into validating the quantitative results from the DO model against past experimental work in this field. Liu et al published a paper in 2004 comparing several analytical and numerical radiation models including the DO model (Liu, Ducoste, Jin, &

Linden, 2004). The DO model simulation used in the paper was conducted on a similar platform as the DO model used for this paper.

Considering the radiation profiles simulated in Figure 3-7, the source of radiation in these simulations is the surface of a cylindrical tube labelled the lamp core as seen in Figure 3-4. The radiation that leaves the lamp core passes through the lamp plasma and a thin layer of quartz before radiating out into the surrounding media (air). The interfaces between the thin layer of quartz and lamp plasma as well as surrounding air reflects a portion of radiant energy. Additionally, the radiation beams passing the quartz media is refracted as it passes through media of different index of refraction. This consideration for the modelled lamp is similarly applied to the spherical quartz actinometers. The beam passing into the actinometer will have to pass a thin layer of quartz before entering the inner actinometer fluid media. A portion of the radiant energy from the incoming beam is reflected back and contributes to radiant energy in different direction. This phenomenon could account for the increased incident radiation values close to the center of the row of actinometers as seen in Figure 3-7 (especially in 6(a)).

Another observation that could be made about the radiation profiles simulated for this study is the full absorption of intensity by the actinometer fluid. Observing Figure 3-7, the values of intensity drops drastically as it enters into the actinometer fluid media. The absorption coefficient of this media was set to a high value to achieve this effect as it is similar to how actinometers function. Actinometer houses chemical fluid that changes concentration based on the reaction between absorbed fluence and the chemical. More detailed discussion on spherical actinometry can be obtained by reviewing papers from Rahn, Linden and Moffidi (Rahn, 1997) (Linden & Mofidi, 1999). The change of concentration in the actinometer fluid can be analyzed and fluence rate can be estimated by calculation. In the simulated radiation profile, the actinometer

completely absorbs the radiant energy as it enters the fluid region of the actinometer which is in agreement with the actual operation of spherical actinometry experiments. Therefore, the fluence rate values from the simulation can be obtained by integrating the incident radiation values passing through the entire surface of the inner actinometer fluid body.

As noted before, the authors of the experimental work referred to, Liu et al also conducted his study to evaluate DO model as one of the fluence rate distribution models (Liu, Ducoste, Jin, & Linden, 2004). Liu et al used a similar platform to study DO model (FLUENT); however, the published results from DO model in that paper were grossly overestimated the actual measured fluence rates from the actinometers as shown in Figure 3-8. The authors noted this error and concluded the source for this error was the DO model inability of incorporating refraction effects into the simulation. This is in contradiction the findings from the previous set of study performed in this paper (basic optic principles validation). In the previous set of study, DO model was demonstrated to account for reflection, refraction, shadowing and absorption. Intricate considerations to modeling the lamp and spherical actinometers accounted for reflection and refraction effects of quartz in this study. Taking the reflection and refraction into consideration in this study, the fluence rate values obtained from DO model matches the experimentally determined values from Liu et al's experiment relatively well. The importance of reflection, refraction, shadowing effect and absorption to accurate radiation modeling was discussed by Bolton as mentioned previously and is evident from the improvement in DO model simulation result as shown in Figure 3-8 (Bolton, 2000).

Lastly, the final set of studies conducted for this paper studies the scalability of the DO model against complex radiation problems. Specular radiation cases are complex radiation problems and would require complex work to solve the case through an analytical radiation approach;

however, utilizing the DO model, this complex case was solved using a similar set-up to the simpler cases (as described in the "Configuring FLUENT for simulation" section). The DO model allows leveraging computing power to handle the complexity of a specular radiation case. With the trend of continually increasing computing power, the DO model approach to solve radiation problems can be perform faster and easier. This is particularly useful for researchers to test out different radiation configurations and study the results.

3.7 Conclusion

The use of DO model to obtain accurate radiation results have been qualitative and quantitatively validated in this chapter by three sets of studies. The first set of study demonstrated DO model's consideration for basic optic principles such as reflection, refraction, shadowing and absorption. This was achieved by simulating a set of simple 2D cases to address each optic principle independently. As seen in Figure 3-6, DO model can account for these optic principles which is integral to achieving an accurate radiation model.

The second set of study quantitatively validated DO model simulation values by referencing published experimental radiation work performed by Liu et al. As seen in Figure 8, the simulated fluence rate values from DO model in this study is in good agreement with the measured fluence rate values in the published work. In this study, close intricate attention was paid to modeling of quartz surrounding lamp and spherical actinometer as quartz will reflect and refract portions of radiant energy as beam passes through media. This consideration was omitted in the previously published work but considered here. Consideration of reflection, refraction effects from quartz resulted in much better agreement between DO model simulation and experimental results.

The third set of study discussed in this chapter demonstrates the scalability of DO model to handle complex radiation cases. A sample complex case was established with tubular lamps

enclosed in a tubular reactor with non-reflective and specular walls. The multiple lamps consideration in this simulation acts as a sources of radiation as well as an optical media as it receives radiation from other sources. The case with specular wall enclosure further complicate the radiation case and is analytically challenging to compute for fluence rate distribution while accounting for all the optical principles as the numerical approach. However, using a similar methodology (as outlined in the appendix) to modeling simpler radiation cases can be applied to complex radiation cases just as well. The simplicity of using DO model to solve complex radiation cases while including comprehensive optical principle considerations are demonstrated in this set of study.

It is demonstrated that DO model can be a viable radiation model that leverages computing power to solve simple and complex radiation cases easily. Additionally, DO model can be an effective numerical radiation model to use in conjunction with turbulence models for UV disinfection studies because both CFD and radiation modeling can be performed on a single platform (FLUENT 14)

3.8 References

Baas, M. M. (1996). Latest Advances in UV Disinfection Hydrodynamic Simulation and Relation to Practical Experiences. *Proceedings AQUATECH.* Amsterdam.

Blatchley III, E. R. (1997). Numerical modeling of UV intensity: application to collimated-beam reactors and continuous-flow system. *Wat. Res., 31*, 2205-2218.

Bolton, J. R. (2000). Calculation of Ultraviolet Fluence Rate Distributions in an Annular Reactor: Signifiance of Refraction and Reflection. *Wat. Res., 34*, 3315-3324.

Buffle, M. O., Chiu, K. P., & Taghipour, F. (2000). UV reactor conceptualization and performance optimization with computational modeling. *Proceedings of the Water Environmental Federation, 2*, pp. 401-410.

Chandrasekhar, S. (1960). *Radiative Transfer.* New York: Dover.

Chiu, K., Lyn, D. A., Savoye, P., & Blatchey III, E. R. (1999). Integrated UV Disinfection Model Based on Particle Tracking. *Journal of Environmental Engineering ASCE, 125*(1), 7-16.

Do-Quang, Z., Janex, M. L., & Perrin, D. (2002). Predictive tool for UV dose distribution assessment: Validation of CFD models by bioassays. *Proceedings AWWA National Convention.* New Orleans.

Ducoste, J. J., Liu, D., & Linden, K. (2005). Alternative Approaches to Modeling Dose Distribution and Microbial Inactivation in Ultraviolet Reactors: Lagrangian vs Eulerian. *Journal Environmental Engineering.*

Fluent Inc. (2006, 09 20). *Fluent 6.3 User's Guide.* Retrieved January 2014, from http://aerojet.engr.ucdavis.edu/fluenthelp/html/ug/main_pre.htm

Georgios, N. L., & Nikolos, I. K. (2012). Using the Finite-Method and Hybrid Unstructured Meshes to Compute Radiative Heat Transfer in 3-D Geometries. *Numerical Heat Transfer, 62*, 289-314.

Jacob, S. M., & Dranoff, J. S. (1970). Light intensity profiles in a perfectly mixed photoreactor. *A.I.C.H.E*, 359-363.

Kim, M. Y., Baek, S. W., & Park, J. H. (2001). Unstructured finite-volume method for radiative heat transfer in a complex two-dimensional geometry with obstacles. *Numerical Heat Transfer, 39*, 617-635.

Kowalski, W. (2009). *Ultraviolet germicidal irradiation handbook: UVGI for air and surface disinfection.* Springer.

Linden, K. G., & Mofidi, A. A. (1999). Measurement of UV irradiance: tools and considerations. *Proceedings, Water Quality Technology Conference, AWWA*, (pp. 1-3). Tampa Bay, Florida.

Liou, B. T., & Wu, C. Y. (1996). Radiative transfer in a multi-layer medium with fresnel interfaces. *Heat and Mass Transfer, 32*, 103-107.

Liou, K. N. (1973). A Numerical Experiment on Chandrasekhar's Discrete-Ordinate Method for Radiative Transfer: Applications to Cloudy and Hazy Atmosphere. *Journal of Atmospheric Science, 30*, 1303.

Liu, D., Ducoste, J., Jin, S., & Linden, K. (2004). Evaluation of alternative fluence rate distribution models. *Journal of Water Supply: Research and Technology AQUA, 53*(6), 391-408.

Mishra, B., & Rajamani, R. (1992). The discrete element method for the simulation of ball mills. *Applied Mathematical Modeling, 16*, 598-604.

Modest, M. (1993). *Radiative Heat Transfer.* New York: McGraw-Hill.

Murthy, J. Y., & Mathur, S. R. (1998). Finite volume method for radiative heat transfer using unstructured meshes. *Journal of thermophysics and heat transfer, 12*(3), 313-321.

Murthy, J. Y., & Mathur, S. R. (2000). A finite volume scheme for radiative heat transfer in semitransparent media. *Numerical Heat Transfer, 37*, 25-43.

Neofotistos, P., Do-Quang, Z., & Perrin, D. (2002). Ultraviolet Light: CFD Modeling Overlay with Fluence Rate Modeling as a Predictor of Reactor Performance for Drinking Water UV systems. *Proceedings AWWA National Convention.* New Orleans.

Rahn, R. O. (1997). Potassium iodide as a chemical actinometer for 254 nm radiation: use of idate as an electron scavenger. *Photochem. Photobiol., 66*(4), 450.

Rahn, R. O., Stefan, M. I., & Bolton, J. R. (2000). The iodide/iodate actinometer in UV disinfection: characteristics and use in the determination of the fluence rate distribution oin UV Reactors. *Proceedings Water Quality Technology Conference.* AWWA.

Raithby, G. D. (1999). Discussion of the finite-volume method for radiation and its application using 3D unstructured meshes. *Numerical Heat Transfer, 35*, 389-405.

Rokjer, D., Valade, M., Keesler, D., & Borsykowsky, M. (2002). Computer modeling of UV reactors for validation process. *Proceedings AWWA WQTC.* Seattle.

Stamnes, K., Chee Tsay, S., Wiscombe, W., & Jayaweera, K. (1988). Numerically stable algorithm for discrete-ordinate-method radiative transfer in multiple scattering and emitting layered media. *Appl. Opt., 27*(12), 2502-2509.

3.9 Appendix

3.9.1 Setting up model in FLUENT for simulation

This section of the document explains the general configuration steps taken to perform the DO model radiation simulation using FLUENT. Both complex and simple radiation cases share a common approach to setting up the problem.

1. The model should have different section (media) considering quartz, plasma, etc. Each section should be specify in the meshing process using different names.
2. Activate DO radiation model
    a. The angular discretization controls the refinement of the DO model as described in the theory section. The default values for the theta and phi divisions is 2 x 2, which is coarse. A finer discretization is recommended to achieve better radiation simulation results (i.e. 5x5 or 10x10). The default for theta and phi pixelation is 1 x 1. The FLUENT user guide recommends using at least 3x3 for specular or semi-transparent boundaries cases (Fluent Inc, 2006). Increasing the discretization and pixelation will result in higher computation time.
3. Assigned appropriate materials for each section of the model
    a. Properties of materials of interest can be defined here. For example the properties of the quartz of the lamp can be defined as a new material if it does not exist in the default material database.
    b. Absorption coefficient values of materials can defined to reflect the UV transmittance (UVT), where:

$$UVT = \frac{I}{I_o} = e^{(-ax)} \tag{6}$$

where $\frac{I}{I_o}$ is the reduction in intensity over distance, $x = 1\ cm$. Therefore, the absorption coefficient, a can be rearranged as:

$$a = -ln\left(\frac{I}{I_o}\right) \times 100 \tag{7}$$

where 100 is used to convert cm^{-1} to m^{-1}. For example, if UVT for material is 0.9 (90%), the absorption coefficient is 10.54 m^{-1}.

    c. For semi-transparent materials that allows for radiation passing the body, refractive indices can be defined.

4. Define cell zone conditions
    a. The imported CFD models are divided into separate cell zones as defined in the meshing step of modeling. These zones can be categorized as either a solid or fluid cell zone.
    b. By default, if a zone is specified as a solid zone, the zone does not participate in radiation. If model case involves semi-transparent solid zones (i.e. quartz), turn on radiation participation by editing the properties of the cell zone.
    c. Another important note is to fix temperatures of all zones to 1K in order to avoid thermal radiation effects (I_b in Equation 1) in the final simulation result.
        i. Select any cell zone and check the fixed values property.
        ii. Under the Fixed values tab, scroll down to temperature and set it to 1.
5. Define proper boundary conditions
    a. Boundary conditions of walls, interfaces, inlets, outlet, etc. can be defined here. If the model case involves radiation participation and propagation pass separate cell zones, interfaces between these zones needs to be created.
        i. Interfaces can be defined if the surface of the zones were named properly in the meshing step. For each interface, there are two adjacent cell zone bodies; therefore, there are two surfaces that needs to be combined into an interface. These surfaces should be identified and be converted into interface type when defining boundary conditions.
        ii. After the appropriate surfaces have been defined as an interface. A new interface can be created.
            1. For cases of defining interfaces between a solid and fluid, the coupled wall option should be used. (Note the newly created "walls" and "wall-shadows" after coupling surfaces, these walls will be used to specify the boundary condition of that interface)
    b. For the surfaces that are specular or semi-specular (reflective), emissivity values at the boundary conditions can be specified to account for this effect:
        i. Under the Thermal tab, internal emissivity (ε) can be set here. This plays a role in the diffusely reflected energy, $f_d(1-\varepsilon)q_{in}$ and the absorbed energy, $f_d(\varepsilon)q_{in}$. The specular reflected energy is $(1-f_d)q_{in}$, where f_d is the diffuse fraction, ε is the emissivity, and q_{in} is the radiative energy incident on the wall.
    c. Surfaces can be defined as semi-transparent or opaque. In addition, the diffuse fraction (f_d) can be defined.

6. To minimize the effect of thermal radiation from temperature differences between cells set the temperature of the all bodies to 1 K during initialization.

Chapter 4:Validating DO model with multi-lamp 3-dimensional radiation measurement experiment

4.1 Abstract

In this study a multi-lamp 3-dimensional radiation experiment was conducted in effort to validate DO radiation model. The experimental setup consists of 5 UV lamps and 2 radiometers. One radiometer was located at fixed position while the second radiometer was attached to a robotic arm capable of moving in a 3-dimensional space during experiment. A LabVIEW program was developed to automatically control the position of robotic arm using Arduino Duo board and collected data from two radiometer via two USB ports. Overall, 1978 data points were collected on each different layer with a fixed z-distance away from the lamp. The experimental data was used to validate the results of modeling using DO model. Important findings on the varying lamp intensities and lamp plasma absorption coefficient was addressed as included in the DO model simulation setup. DO model simulation results were qualitatively compared to the experimentally measured data; however, there are discrepancies between the experimental measurements and simulation results. Although the DO model simulation results did not match the experimentally measured data entirely, findings from this study is very valuable for future work on using DO model in the field of UV lamp radiation modeling.

4.2 Introduction

Ultra-violet (UV) irradiation commonly emitted by UV lamps can be used for air disinfection by de-activating microbes (Kowalski W. , 2009). One of the main components to modeling the efficiency of these air disinfection systems is the radiation modeling of the UV lamps. Various approaches to radiation model of UV lamps were studied by researchers in the past including: variations of point and line source models (Multiple Point Source Summation (MPSS), Multiple Segment Source Summation (MSSS), Line Source Integration (LSI)), view factor model, Monte

Carlo model, P-1 model and Discrete Ordinate (DO) model (Jacob & Dranoff, 1970) (Blatchley III, 1997) (Bolton, 2000) (Stamnes, Chee Tsay, Wiscombe, & Jayaweera, 1988) (Mishra & Rajamani, 1992) (Modest, 1993) (Kowalski W. , 2009). Between all the listed radiation models, DO model is one of the most comprehensive model which account for all the basic optical principles (reflection, refraction, shadowing and absorption) and can leverage the ever growing computing power of today.

DO model is based on solving sets of radiative transfer equations (RTE) in all angular directions. The iterative numerical approach to solving RTE is similar to how a computational fluid dynamic (CFD) software solves fluid flow and convective heat transfer problems (Raithby, 1999). Therefore, DO model is easily accessible for use through commercial CFD software such as FLUENT (ANSYS Inc, n.d.). As mention, DO model uses an iterative numerical approach to solve the RTE equation; consequently, DO model could be subjected error propagation issues similar to various other iterative numerical models. In the previous chapter, DO model was validated against experimental data published by past researchers. The fluence rate values published by Liu et al matches the DO model simulation result as discussed in the previous chapter. However, the experiment conducted by Liu et al is a simple single lamp 2-dimensional experimental setup with actinometers (Liu, Ducoste, Jin, & Linden, 2004). A more comprehensive full 3-dimensional multi-lamp radiation experimental setup still has not be published to compare and validate the DO model against.

In effort to validate DO model for use in a complex multi-lamp radiation case, a multi-lamp further experimental design consisting of 5 UV lamps and two radiometers was designed. The radiometers used only respond to UVC radiation which is the same band of radiation emitted by the LP mercury lamps used. The radiometer measures the incident radiant flux (power) passing

through the photovoltaic sensor by converting the incident radiant flux received into electrical power. Therefore, the electrical signal readings from the radiometer correlates directly with incident radiant flux. The first radiometer is located in a fixed position during all the experiments as a control point while the other radiometer is attached to a robotic arm that can be moved in a 3-dimensional space remotely. This experimental setup allows the radiometer to capture radiant flux data in a full 3-dimensional space. The movement of the probe is controlled remotely by a computer and automatically increments to the next position after capturing data.

4.3 Procedures and Methods

The methodology taken to validate the DO model in this chapter includes performing a complex multi-lamp 3-dimensional radiation measurement experiment and running a DO model simulation of the same multi-lamp experimental setup. The measured data and simulated DO model radiation analysis will be presented in the following section and discussed thoroughly.

4.3.1 Main experimental setup

In this study, a multi-lamp experimental setup consisting of 5 lamps was designed. Five low pressure (LP) mercury UV lamps were used for this experiment. The dimensions of the lamps and position details of the experimental design are shown in Figure 4-1.

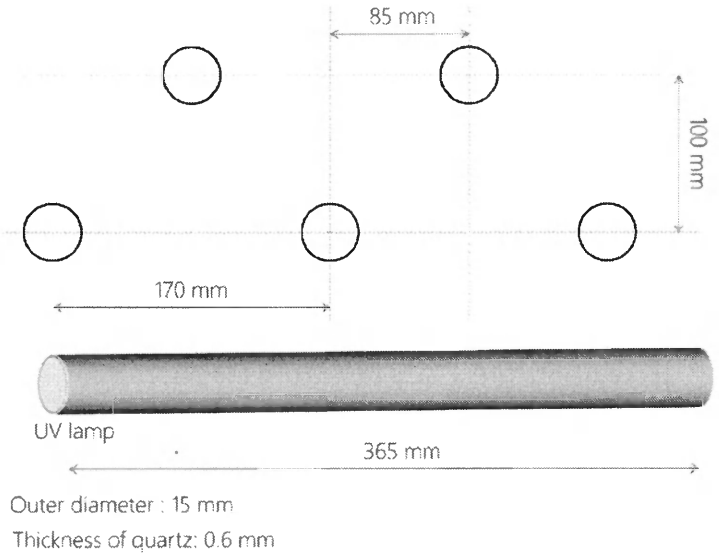

Figure 4-1: Lamp position and dimension details

Custom fitted plexiglass holders painted with matte black paint was attached on either side the UV lamps to hold the lamps in position for this experiment. Similar to generic window glass, plexiglass (Poly methyl methacrylate (PMMA)) filters UV radiation at wavelengths below 300nm. Therefore, the reflection contributions from the holders to the experimental data should be minimized.

The radiometers used in this experiment responds to UVC radiation (wavelength between 200-280nm) which corresponds to the germicidal range for air disinfection applications (Bedford, 1927). The first radiometer is fixed in position for all the experimental runs while the second radiometer is attached to a probe that can navigate in a three dimensional space shown in Figure 4-2. This experimental apparatus is custom built and consist of three stepper motors moves the probe along 3 different axis (X-axis, Y-axis, and Z-axis).

Figure 4-2: 3D Scanner Apparatus with attached radiometer on probe

The stepper motors are connected to the computer controlling the apparatus using an Arduino Duo board (Arduino, 2014) and LabVIEW software (National Instruments Corporation, n.d.). The radiometer controller is also connected to the computer via the Arduino Duo board. The computer communicates with the Arduino board and is capable of moving the probe in a 3-dimensional space and receive and/or record the signals from the 2 radiometers in this experimental setup using the LabVIEW software.

A set of instructions (visual code) was developed in LabVIEW to systematically study the signals received from radiometers and moving the probe systematically to obtain radiant flux measurements at various positions on a plane (XY plane) before moving to the next plane. Experimental data was collected at 4 specific z-planes as shown in Figure 4-3(a) at distances 50mm, 100mm, 150mm and 200mm away from the center plane of the bottom row of UV lamps.

The range of motion for probe is between 0 – 450mm along the Y-axis and 0 – 420mm along the X-axis for any specific z-plane (see Figure 4-3(b)). The experimental apparatus was calibrated

and aligned so the probe's origin point starts 225mm along the Y-axis away from the center and 210mm along the X-axis away from the center as shown in Figure 4-3(b). The probe was set up to move in 10mm increments along each axis and record a data at every point which results a total of 1978 data points per z-plane. The experiment is repeated twice on each plane which results in a total of 8 experimental runs with 1890 data points each run. A full experimental overview of the radiometer positions and UV lamp positions is shown in Figure 4-4(a).

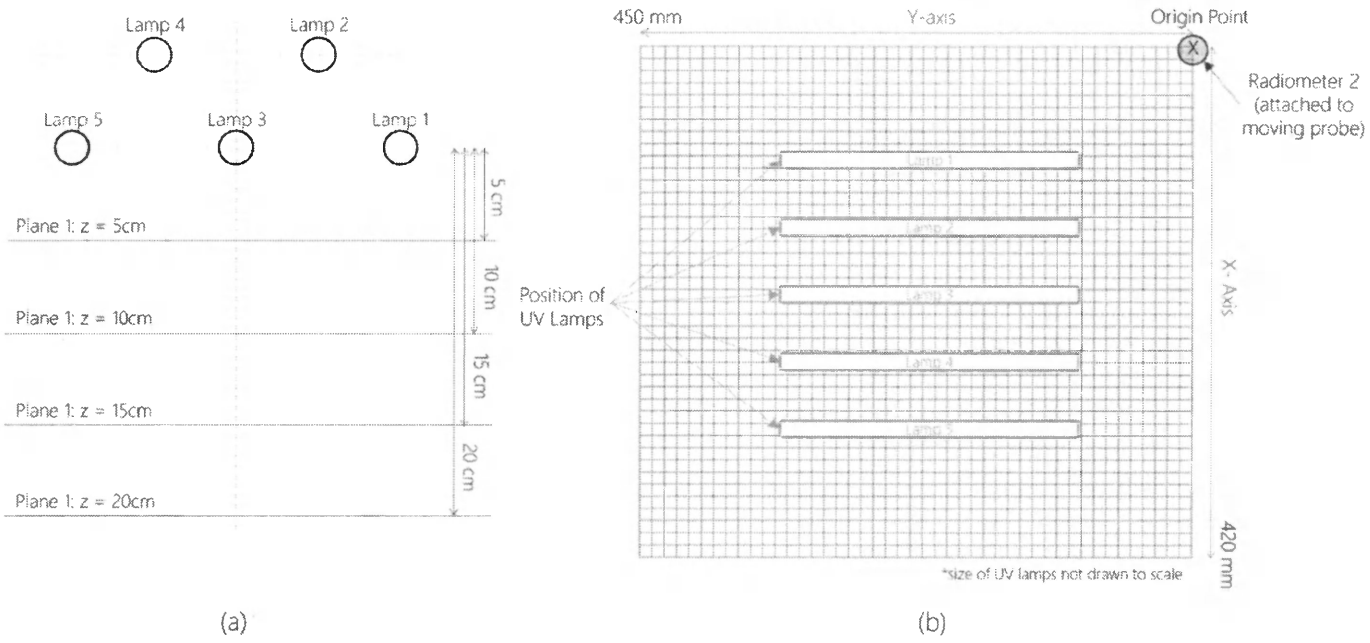

Figure 4-3: Positions of planes and grid system used for gathering data

The UV lamp experiments were conducted in a lab area with no personnel interference during the course of the experiment to minimize the effect of temperature changes and turbulence in the lab room area. No additional light sources were present during the course of the experiment to minimize external contributions of UV radiation to the experimental setup as well. Additionally, all the UV lamps were turned on for 1 hour before experimental measurements were taken to minimize the effect of the initial UV irradiation fluctuations into the dataset. This duration is determined by studying the stability of the radiometer readings after the UV lamps are turned on.

Since the experimental setup is entirely connected to the computer, the entire experiment is conducted remotely. A snapshot of the UV lamp experiment running is shown in Figure 4-4(b).

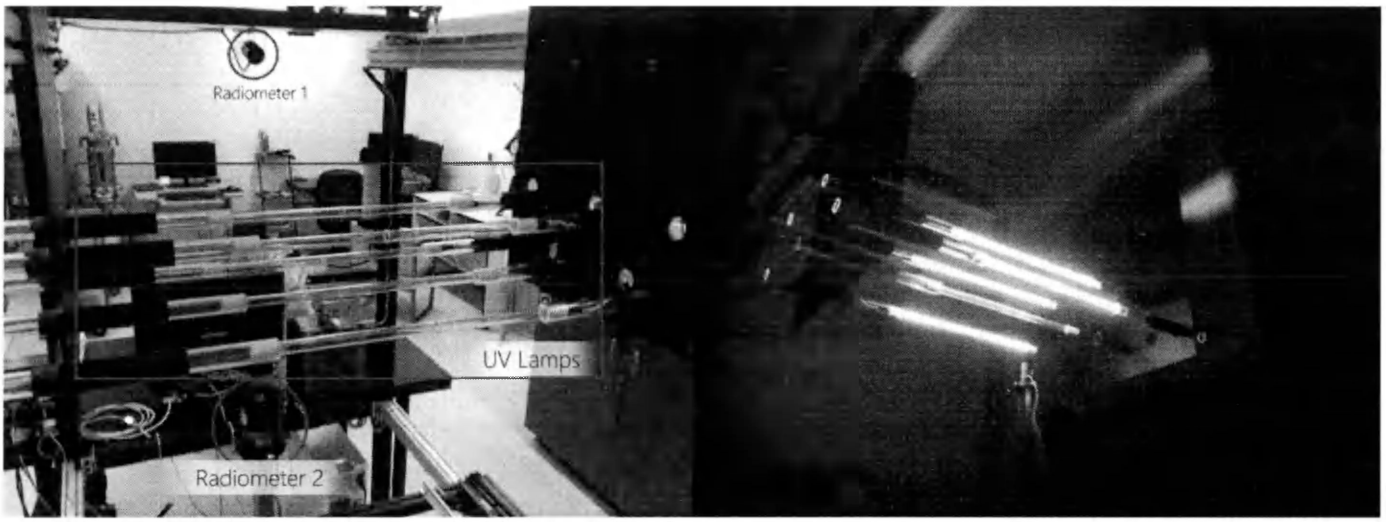

Figure 4-4: Full general overview of experimental setup and a snapshot of experiment running.

4.3.2 Simulation setup

In order to validate DO model against experimental radiation measurement, the experimental setup detailed previously is constructed and meshed using ANSYS 14 (ANSYS Inc, n.d.) as a platform. ANSYS 14 is a commercially available CFD software package that includes the FLUENT solver. DO model is easily accessible through the FLUENT software and it used to solve this complex multi-lamp radiation experimental setup.

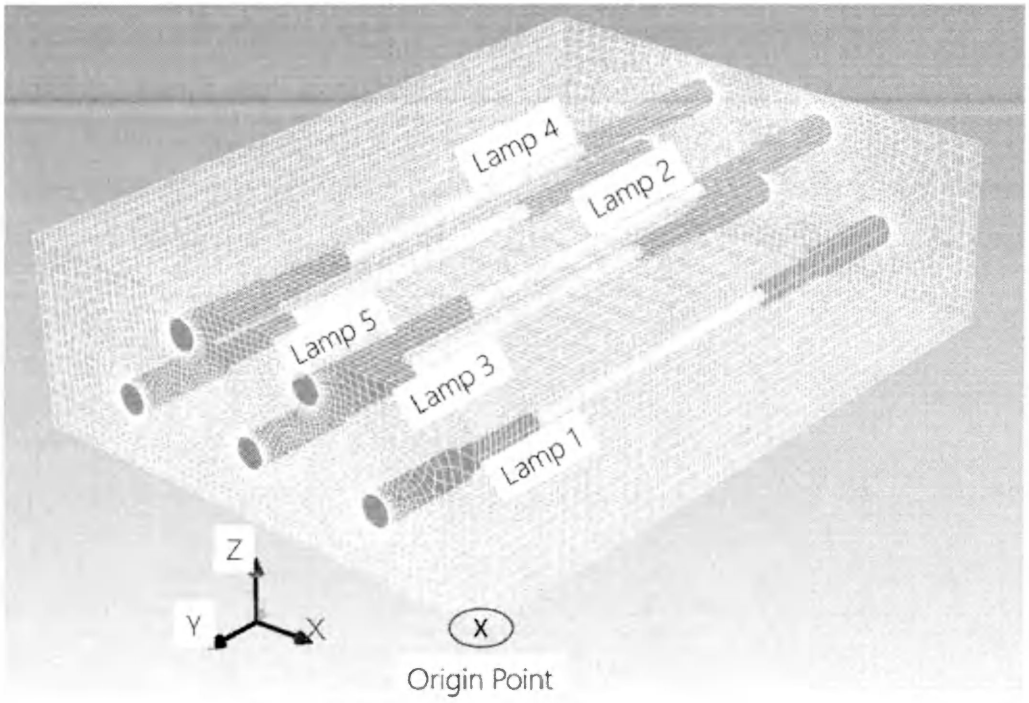

Figure 4-5: Geometry and mesh of complex multi-lamp experimental setup in ANSYS

The lamps used in the simulation setup is modelled as 15mm outer diameter cylindrical tube with a quartz housing of 0.6mm thick as shown in Figure 4-1. The thin quartz housing for the lamps are modeled with a refractive index, n of 1.5 with emissivity, ε of 0.92 (these estimations were obtained from past research work on modeling quartz properties with UV irradiation (Bolton, 2000)). The custom fitted plexiglass holders holding the lamps on either side is also modelled according to the dimensions of the holders used in the experiment. The UV absorption properties of the plexiglass holder material is set to 100% (ε of 1) as it is coated with matte black paint in the experiment (see Figure 4-4a). In this complex multi-lamp radiation case, it is assumed that there are no particulates in the medium and effects of scattering is not modeled. In order to model the radiation inside the lamp (to study the interactions between radiation and the lamp plasma), a small diameter lamp core (0.5mm) was modeled with a diffuse irradiation boundary condition. The absorption coefficient, a of the lamp plasma and output radiation intensity, I

values from the each lamp core is determined through initial experiments which will be detailed below. The geometry and mesh of the final setup is shown in Figure 4-5.

Since the radiometers used for this experiment only respond a small range of UV irradiation, this case can be assumed to follow a single gray band radiation model. Additionally, the DO model was set up with angular discretization of 5 x 5 ($N_\theta \times N_\phi$) for each quadrature and pixelation of 3x3 (as recommended by the FLUENT user manual) (Fluent Inc, 2006).

4.3.3 Initial experimental setup

Five LP mercury UV lamps were used for these experiments. In order to account for the possible variance in intensity between each lamp, an experiment needed to be conducted to determine the variance in light intensity emitted. Additionally, the UV lamps contain LP mercury plasma which absorbs a portion of the radiant energy passing through. An experiment needed to be conducted to determine the absorption coefficient values of the lamp plasma. The findings from these experiments will be used in the final DO model simulation setup.

4.3.3.1 Intensity variation between each lamp experiment

To determine the slight emitted intensity variation between each lamp, the Radiometer 2 is placed 100mm away from the center plane of the lamp as shown in Figure 4-6. The probe is then programmed to move in 10mm increments along the Y-axis (longitudinal axis along the lamp) during the experiment. The experimental conditions for this experiment is similar to the main experimental conditions as described above:

1. The probe and data collection is performed remotely via a computer
2. Experiment is conducted in a lab area with no additional light sources or personnel interrupting

3. The lamp is switched on for 1 hour before any data is collected

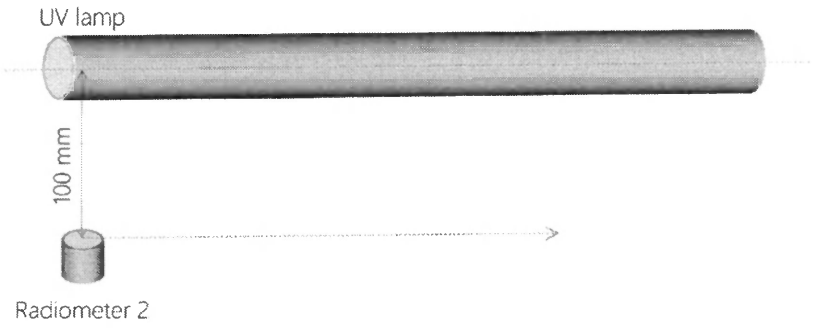

Figure 4-6: Initial experimental setup to determine lamp intensity variations

This experiment is conducted for each lamp of the 5 lamps used in this experiment individually. The data obtained from this experiment is analyzed and used in the final DO model simulation.

4.3.3.2 Lamp plasma absorption experiment

The LP mercury UV lamps contains a medium of pressurized gas mercury which contributes the absorption of UV radiation as the UV radiation passes through. In determine the absorption coefficient to use for this medium in our simulation setup, an experiment is designed. In this experiment, a setup of two lamps tied together is used where the top lamp is labelled Lamp 1 and the bottom lamp is labelled Lamp 2 and the radiometer is fixed at 100mm away from the center line of Lamp 1 as shown in Figure 4-7. The probe is fixed in location for this experiment and four conditions of this setup is studied as listed below:

Case 1: Lamp 2 is removed and only Lamp 1 is turned on

Case 2: Lamp 2 is placed in position and only Lamp 1 is turned on

Case 3: Both Lamp 1 and 2 are turned on

Case 4: Only Lamp 2 is turned on.

The experimental conditions for this experiment is similar to the main experimental conditions as described above:

1. The probe and data collection is performed remotely via a computer
2. Experiment is conducted in a lab area with no additional light sources or personnel interrupting
3. The lamp is switched on for 1 hour before any data is collected

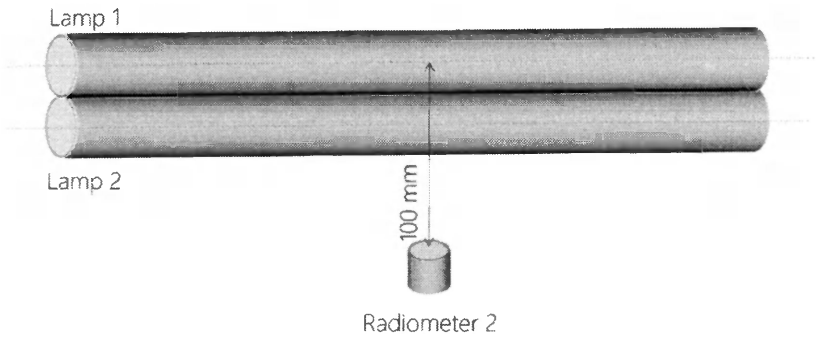

Figure 4-7: Lamp plasma absorption experiment

It should also be noted that the computer code is slightly altered for the radiometer readings for this particular part of the experiment. The computer is coded to record 270 data points from radiometer 2 without moving the probe position.

4.4 Results

4.4.1 Stability test results

A quick experiment to determine the stability of the UV lamps when turned on initially was conducted. The radiometers were fixed in place and measured the radiant flux of the UV lamp setup during operation. Observing the results (Figure 4-8) of the stability test, it was concluded that it takes approximately 3600 seconds for the radiometer readings to reach a plateau.

Therefore all preceding experiments were conducted after leaving the UV lamps turned on for 1 hour.

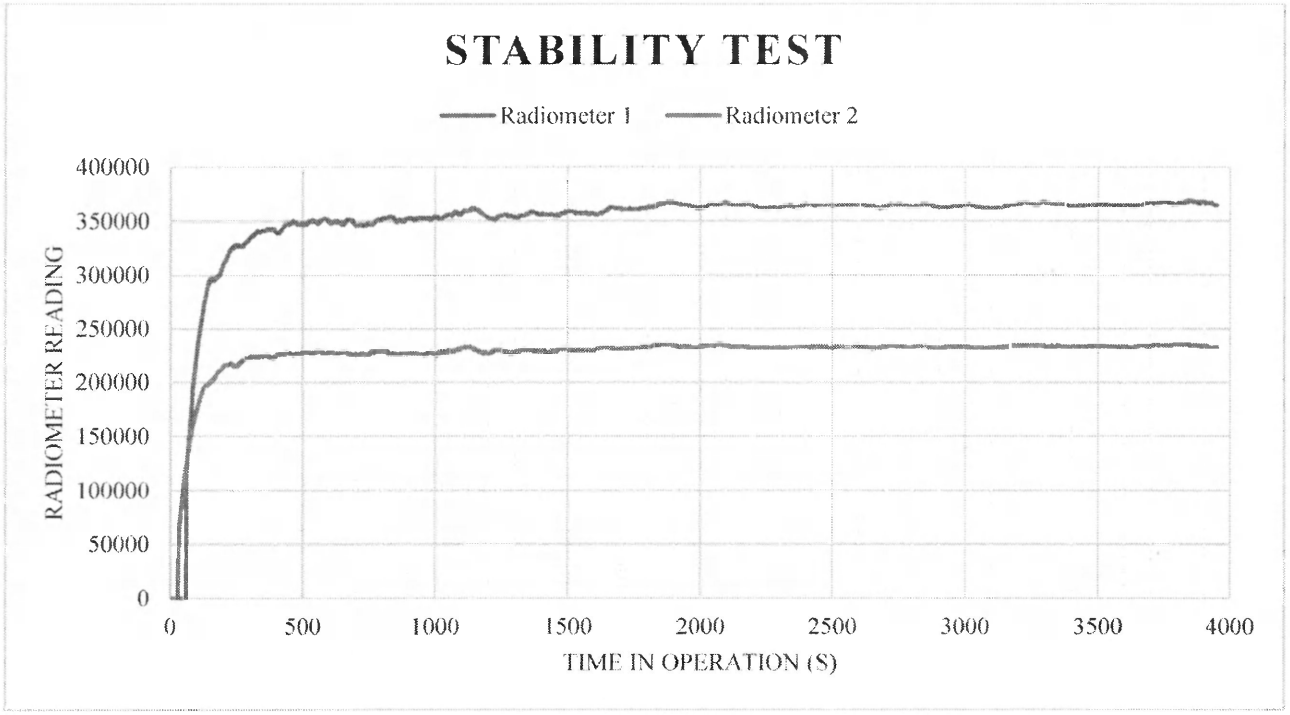

Figure 4-8: Initial UV lamps stability test

4.4.2 Main experiment results

A total of 15,824 data points were taken for the main radiation experiment. The data is represented in this paper as contours for ease of understanding and to help visualize the radiation data. A summary of the experimental data collected is shown from Figure 4-9 -13.

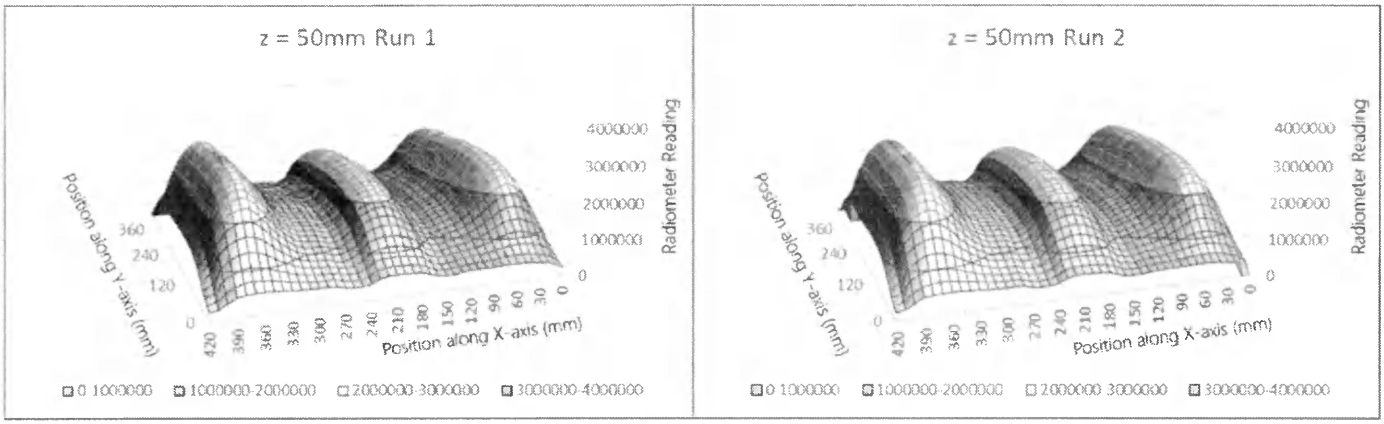

Figure 4-9: Contoured radiation readings obtained for z-plane distance = 50mm

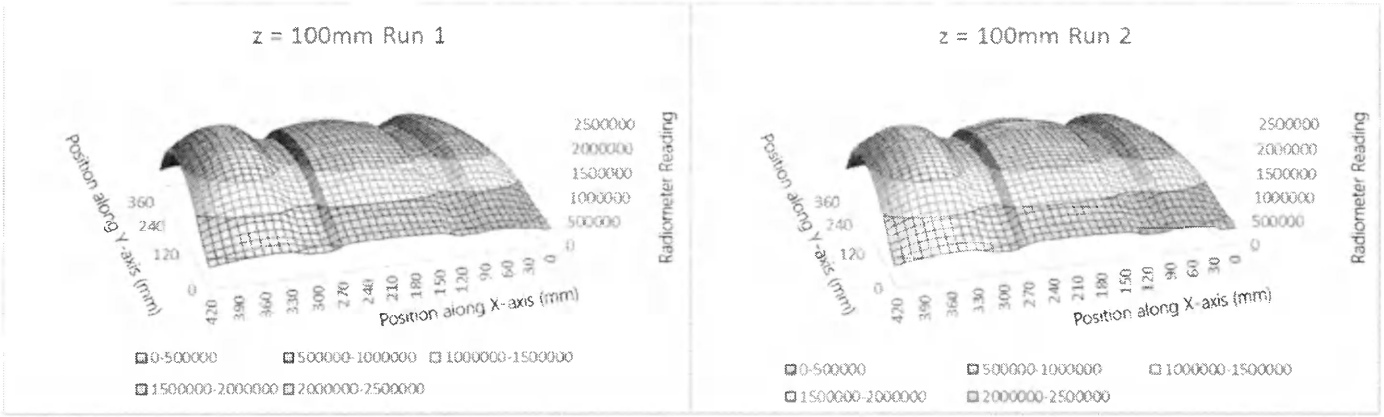

Figure 4-10: Contoured radiation readings obtained for z-plane distance = 100mm

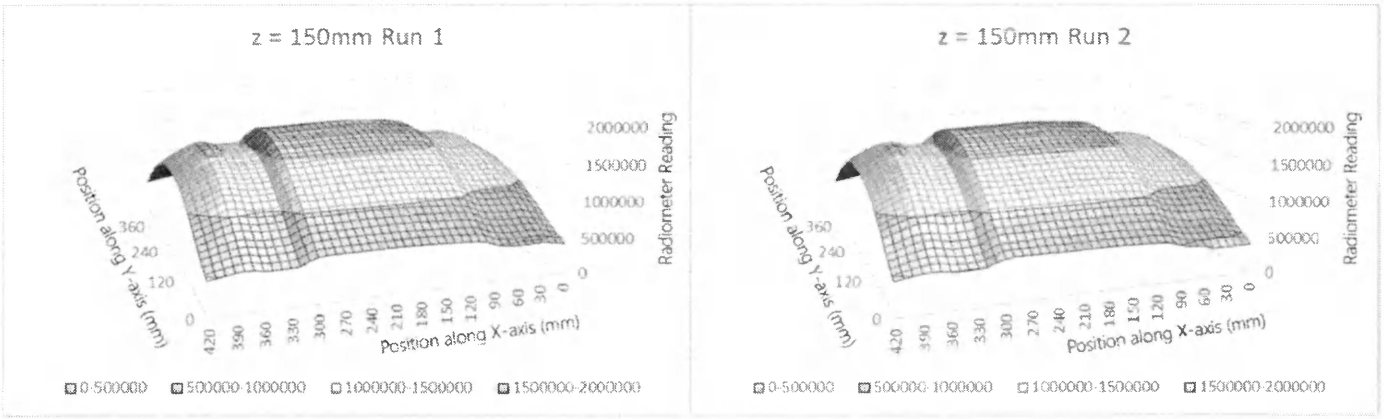

Figure 4-11: Contoured radiation readings obtained for z-plane distance = 150mm

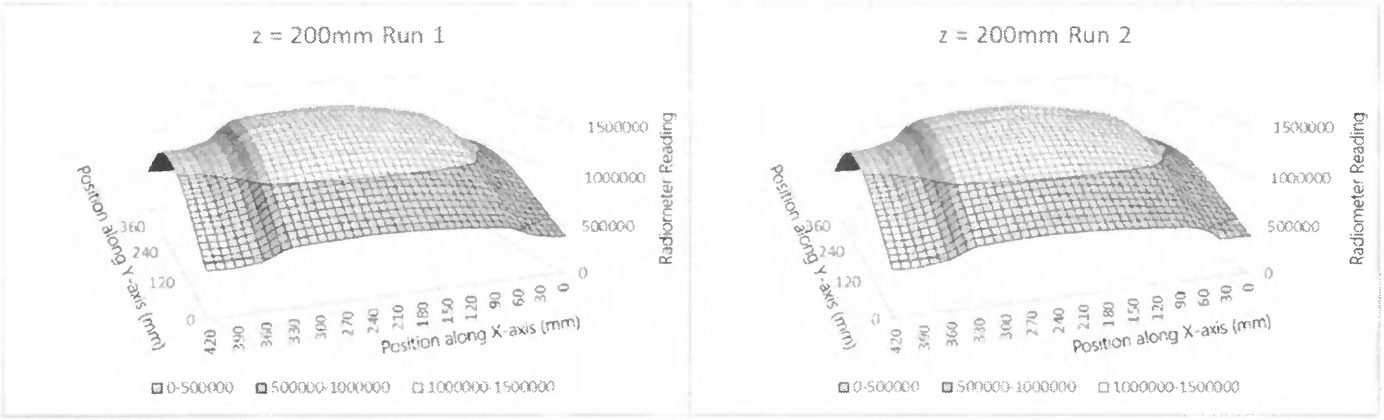

Figure 4-12: Contoured radiation readings obtained for z-plane distance = 200mm

Observing the experimental data, the contoured radiation readings between Run 1 and Run 2 is similar for each z-plane as shown by Figure 4-9 – 13.

4.4.3 Additional experiments for simulation

Additional experiments was required to obtained radiation intensity values to be used in the DO model simulation and to define an absorption coefficient value for the lamp plasma material.

4.4.3.1 Intensity variation experiment results

In the intensity variation experiment, 5 lamps were individually measured as described in the procedures and methods section above. The radiometer reading profiles for each lamp is summarized in Figure 4-13.

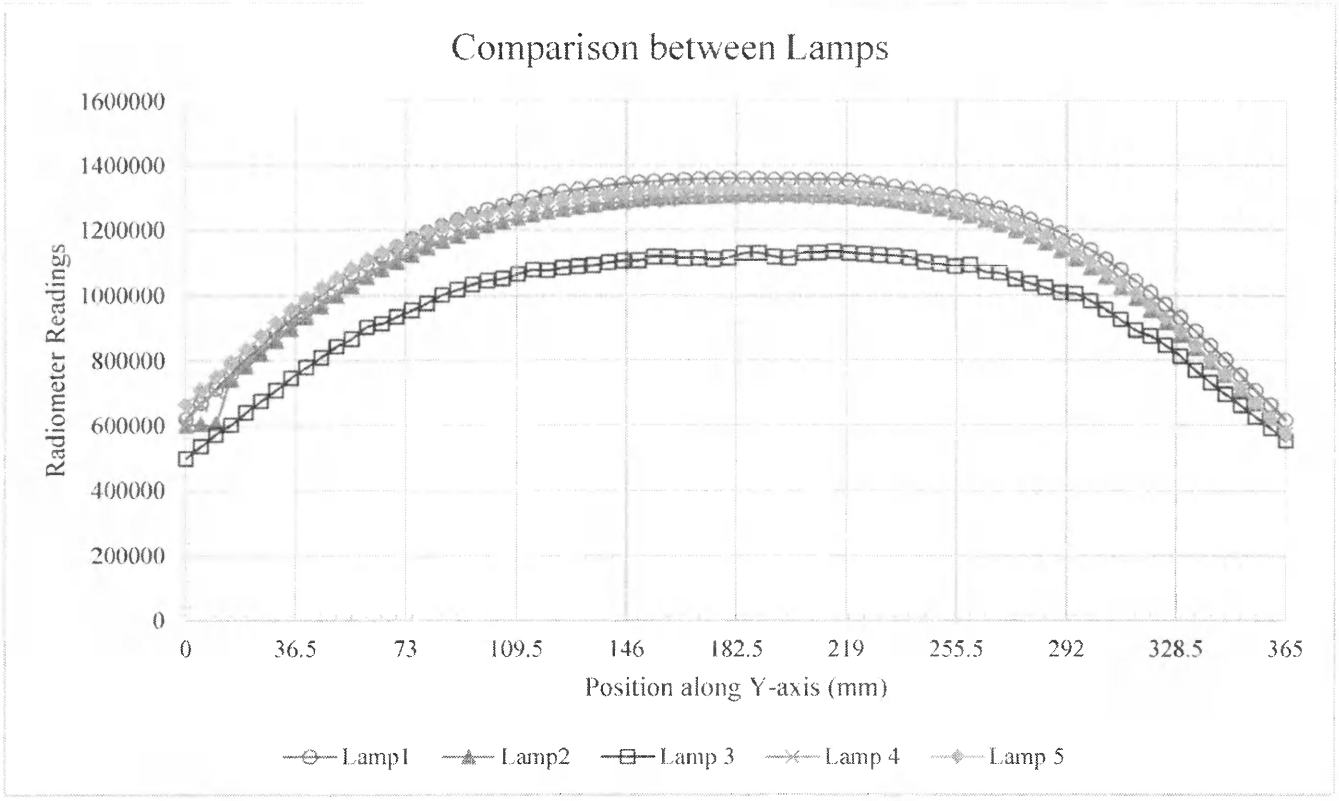

Figure 4-13: Radiometer reading profiles along longitudinal (Y-axis) of each lamp used in the experiment

Observing the measured radiometer readings from the experiment, it can be noted that lamp 3 is the least intense lamp used in this experiment. Therefore, the intensity values of the other lamps are normalized against lamp 3. Values that fall between 110mm and 250mm long the Y-axis of the lamps were average and compared to lamp 3. This ratio will be used when entering intensity values to the DO model simulation. The intensity ratio results between the lamps are summarized in the table below.

Table 4-1: Intensity ratio between lamps against lamp 3

Lamp	Intensity Ratio to Lamp 3
Lamp 1	1.21:1
Lamp 2	1.16:1
Lamp 3	1:1
Lamp 4	1.16:1
Lamp 5	1.18:1

Therefore, the intensities of each lamp is appropriately assigned in the DO model simulation according to this result.

4.4.3.2 Lamp plasma absorption experiment results

An additional experiment was also conducted to determine the absorption co-efficient to use for the lamp plasma material in the DO model simulation. Four separate experimental cases were studied in this part of the experiment as detailed above. A total of 270 data points were recorded for each case and is summarized below:

Table 4-2: Summary of radiometer readings obtained from absorption experiment

Case	Mean	Standard Deviation
Case 1: Only Lamp 1 is turned on without Lamp 2	856.22	1.29
Case 2: Only Lamp 1 is turned on with Lamp 2 (not turned on)	355.99	4.84
Case 3: Both Lamps are turned on	1089.31	5.23
Case 4: Only the Lamp 2 is turned on	908.26	1.38

Evidence of radiant energy absorption is immediate evident by comparing case 1 and case 2. The radiometer reading when a LP UV lamp was present is significantly lower (case 2) compared with the radiometer reading when a LP UV lamp is not present (case 1). According to the radiometer readings, the radiant flux was reduced by 58.47% when passing through the LP UV lamp. Additionally, comparing the results between case 3 and case 4 + case 1, a reduction of 38.26% in radiant flux was observed. It should be noted that in case 3, both lamps are turned on which might alter the absorption coefficient of the plasma medium as opposed to case 2. Through trial and error, it was found that an absorption coefficient of $46.5m^{-1}$ (assigned to the lamp plasma material) achieve approximately 38% reduction in radiant flux in a sample DO model case of this experiment.

4.4.4 DO model Simulation results

The main experiment described in this paper consisting of 5 UV lamps was modeled and meshed in ANSYS CFD software. Using FLUENT as a platform, DO radiation model was performed for multiple z-plane distances away from the lamp of: 50mm, 100mm, 150mm and 200mm. The additional experiments performed provided important values to be used in the DO model simulation setup. The result of the DO model simulation was completely 3-dimensional; however, only the incident radiation flux contours on the z-plane surfaces is studied. A summary of the DO model simulation results is shown in Figure 4-14 to 16.

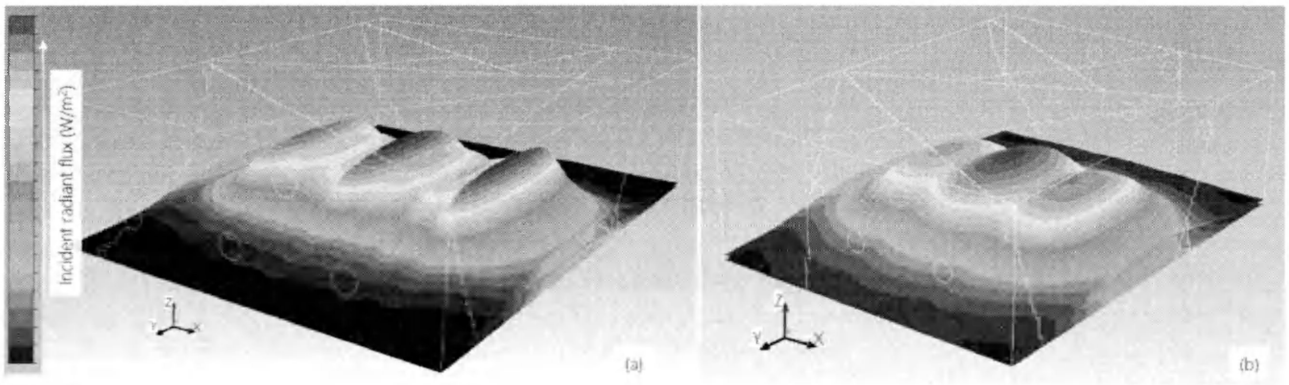

Figure 4-14: Incident radiant flux contours from DO model simulation of z-plane distance away = 50mm (a) and 100mm (b)

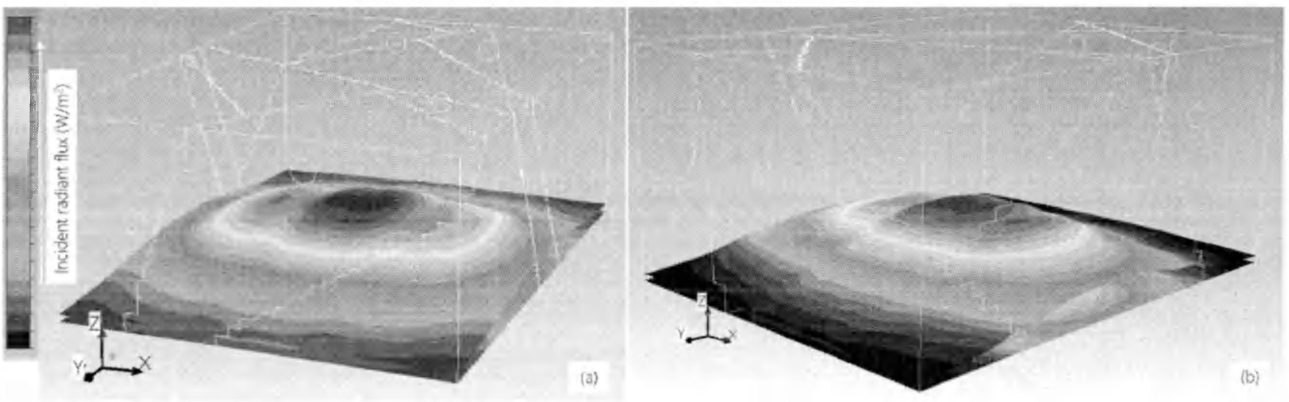

Figure 4-15: Incident radiant flux contours from DO model simulation of z-plane distance away = 150mm (a) and 200mm (b)

Comparison between the experimentally measured radiant flux and the DO model simulated radiant flux is performed by utilizing ANSYS CFD-Post software. In this post-processing software, both dataset from the experiment and simulation can be overlaid for additional analysis.

4.5 Discussion

The aim of the work performed in this chapter is validate DO radiation model against experimentally obtained radiation data. DO radiation model is a comprehensive radiation model that accounts for basic optical principals such as (reflection, refraction, shadowing effect, and absorption) which are all essential to the modeling radiation accurately as discussed in the previous chapter (Bolton, 2000). DO model solves sets of RTE equations similar to the approach CFD software uses to solve sets of Navier-Stokes equation in hydrodynamic modeling (Raithby, 1999). This numerical iterative approach to radiation modeling is useful because it can leverage the ever increasing computing power to solve the complex radiation problems; however, this numerical iterative approach is also susceptible to error-propagation issues that affect all numerical iterative models. Therefore, it is important to validate DO model for use in UV radiation modeling against experimental data.

According to our knowledge and reviews, there are no available published multi-lamp fully 3-dimensional UV lamp radiation experimental work or data to refer to for the validation of DO model. Therefore, careful precautions are considered when running these experiments (such as allowing the UV lamp to stabilize for 1 hour before experimental data is collected, running the experiment remotely to avoid personnel interference, and conducting the experiment in a dark room with no additional light source). This methodology is proven to be an effective way to conduct this experiment as the shown by the data collected in (Figure 4-9 -13). For each z-plane

distance, the experiment is repeated and the data collected for both runs (of the same z-plane distance) are in very close agreement. As expected, the radiometer readings for z-plane distances closer to the light source (z-plane distance = 50mm) is significantly higher than radiometer readings for z-plane distances further away from the light source (z-plane distance = 200mm).

A total of 15,824 data points was collected from this experiment. This raw data collected is the foundation of the DO radiation model validation effort in this paper. DO radiation model has been utilized poorly by researchers in the past and been concluded to be unable to consider refraction in a study by Liu et.al (Liu, Ducoste, Jin, & Linden, 2004). However, a study of DO model with basic optic principles was conducted in the previous chapter showed DO model was capable of considering such basic optic principles in its solution as discussed in the previous chapter. Intricate details of the lamp design (inner-lamp plasma material, inner-lamp core, and outer-lamp quartz) was included in the construction and design of the DO model for simulation. These considerations are important to obtain the most accurate simulation results possible from the DO model.

In order to include the intricate details of the lamp, experimental work on the lamps was conducted to obtain these values (emitted intensity variation between each lamp and lamp plasma absorption coefficient). The lamp intensity variation experiment provided emitted radiation intensity differences between each lamp. Observing Figure 4-13, it should be noted that lamp 3 emitted significantly less radiation compared with the other lamps used for this experiment. This shows that each UV lamp has slightly emitted UV radiation intensity differences and cannot be assumed to be the same in the DO model simulation. The low emitted radiation intensity from lamp 3 could be attribute to manufacturing defects but further testing is required to validate this assumption. Another interesting observation that can be noted from

Figure 4-13 is the radiant flux (W/m^2) profile along the longitudinal axis of each lamp. The maximum measured radiant flux regions along the longitudinal axis of the lamp lies between 120mm – 240mm along the 365mm long UV lamp.

The intensity ratios were obtained from the intensity variation experiment (Table 4-1) and appropriately assigned in the DO model simulation. Additionally, another experiment was designed and conducted to determine the absorption coefficient of the lamp plasma medium. In this experiment, radiometer 2 was fixed directly the middle point of the lamp 1 with a z-plane distance of 100mm. Four cases were tested and the results show that there is significant loss in radiant flux when radiation is passed through a lamp (see Table 4-2). Observing the results from this experiment, it is calculated that the reduction in radiant flux between case 1 and case 2 is 58.47%. The reduction in radiant flux between case 1 + case 4 and case 3 was calculated to be 38.26%. This significant difference in radiant flux absorption between these cases could suggest that absorption values for the lamp plasma is dependent on the state of the lamp plasma (activated when lamp is turned on and de-activated when lamp is not turned on).

In the DO model simulation setup, the lamps are modelled when they are turned on; therefore, an absorption coefficient of 46.5 m^{-1} was assigned to the lamp plasma material. The value of the absorption coefficient was determined by trial and error by modeling the lamp absorption experiment in ANSYS, and manipulating the value of lamp absorption coefficient until an incident radiant flux reduction of approximately 38% is achieved on the mid-point at z-plane distance = 100mm from lamp 1. It was assumed in the DO model that all the lamps share a common lamp plasma absorption coefficient value of 46.5 m^{-1}.

With all the necessary details obtained from these experiments, the DO model simulation of the main experiment is performed for z-plane distances of 50mm, 100mm, 150mm, and 200mm. The

results from the DO model simulation was imported to ANSYS's CFD-Post software for post-processing work. In CFD-Post, the experimental dataset and the DO model simulation result dataset was compared and studied. Figure 4-16-21 shows the results for z-plane distance of 50,100, 150 and 200mm.

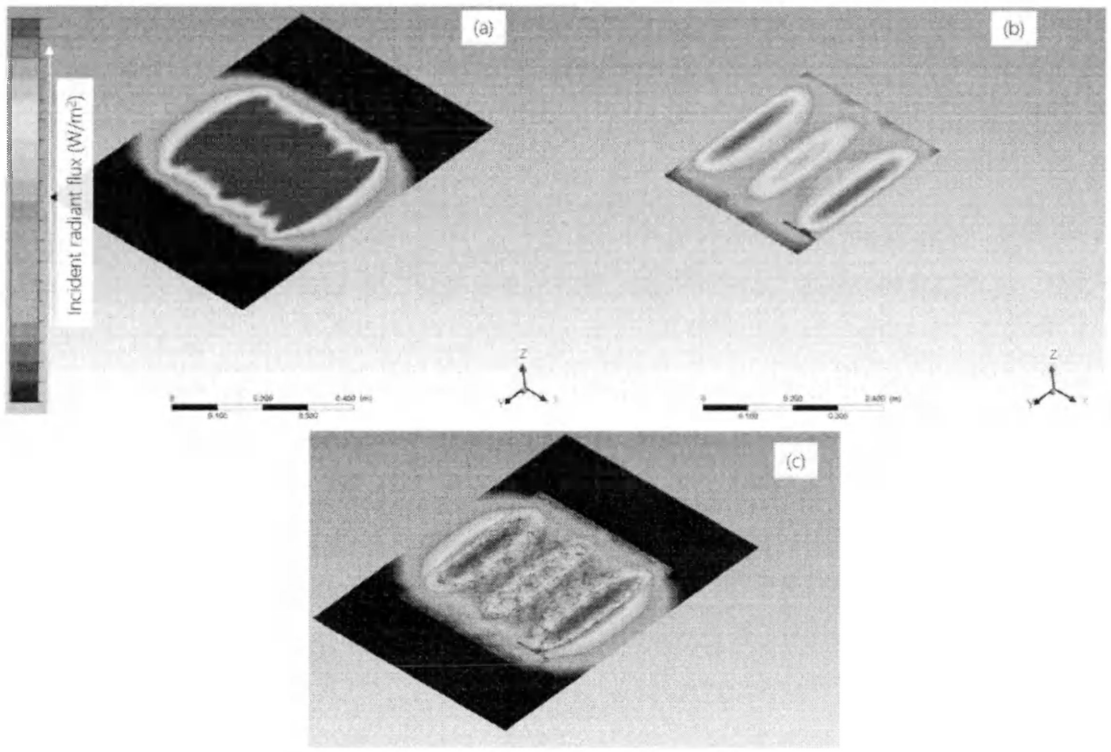

Figure 4-16: Comparison between incident radiant flux (W/m^2) contours of DO model simulation (a), experimental data (b), and overlaid contours (c) at z-plane distance = 50mm

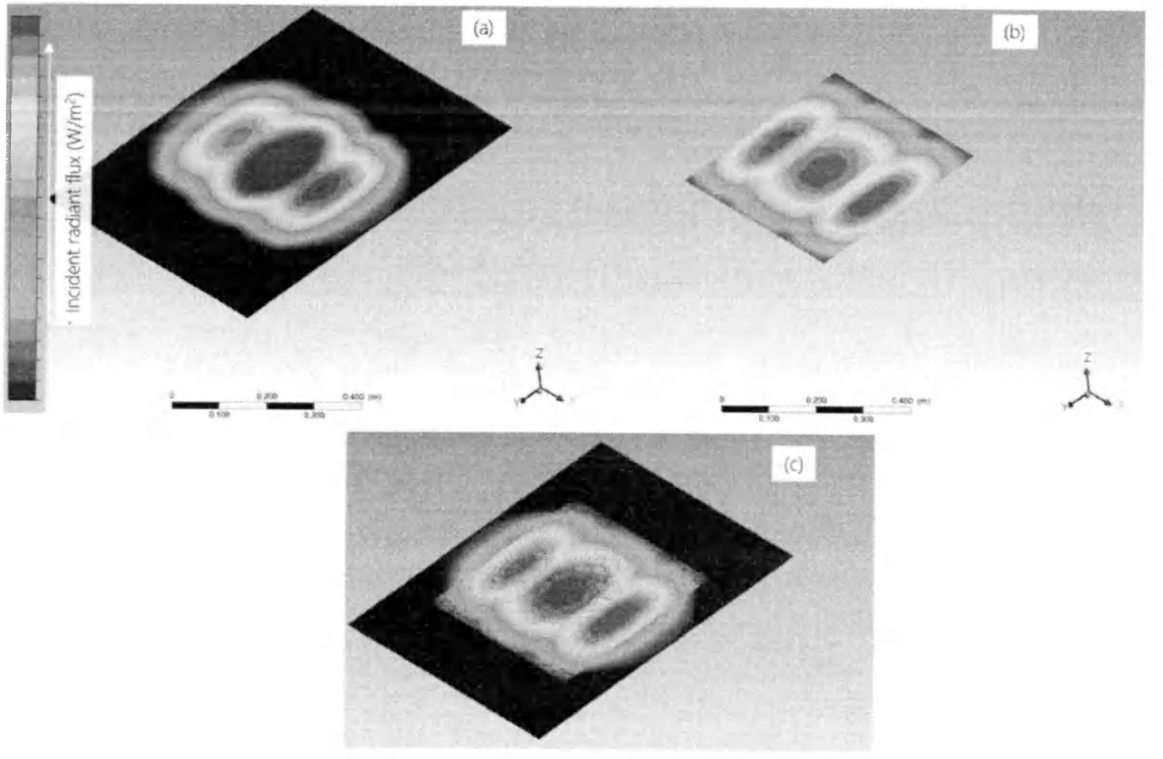

Figure 4-17 Comparison between incident radiant flux (W/m2) contours of DO model simulation (a), experimental data (b), and overlaid contours (c) at z-plane distance = 100mm

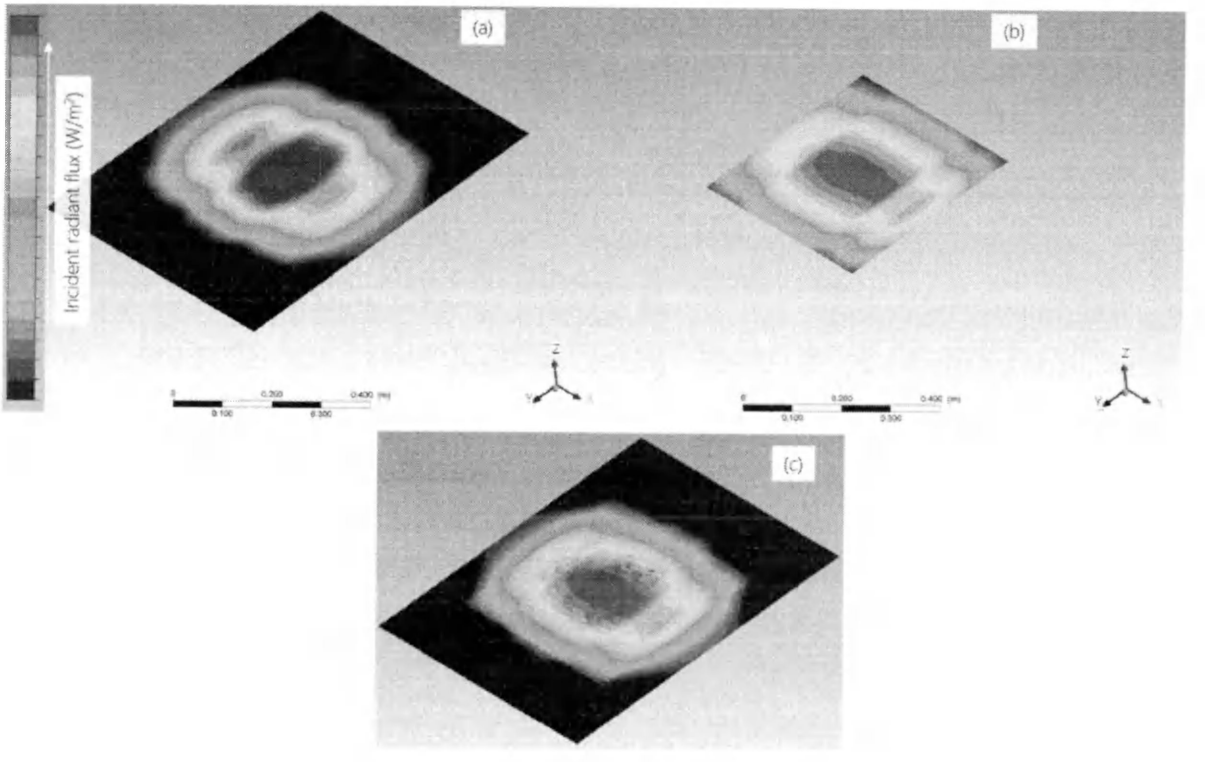

Figure 4-18 Comparison between incident radiant flux (W/m2) contours of DO model simulation (a), experimental data (b), and overlaid contours (c) at z-plane distance = 150mm

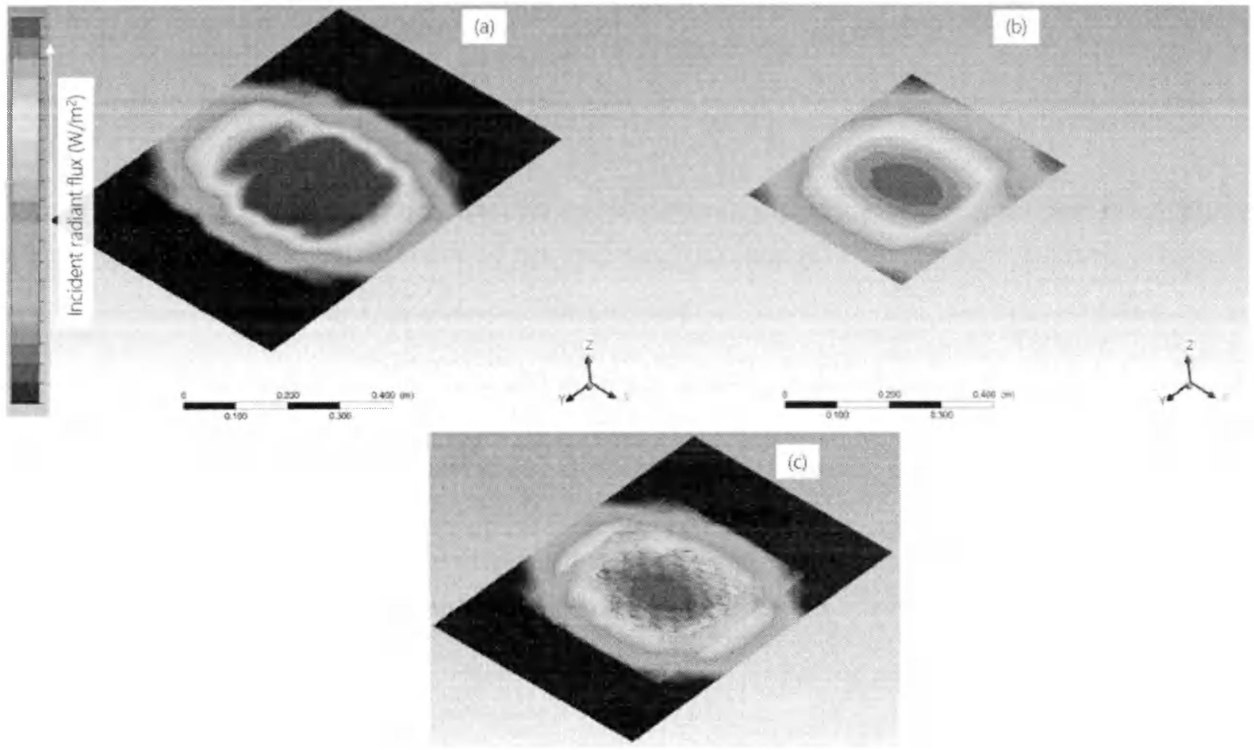

Figure 4-19 Comparison between incident radiant flux (W/m2) contours of DO model simulation (a), experimental data (b), and overlaid contours (c) at z-plane distance = 200mm

Referring to Figure 4-16- 21, the contour shape obtained from the simulation portion (a) and experimental portion (b) can be visually enhanced by overlaying the two contours as shown in (c). This comparison allows the shape of the contours from the DO model simulation and experimental measurement to be compared qualitatively.

Comparing z-distance = 50mm (Figure 4-16) and z-distance = 100mm (Figure 4-17), the contour similarities between the simulation and experimental results are in bad disagreement. The shapes of the contours from the simulation do not agree with the measured dataset. However, comparing z-distance = 150mm (Figure 4-18), the similarities are getting better. The best simulation and measured dataset agreement can be seen at z-distance = 200mm (Figure 4-19) for this experiment.

The contour overlay shows that the DO model simulation incident radiant flux contours did not fully agree with the experimentally measured data. It should be noted that the contour comparison results for z-plane distance of 50mm was the poorest while the comparison results for z-plan distance of 200mm was the best. The poor contour comparison agreement between the DO model simulated result and experimentally measured data could be attributed the angle of view of the radiometer sensor which does not covered all angles (180 degree). Due to time constrain it was not possible to implement the angle of view in the DO model.

In the previous chapter, the DO model shows great agreement with the experimentally measured actinometer results Figure 3-8. However, the experimental work performed in this chapter did not match the DO model results entirely. This discrepancy could be attributed to many factors.

The first factor of the consideration is how the way radiant flux values are collected experimentally and studied in the DO model simulation result. In the previous chapter, the radiant flux values are collected by a spherical actinometer, which results in collecting fluence rate values. The incident radiation flux values along the spherical surfaces in the DO model simulation result is integrated along the entire surface to obtain the fluence rate values to compare with the experimental actinometer result. The approach to studying the values experimentally is very similar to the studying the values in the DO model simulation.

In this chapter, the radiometers used for the experiment consist of a flat photovoltaic sensor that is housed by a plastic casing and lens. However, in the DO model simulation, the radiometer housing with a plastic casing and lens is not modelled; instead, the DO model results are based on studying the incident radiation flux passing a totally flat surface. This slight discrepancy between the experimental measurement methodology and simulation result study methodology

could have affected the agreement between the simulation results and experimentally measured values.

Additionally, an oversimplified assumption when performing the DO model simulation of assuming all the lamps to have equal lamp plasma absorption coefficient could have also affected the agreement between the simulation results and experimentally measured values; it was could be possible that each lamp in this experiment attributed different absorption coefficients, during operation or when turned off. It was observed in the lamp intensity comparison experiment (Figure 4-6) that lamp 3 was emits significantly less radiant flux compared to other lamps. This suggests a potential manufacturing defect in lamp 3 that could have affected the lamp plasma absorption coefficient of that lamp.

4.6 Conclusion

The DO radiation model is a robust and comprehensive radiation model that is capable of incorporating all basic optic principles (reflection, refraction, shadowing effect and absorption) into the solution as it is integral to developing an accurate radiation model (Bolton, 2000)). However, the numerical iterative approach used to solve the sets of RTE equation in DO model could potentially introduce errors that invalidate the radiation model. Therefore, validation work on DO model is important. The DO radiation model is a model of interest particularly because of the similarities with the way hydrodynamic models are solved in CFD software (Raithby, 1999). This allows DO model is to be easily accessible in commercial CFD software like ANSYS 14 CFD software packaged used in this paper as a platform for studying DO model. Additionally, radiation modeling and hydrodynamic modeling are both important aspects when studying air UV disinfection systems and can be simultaneous combined on a single CFD software package

platform. The potential of radiation modeling using DO model for studying UV air disinfection systems is great but validation work on DO model needs to be addressed.

In this paper, a full multi-lamp 3-dimensional experimental setup was used in effort to validate DO model. The experimental apparatus consisted of 5 LP UV lamps and 2 radiometers. Experimental data was collected at 4 specific z-planes as shown in Figure 4-3(a) at distances 50mm, 100mm, 150mm and 200mm away from the center plane of the bottom row of UV lamps. The range of data collection was a fine 10mm increments along the X and Y-axis of the z-planes as shown in Figure 4-3(b). The data collected is very valuable for further studies of radiation models beyond the scope of this study. In this study, the data is visualized into radiant flux contours as shown in Figure 4-9-13.

Using the same experimental apparatus, several additional experiments was conducted to obtained values to use in the DO model simulation. These experiment included a study on the variation in emitted radiation intensity between each lamp. Each UV lamp used in the experiment emits radiation in different intensities as shown in Figure 4-6. Therefore, the assumption of lamps emitted the same radiation intensity is invalid. Additionally, the radiant flux absorption of lamp plasma experiment was also conducted. The results from this experiment suggests that lamp plasma absorption coefficient values is dependent on the state of the lamp plasma (depending on whether the lamp is turned on or off). A reduction in radiant flux by approximately 38% is found when the lamp was turned on. This finding was appropriately adjusted in the final DO model simulation setup.

The radiant flux contours obtained from the DO model simulation in this study was not in perfect agreement with the measured experiment data as shown in Figure 4-16 to 19. Even though many intricate details of the DO model was studied and applied (varying lamp intensities, refraction by

thin lamp quartz, and lamp plasma absorption), there could potentially be other external factors of the experiment that was not considered in the DO model simulation. The use of DO model in this study demonstrated the depth of optical principles the DO model can include in the radiation model solution. Although the DO model simulation results did not match the experimentally measured data completely, a lot of important optical considerations to include in the DO model simulation was explored (varying lamp intensities and lamp plasma absorption). Findings from this study is valuable future work on using DO model in the field of UV lamp radiation modeling. Further experimental validation work is recommended to ensure the accurate use of DO model in radiation modeling work for field of UV air disinfection.

4.7 References

ANSYS Inc. (n.d.). Retrieved January 2014, from http://www.ansys.com/Products/Simulation+Technology/Fluid+Dynamics/Fluid+Dynamics+Products/ch.ANSYS+CFX.pl

Arduino. (2014). Retrieved from Arduino: http://arduino.cc/

Bedford, T. B. (1927). The nature of the action of ultra-violet light on microorganisms. *British journal of experimental pathology, 8*(6), 437.

Blatchley III, E. R. (1997). Numerical modeling of UV intensity: application to collimated-beam reactors and continuous-flow system. *Wat. Res., 31*, 2205-2218.

Bolton, J. R. (2000). Calculation of Ultraviolet Fluence Rate Distributions in an Annular Reactor: Signifiance of Refraction and Reflection. *Wat. Res., 34*, 3315-3324.

Chandrasekhar, S. (1960). *Radiative Transfer.* New York: Dover.

Fluent Inc. (2006, 09 20). *Fluent 6.3 User's Guide*. Retrieved January 2014, from http://aerojet.engr.ucdavis.edu/fluenthelp/html/ug/main_pre.htm

Georgios, N. L., & Nikolos, I. K. (2012). Using the Finite-Method and Hybrid Unstructured Meshes to Compute Radiative Heat Transfer in 3-D Geometries. *Numerical Heat Transfer, 62*, 289-314.

Jacob, S. M., & Dranoff, J. S. (1970). Light intensity profiles in a perfectly mixed photoreactor. *A.I.C.H.E*, 359-363.

Kim, M. Y., Baek, S. W., & Park, J. H. (2001). Unstructured finite-volume method for radiative heat transfer in a complex two-dimensional geometry with obstacles. *Numerical Heat Transfer, 39*, 617-635.

Kowalski, W. (2009). *Ultraviolet germicidal irradiation handbook: UVGI for air and surface disinfection.* Springer.

Liou, B. T., & Wu, C. Y. (1996). Radiative transfer in a multi-layer medium with fresnel interfaces. *Heat and Mass Transfer, 32*, 103-107.

Liou, K. N. (1973). A Numerical Experiment on Chandrasekhar's Discrete-Ordinate Method for Radiative Transfer: Applications to Cloudy and Hazy Atmosphere. *Journal of Atmospheric Science, 30*, 1303.

Liu, D., Ducoste, J., Jin, S., & Linden, K. (2004). Evaluation of alternative fluence rate distribution models. *Journal of Water Supply: Research and Technology AQUA, 53*(6), 391-408.

Mishra, B., & Rajamani, R. (1992). The discrete element method for the simulation of ball mills. *Applied Mathematical Modeling, 16*, 598-604.

Modest, M. (1993). *Radiative Heat Transfer.* New York: McGraw-Hill.

Murthy, J. Y., & Mathur, S. R. (1998). Finite volume method for radiative heat transfer using unstructured meshes. *Journal of thermophysics and heat transfer, 12*(3), 313-321.

Murthy, J. Y., & Mathur, S. R. (2000). A finite volume scheme for radiative heat transfer in semitransparent media. *Numerical Heat Transfer, 37*, 25-43.

National Instruments Corporation. (n.d.). *NI LabVIEW*. Retrieved 2014, from NI LabVIEW: http://www.ni.com/labview/

Raithby, G. D. (1999). Discussion of the finite-volume method for radiation and its application using 3D unstructured meshes. *Numerical Heat Transfer, 35*, 389-405.

Stamnes, K., Chee Tsay, S., Wiscombe, W., & Jayaweera, K. (1988). Numerically stable algorithm for discrete-ordinate-method radiative transfer in multiple scattering and emitting layered media. *Appl. Opt., 27*(12), 2502-2509.

Chapter 5:Conclusion of study and future work

UV air disinfection modeling can be divided into two major parts: radiation and hydrodynamic modeling (Chapter 1). This thesis focuses heavily on the radiation modeling aspect of UV air disinfection modeling, and in particular the proper utilization of DO radiation model. DO model is a unique radiation model compared with other radiation models because this model can be solved with a similar calculation methodology used for solving hydrodynamic problems in commercial CFD software such as FLUENT (Chapter 2). Therefore, there is potential of combining both aspects of UV air disinfection modeling onto a single platform. Additionally, DO model is a robust and comprehensive radiation model that is capable of considering many basic optical principles and solving complex radiation problems efficiently. DO model has been extensively developed over the years but it is underutilized in UV air disinfection radiation research work. Therefore, thorough validation work was performed to validate DO model to further the understanding and use of this model for UV air disinfection work.

In Chapter 3, a simple set of studies demonstrated DO model's consideration for basic optic principles such as reflection, refraction, shadowing and absorption. Consideration for these basic optic principles are the foundation to the developing an accurate radiation model as heavily emphasized by Bolton (Bolton, 2000). A published research by Liu studying several fluence rate distribution models including the DO model in 2004 concluded that DO model cannot account for refraction effects in the solution (Liu, Ducoste, Jin, & Linden, 2004). However, results for the simple simulation cases demonstrated that DO model can account refraction. This discrepancy was investigated more thoroughly by re-constructing Liu's experimental setup in FLUENT with intricate considerations for the reflection, and refraction effects of the lamps and actinometers. The results from that DO model simulation shows comparable quantitative values to the

experimentally obtained data. This demonstrated that DO model could be a viable radiation model that can be validated quantitatively. Scalability of the DO model to solve complex radiation was studied in chapter 3 as well. The simplicity of using DO model to solve complex radiation problems was demonstrated by solving both simple and complex radiation problems using a similar approach. Other radiation models may require tedious analytical work to solve complex radiation problems but DO model can account for this complexity leveraging the computation power of a computer (Chapter 3). Although considerable validation work was performed on the DO model in chapter 3, further validation effort to test the DO model against a complex 3-dimensional multi-lamp experiment was considered in chapter 4.

In Chapter 4, a full 3-dimensional multi-lamp experiment was conducted to further validate DO model. An experiment setup consisting of 5 lamps and 2 radiometers was used. One radiometer was fixed in location while the second radiometer was attached to a probe that is capable of moving in a dimensional space using a computer. The experiments were conducted remotely and precautions were taken to ensure the stability of the UV lamp emission before any data was collected. However, despite the efforts to consider intricate details of lamp emission variability, and consideration of lamp plasma absorption, the experimental data obtained from the radiometer did not fully agree with the DO model simulation results as discussed in chapter 4.

The discrepancy between the DO model simulation results and the experimental data obtained in chapter 4 could be attributed to many factors. In chapter 3, the experimentally obtained data was collected by an actinometer. The radiant flux passing by the surface of the actinometer is absorbed and compared against summed surface incident radiation flux values along the spherical surface of the actinometers of the DO model simulation result. In chapter 4, the experimentally obtained data was collect by a radiometer which has a flat photovoltaic sensor

that is housed by a cylindrical plastic casing and lens on top. This experimental data was compared against an assumed flat surface incident radiation flux value of the DO model simulation result. The intricate details of the radiometer housing and lens was not considered in the DO model simulation result and could have resulted in the bad agreement between the experimental data and simulated result. Additionally, an oversimplified assumption when performing the DO model simulation of assuming all the lamps to have equal lamp plasma absorption coefficient could have also affected the agreement between the simulation results and experimentally measured values. An experiment conducted in chapter 4 shows that each UV lamp used have variable intensities; this could also suggest that lamp plasma absorption values for each lamp could also vary.

The work presented in this thesis shows thorough validation effort to validate DO model for use in radiation modeling of UV air disinfection systems. This work in important in advancing the field of radiation modeling using the DO model as guidelines to use DO model to correctly was establish in chapter 3 (Refer to 3.9.1). A complex or simple radiation problem can be solved using a similar DO model set up approach that utilizes powerful computing hardware, avoiding tedious analytical work. Many factor of considerations and challenges of performing an accurate DO model simulation was presented and discussed in this work and is useful for future work in this area of DO model validation. Although DO model was demonstrated to account for many basic optical principles and accurately representing fluence rate values in the actinometer experiment, DO model simulation results did not agree with the 3-dimensional multi lamp experiment. DO model still requires further validation before extensive use in radiation modeling for UV air disinfection applications. Potential researchers in this field can benefit from the observations and conclusions obtained from this work.

5.1 References

Bolton, J. R. (2000). Calculation of Ultraviolet Fluence Rate Distributions in an Annular Reactor: Signifiance of Refraction and Reflection. *Wat. Res., 34*, 3315-3324.

Liu, D., Ducoste, J., Jin, S., & Linden, K. (2004). Evaluation of alternative fluence rate distribution models. *Journal of Water Supply: Research and Technology AQUA, 53*(6), 391-408.